Xiaoming Lai

Signal Processing in Doppler Ultrasound for Blood Velocity Measurement

NTNU Trondheim
Norges teknisk-naturvitenskapelige universitet

Doktor ingeniøravhandling 1997:120
Institutt for teknisk kybernetikk

ITK-rapport 1997:65-W

To my lovely Sonja

Signal Processing in Doppler Ultrasound for Blood Velocity Measurement

Xiaoming Lai

A DISSERTATION SUBMITTED TO THE DEPARTMENT OF ENGINEERING CYBERNETICS AT NORWEGIAN UNIVERSITY OF SCIENCE & TECHNOLOGY IN PARTIAL FULLFILLMENT OF THE REQUIRMENTS FOR THE DEGREE OF DOKTOR INGENIØR

January, 1998, Trondheim, Norway

Contents

Acknowledgments

I am deeply indebted to my supervisor Dr. Hans Torp, for introducing me into the area, for his patient guidance and enthusiastic support during my Dr. Ing. study. His insights and creativity in medical ultrasound systems and signal processing have been a source of progress in my research.

I am also most grateful to my supervisor Dr. Bjϕrn A. J. Angelsen, for offering me the opportunity to do this research. His open minded attitude towards all the science, technology, social problems and his wide and deep knowledge are inspirational. Without his support, this work could not be completed.

I am indebted to Dr. Kjell Kristofersen, Chief scientist and Vice President of Vingmed Sound AS, Horten, Norway, for his support and arrangement. Much of the research work was carried out at Vingmend Sound during July, 1995 and April, 1997.

I am grateful to all faculty members and students at department of Dept. of Physiology and Biomedical Engineering, Norwegian University of Science & Technology, Trondheim for their support and friendship. Special thanks go to Mr. Steinar Bjaerum, Mr. Olaf. N. Norman, Dr. Michael Nickel and Mr. Johan Kirkhorn.

I wish to express my appreciation to all staff at Vingmed Sound AS, especially Eva Nilsson, for correcting the first paper in this thesis and Mr. Torbjϕrn Bakke, Mr. Inge Hϕivik, Dr. Lars Ø degaard, Mr. Dagfinn Saetre, Miss Ellen Ȧ se Thu, Mrs. Ragnhild Bast and Mr. James Brandal for their help.

NTNU is gratefully acknowledged for the financial support during the research in Norway.

The final revision of the thesis was made at Department of Medical Biophysics, Sunnybrook Health Science Centre, University of Toronto, Canada. I am indebted to Dr. Peter N. Burns for his support in the last stage of this study. I sincerely thank Mr. David. Hope Simpson, Mr. Chien Ting Chin, Miss Heather Fedash and Dr. Zvi Margaliot for reviewing and correcting the thesis.

I must thank my husband, Dr. Renyuan Li, for his encouragement, support, understanding, patience and tolerance during the study. The meaningful and cheerful days we spent together in Norway will remain in my memory forever. I feel grateful for the holidays and evenings he had to take care of Sonja, our daughter, while I was working for this thesis.

Finally, I like to thank my family and friends.

Abbreviations:

AM:	Autocorrelation method
A/D:	Analog -to-digital converter
CCM:	Cross-correlation method
CFI:	Color flow imaging
CFM	Color flow mapping
CW:	Continuous wave Doppler
IIR:	Infinite impulse response
EAM:	Extended autocorrelation method
FIR:	Finite impulse response
FTC:	Fixed target canceller
MRG	Multirange gated
MLE:	Maximum Likelihood Velocity Estimator
PRF:	Pulse repetition frequency
PW	Pulsed wave Doppler
RF:	Radio frequency
SNR:	Signal to noise ratio
VLSI:	Very large scale integrated circuit
2-D:	Two dimensional

Nomenclature

c:	Ultrasound velocity,
v:	Blood velocity
$\hat{v}$:	Estimated blood velocity
T:	Pulse repetition period.
prf or *PRF:*	Pulse repetition frequency
f_0:	Center frequency of transmitted signal,
f_c:	Mean frequency of the received signal
f_s:	Sampling rate
Δf:	Deviation of the received signal center frequency
ω_0:	Center frequency of the transmitted signal
ω_c:	Mean frequency of the received signal
$\Delta\omega$:	The deviation of the received signal center frequency
θ:	Angle between the ultrasound beam and the blood vessel
$p(t,k)$:	Received 2-D RF signal, where t: Elapsed time after pulse transmission; k: Pulse number
$x(t,k)$:	Complex demodulated signal
$h(t,k)$:	Echo response of a single moving scatterer
$n(t,k)$, $n_0(t,k)$:	2-D Gaussian white noise
$r(t)$:	Envelope of the transmitted signal
$f(t)$:	Transmitted pulse
$s(t)$:	Received signal from a single scatterer
$e(t)$:	Envelope of the received pulse
BW:	Bandwidth
B:	Beam width.
$w(n, 1)$:	Function after L-1 new zero values between each pair of sample values of $\hat{R}(m, 1)$ has been padded.
ϖ	Normalized mean frequency in the temporal direction
N:	Depth averaging samples
K:	Temporal averaging samples
σ:	Standard deviation
v_{NY}:	Nyquist limit

3 Abstract

Blood flow velocity in the human body is an very important information for the diagnosing of diseases. Doppler ultrasound is now commonly used to measure blood velocity. Some of the advantages are its non-invasiveness, short investigation time and low cost. The color flow imaging (CFI) in the Doppler ultrasound scanners has become an indispensable tool in modern hospitals, because it provides an excellent spatial visualization of flow pattern. The purpose of this thesis is to improve color flow image quality by using signal processing method.

Signal processing plays an important role in the CFI technology. Among the challenges in the CFI signal processor, parameter estimators and clutter filter are of major interests in this study. Parameter estimators in CFI seek to quantify blood velocity, bandwidth and power of the blood signal. All of which have haemodynamic significance. One aim of my study is to develop unaliasing velocity estimators with high estimation accuracy, small estimation variance and potentially for real-time implementation.

The unaliasing RF-signal cross-correlation velocity estimator has been regarded as a wideband velocity estimator which has small estimation variance and high spatial resolution. However, it suffers from large computation. Four new interpolation methods have been presented in this work (Paper B). All four methods reduce the computation in the RF-signal cross-correlation method without sacrificing the performances of the estimators. The matched filter interpolation method in paper B has improved the performance of the estimator when the signal to noise is low, as is typically the case for the received blood signal.

In addition, a novel velocity estimator for extending the traditional autocorrelation approach is described in Paper A in this thesis. The new method can estimate velocities above the Nyquist limit and its performance is similar to the RF cross-correlation method. It has similar estimation variance to the cross-correlation method and smaller estimation variance than the conventional autocorrelation method when applied to wideband cases. Moreover, it uses much less calculation.

A clutter filter is a kind of highpass filter which is used to remove the strong clutter signals from boundaries and slowly moving solid tissue. The other aim of this study is to investigate of

clutter filter. In order to achieve an acceptably high frame rate in CFI, only 4-16 pulses are available for analysis from a line of sight. Conventional highpass filtering methods are not suitable for application to such a short time period. The third part of this study is to investigate the clutter filter which is capable of eliminating the strong clutter component in a short sample segment (Paper C). The highpass filter may also remove the blood signal power which limits the low velocity estimation range. Due to its sampled nature, the frequency response feature of the wall filter is also repeated with the pulse repetition frequency (PRF), therefore, it also removes some of the signal power with high velocities. The last part of this study is to investigate the effects of the highpass filter on the estimation of high blood velocity (Paper D).

4. Introduction

4.1 Continuous wave Doppler and pulsed wave Doppler Measurement.

The principle and history of Doppler ultrasound

Blood flow characteristics are important for the diagnosing of vascular diseases. Clinical applications include detection and velocity estimation of blood flow in the great vessels; real-time flow mapping of the heart, peripheral vascular diagnosis and venous diagnosis.

The Doppler effect can be used to measure the blood velocity. The principle of this Doppler effect can be explained by the frequency shift of backscattered acoustic echoes from moving targets with respect to the frequency transmitted. By estimating the frequency shift from the received signal, the blood velocity of the moving target is obtained.

A continuous wave Doppler (CW) technique which used the Doppler effect to measure blood velocity was reported in 1957 [1]. Ten years later, a pulsed wave Doppler (PW) instrument was introduced [3] which is based on the phase-shift measurements of successive echoes. It is widely used at present, because it offers spatial resolution. In the seventies, multirange gated (MRG) pulsed Doppler instruments to measure real time blood velocity profiles in vessels and the heart was developed [4]. It is based on PW Doppler and the sample of the received signal at multiple ranges. In the late eighties, the instruments which display real time two-dimensional (2-D) color flow imaging (CFI) of flow profiles were developed. They are based on the multigated Doppler and the sweeping of the beam across the vessel. In the nineties, new instruments are being developed for high quality, real-time and high frame rate imaging of the blood flow patterns.

CW Doppler Measurement

In this method, an ultrasound beam is continuously transmitted into the tissue with one transducer, while the back-scattered signal is continuously received by another transducer. Thus, all the moving targets within the overlap of beams from the receiving and transmitting transducers are observed. Initially, the received RF Doppler signal is demodulated into the baseband, where the Doppler shift is estimated from the baseband signal. Then, the velocity is obtained using the Doppler equation:

$$f_d = 2f_0\frac{v\cos\theta}{c} \tag{1}$$

where f_d is the Doppler shift, f_0 is the center frequency of transmitted ultrasound, c is ultrasound wave velocity, v is velocity of the scatterer; θ is the angle between the velocity direction and the ultrasound beam.

The basic elements of a CW instrument are illustrated in Figure 1.

The advantage of the CW Doppler method is that it does not limit the maximum velocity which can be measured. The disadvantage of this technique is that it has no range resolution.

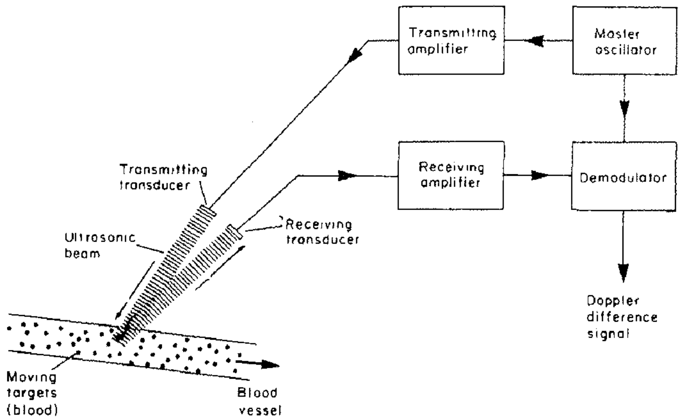

Figure 1 The continuous wave measurement [2]

PW Doppler Measurement

In PW Doppler, sequential short ultrasound pulses with center frequency f_0 and duration T_2 are transmitted into a vessel or the heart at a fixed *pulse repetition frequency* (*PRF*). Return signals are received sequentially after a certain delay following the pulse transmission. The transmitted pulses are phase coherent with respect to an internal reference oscillator. The received signal sequence can be regarded as samples of the continuous Doppler signal as shown in Figure 2. Due to the sampling, it follows the sampling theory that the continuous Doppler signal can be reconstructed without errors by lowpass filtering of the sampled sequence, provided that the sampling rate, or *PRF* here, is larger than twice the maximum frequency of the continuous Doppler signal.

Due to the sampled nature of PW Doppler, the Doppler shift is periodic. Hence the maximum Doppler shift which can be measured is limited. The maximum Doppler shift corresponds to *PRF*/2. Any Doppler shifts which exceed *PRF*/2 will be aliased to the frequency range [-*PRF*/2, *PRF*/2]. This leads to velocity aliasing. The maximum velocity which can be measured is obtained from (1) i.e.:

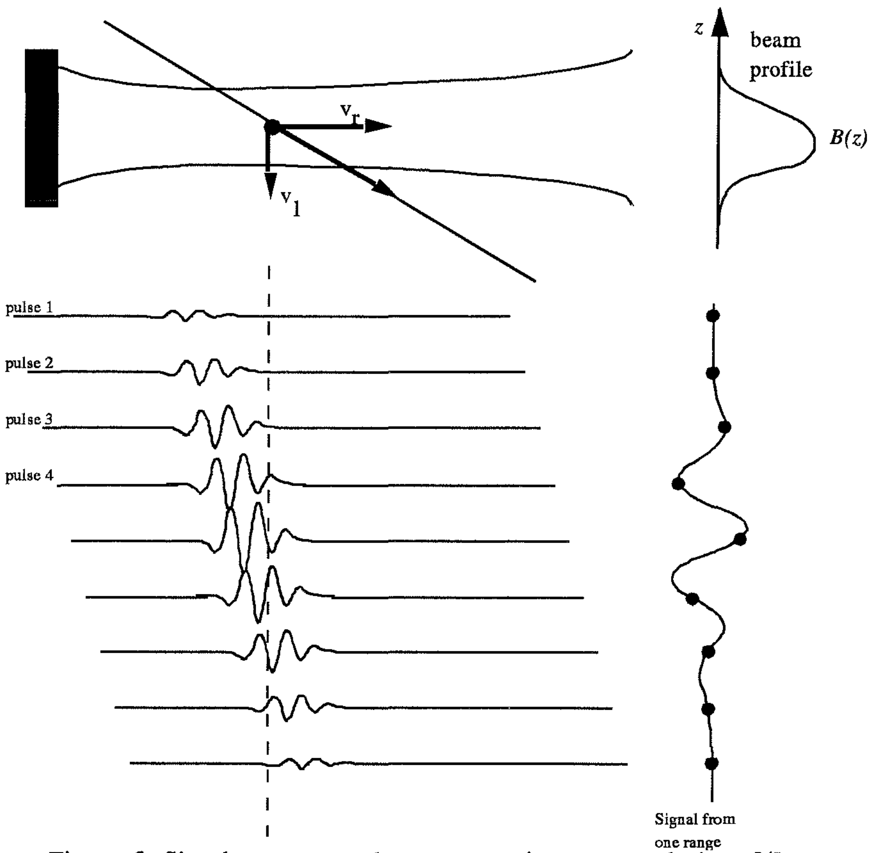

Figure 2 Signal scatterer echo response in range and time [4]. Attenuation is due to transducer beam profile.

$$v_{Ny} = \frac{c \times PRF}{4 f_0 \cos\theta} \tag{2}$$

This velocity is called the Nyquist limit, which can be increased by raising *PRF* and decreasing center frequency f_0. High pulse repetitions frequencies can induce range ambiguity because there may be more than one pulse propagating in the vessel at the same time. Decreasing f_0 may degrade the signal to noise ratio (*SNR*) because the scattered power of ultrasound from blood is proportional to f_0^4 [4].

The width of the range cell is the same as the beam width, and the length is determined by the length of the transmitted pulse. The same transducer can be used for both transmission and reception.

Range and Velocity Ambiguity in the PW Doppler Measurement

When there are several pulses propagating in the tissue at the same time, it is uncertain from which pulse the received echo originates. Therefore, the pulse travelling time t is uncertain, and the range $R=ct/2$ is ambiguous. To avoid range ambiguity, only one pulse is allowed to propagate in the tissue at one time. The second pulse can be emitted only after the first one is received. This leads to a low pulse repetition frequency. The maximum range that can be measured unambiguously is $R=cT/2$. Combining (2), the product of velocity and range that can unambiguously be measured is:

$$v_{Ny} \times R = \frac{c^2}{8 f_0 \cos\theta}$$

It is constant when the center frequency is unchanged. Thus, by increasing the measurable velocity, the detectable range has to be sacrificed, provided that we use some unaliasing velocity algorithms as those described in section **4.3**. For the same reason, the maximum interrogated range can be increased by scarifying the maximum measurable velocity. In PW Doppler the maximum velocity that can be measured unambiguously is inversely proportional to the pulse repetition period T (as shown in Figure 3) and the maximum range which can be interrogated unambiguously is proportional to T. Thus, the choice of PRF produces a tradeoff between the range and velocity ambiguity. The velocity resolution is inversely proportional to the observation time T_1 and the range resolution is inversely proportional to the width of the pulse T_2. Note that the narrower pulse reduces the signal to noise ratio (SNR) for equal mean power. With CW Doppler, the velocity resolution is high due to a long observation time T_1. It does not suffer from velocity ambiguity but it has no range resolution.

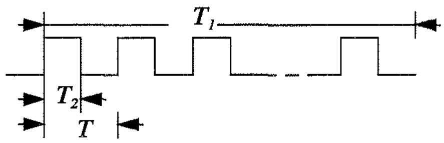

Figure 3 The envelope of the transmitted signal in PW Doppler.

Blood Signal Content from One Pulse

The received return pulse, $p_0(t)$, from a scatterer is determined by the transmit pulse, $f(t)$, the transducer impulse responses [4] and [5]. It can be written as:

$$p_0(t) = f(t) \otimes h_{tt}(t) \otimes h_{rt}(t) \qquad (3)$$

where $h_{tt}(t)$ and $h_{rt}(t)$ are the impulse responses of transmitted and received transducer, respectively. When $f(t)$ is a short pulse, $p_0(t)$ will exhibit ringing since the transducer has a finite bandwidth. The envelope of the received signal, $p_0(t)$, can be described as the rapid rise and more gradual fall of an actual pulse, but an approximation using a Gaussian function is usually adopted in the model for an ultrasound received pulse. Assuming the scatterer in the illuminated region is $n(t, z)$ where $t=2r/c$, and where the beam profile $B(z)$ is taken into account (as shown in Figure 2), the received signal from one pulse is:

$$p(t) = \int_z p_0(t)B(z)n(t, z)dz. \tag{4}$$

The Doppler Signal Spectrum in Each Range

The Doppler signal from a particular range is displayed in Figure 2. The spectrum of the Doppler signal from one range is periodic because of its sampled nature. Besides the blood signal, the received Doppler signal from one range also includes electronic white noise and signal from boundaries and slow moving tissue which is commonly referred to as clutter or wall signal. This clutter signal is usually 60 to 100dB stronger than blood signal. An illustration of the spectrum content of the received signal in one range is in Figure 4. Due to the effect of the scatterer entering and leaving the sampled volume, and the effect of the beam profile, the spectrum is broadened. The effects which cause the spectrum broaden is called transit time effect.

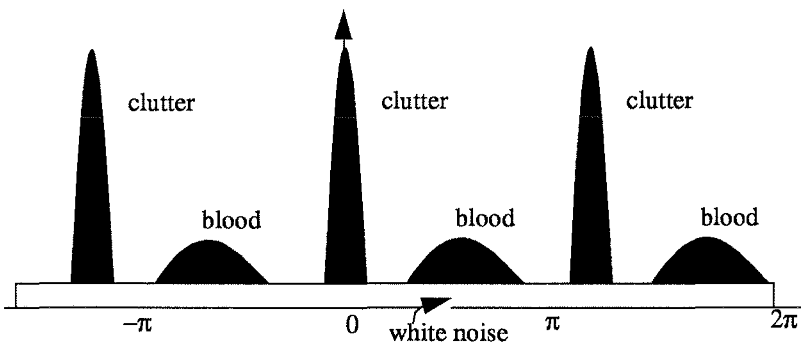

Figure 4 An illustration of typical power spectrum of PW Doppler signal from one sampled range.

The power spectral display in the PW Doppler system

The B-mode image and the power spectrum of the blood signal from the sampled range as shown in Figure 5 are of clinic importance, and they have been widely used today. A B-mode image is used for locating the region of interrogation. The power spectrum is used for obtaining the velocity distribution in the vessel over time. The power spectral display in Figure 5 is also called as a sonogram [31]. Frequency, which is proportional to the velocity, is display as the ordinate. Power density is displayed as the brightness. Some parameters such as peak systolic velocity, minimum diastolic velocity and pulsatility index and volume flow etc. can be measured or calculated from this spectral display and B-mode image. These parameters are important for doctors to diagnose diseases.

The frequency in the sonogram can be obtained by means of spectrum analysis. The blood velocity is pulsatile due to the heartbeats. This means that we can only use a short time signal for spectral analysis. Hence, the estimated spectrum has large variance. This is the reason that the spectrum in Figure 5 has a noise appearance.

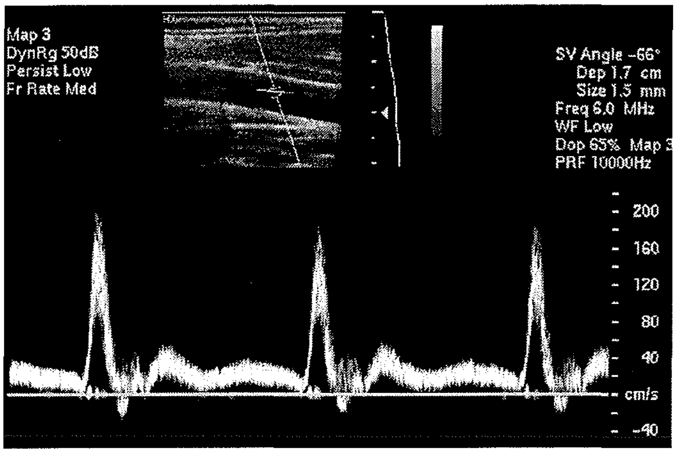

Figure 5 B-mode image (upper) and spectral density display (bottom) from carotid artery.

4.2 Color Flow Imaging System

In the seventies, the multi-range gated pulsed Doppler instruments were developed. Using this approach, the received signal is sampled at multiple ranges, and the signals from each range are processed in parallel. The velocities along the ultrasound beam are measured simultaneously. However, a compact serial signal processing can be used in which each range is processed by the same circuit.

Using the multigated Doppler and sweeping the beam across the vessel, a two-dimensional velocity image is obtained. In CFI, the parameters of the signal power, blood velocity and its variance are combined and presented as a coded color. The color flow image provides an excellent spatial visualization of flow pattern.

Most current scanners are based on the Doppler technique, which extracts the parameters from the complex Doppler signal. The most significant parts of these systems for CFI are plotted in Figure 6. Although the parameters can also be estimated directly from the RF signal, commercial scanners employing this RF processing are still in the development stage [18].

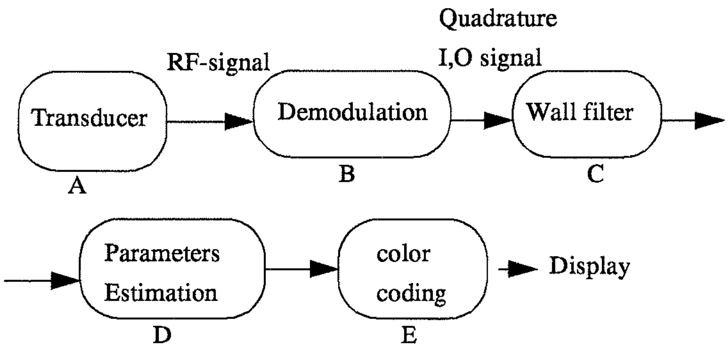

Figure 6 Block diagram of color flow imaging system

The function of each part in Figure 6 is described as follows:

A: A transducer is an energy conversion device. A transmitting transducer converts electrical energy to acoustic energy, while a receiving transducer converts acoustic energy to electrical energy. The most commonly used materials for medical ultrasound transducer are piezoelectric ceramics. The vast majority of transducers are made of one or more piezoelectric elements. The transducer is a key component in the ultrasound system. Electronic beam forming is used to obtain narrow beams with very high sensitivity and low side-lobe levels. Electronically controlled focussing can be obtained by building a transducer out of an array of small elements. The most commonly used array types are: the annular array, the phased array, the linear array and the curved linear array [4]. The annular array is made up of several concentric piezoelectric rings with some curvature for focusing. An adjustable focus can be obtained by putting a spherical delay on the signal from different elements. The advantage of the annular array is that the focus is symmetric. The disadvantage is that it needs mechanical scanning to steer the beam direction. Phased array transducers are composed of a number of elements. By varying the delay for transmission on the echo of the elements, the beam is steered within a sector. This array normally has a small aperture (e.g. 15mm) [14]. A linear array typically has a large aperture (about 40mm) and more elements, which are used to form beams normal to the surface of the transducer. A curved linear array is obtained by curving the linear array slightly which gives a wider image field. Due to the small footprints of the annular array and the phased array, they can image the heart between the ribs. Thus, those arrays are normally used in cardiological application [9]. It is easier to obtain high sensitivity for the Doppler and color flow imaging with the annular array due to the larger and fewer elements. It is also easy to make a high frequency transducer for using an annular array geometry which have special applications in neonatal medicine, endocavity imaging and for guidance of surgical procedures. The phased array with multiple beam can provide very high frame rates for 2-D imaging. Linear array and curve linear array are widely used in abdominal and peripheral. Due to the availability of high-speed analog to digital (A/D) converters and improvements in VLSI technology, digital beamforming has become feasible. Multiple channels (e.g. 256 channels) for digital beamforming have been implemented in the present generation of scanners.

B: Demodulation is a process which consists conversion of the received RF signal into the baseband. In order to detect the sign of the Doppler shift, quadrature demodulation is used (Figure 7)

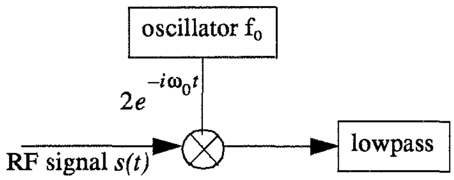

Figure 7 An illustration of quadrature demodulation.

C: A Wall Filter is used to remove the signals from tissue and vessel walls. In CW, an analog highpass filter with sufficiently high stop-band damping and narrow transition band can be used for this purpose [4]. In PW Doppler, due to long measurement time, either a combined highpass and lowpass analog filter or digital highpass filter can surpress the clutter signal [4]. In MGR and CFI with phased array probes, only 4-16 pluses in one beam are available for analysis in order to get a high frame rate. Thus, only a digital filter can be used. In this case, the conventional FIR digital filter is not suitable since the filter order that can be used becomes severely limited and a significant number of samples must thrown away due to the transient effect. IIR filters usually exhibit a long transient response. Thus, special precautions should be taken in order to initialize filters and reduce the transient time as in [10] and [11]. The regression filters described in [12] and [13] have proved to be a better solution in this case. The idea is to make a curve fit to the slowly varying wall signal, and to remove that curve from the received signal; hence separating blood signal from clutter. More details and experimental results are given in Paper C.

D: Parameter Estimation includes velocity, bandwidth and power estimation in CFI. The signal power, mean frequency and square bandwidth can be defined respectively as the zero, first and second order central moments of the power spectrum $G(\omega)$:

$$\text{Signal power: } p = \int_{-\pi}^{\pi} G(\omega)d\omega \tag{5}$$

$$\text{Mean frequency: } \varpi = \frac{1}{P}\int_{-\pi}^{\pi} \omega G(\omega)d\omega \tag{6}$$

$$\text{Bandwidth: } B = \sqrt{\frac{1}{P}\int_{-\pi}^{\pi} (\omega - \varpi)^2 G(\omega)d\omega} \tag{7}$$

The conventional autocorrelation method presented in [14] and [15] is widely used for velocity estimation in the scanner because it is simple and suitable for real time implementation. Since the correlation function $R(n)$ and power spectrum $G(\omega)$ are a Fourier transform pair, the parameters defined by the power spectrum can also be estimated by the autocorrelation coefficients:

$$\text{Signal power: } P = R(0) \tag{8}$$

$$\text{Mean frequency:} \varpi = angle(R(1)) = \operatorname{atan}\left(\frac{Im(R(1))}{Re(R(1))}\right) \tag{9}$$

$$\text{Bandwidth:} B = \sqrt{2}\sqrt{1 - \frac{|R(1)|}{R(0)}} \tag{10}$$

However, the maximum velocity to be measured is limited in this method. Its estimation variance is proportional to the bandwidth of the transmitted signal. It has larger estimation variance when used in the wideband situations which corresponds to high spatial resolution. Some other methods which can solve the velocity ambiguity are discussed in section 4.3.

E: Color Coding refers to the process of representing the parameter estimation results by an assigned color. Some color assignment schemes are describes in [5]. The mean frequency and bandwidth are included in the normalized autocorrelation coefficient which is:

$$\rho(1) = \frac{R(1)}{R(0)} = (1 - B^2)e^{j\varpi} \tag{11}$$

The color is assigned in the complex plane $\rho(1)$. In the most commonly used color assignment scheme, the sign of the frequency is represented by color hue; red is used for positive frequencies, and blue for negative frequencies. The magnitude of the frequency is represented by color intensity. Increasing bandwidth is indicated by including green with red or blue. The power is usually used to discriminate between the region with flow and the region without flow. Using the power and bandwidth parameters, the laminar flow and turbulent flow can be discriminated.

4.3. Algorithms to solve the velocity aliasing in CFM

As mentioned above, the maximum velocity that can be measured is limited in the PW system, due to its sampled nature. The maximum velocity will be slightly higher when using higher *PRF*, but it sacrifices the range that need to be interrogated. Here, some methods that can solve the velocity aliasing in PW system are introduced. By means of these methods, the *PRF* does not have to be increased. Thus, the maximum range that can be interrogated remains unchanged.

We can divide the methods into two types. In one type, the system is different from the conventional PW system. This type includes dual frequency Doppler. In the other type, the system is completely the same as the conventional one and the received blood signal is also the same as in the conventional one. Using some different processing methods such as the RF crosscorrelation method, 2-D Fourier transform, wideband maximum likelihood velocity estimator and butterfly search method, the unambiguous velocity is estimated.

Dual Frequency Doppler

This system was introduced in [16]. In this PW system, two narrow-band pulses with carrier frequencies f_1 and f_2 are transmitted simultaneously. The received signals are fed into two parallel conventional PW systems. The Doppler shifts f_{d1} and f_{d2} are obtained by the conventional autocorrelation method. By combining of the Nyquist limits v_{NY1} and v_{NY2}, and the Doppler shift f_{d1} and f_{d2}, the unaliased velocity is obtained. The new maximum velocity v_{NY}. becomes:

$$v_{NY} = \frac{c}{2(f_2 - f_1)\cos\theta}\frac{PRF}{2} = \frac{f_1}{f_2 - f_1}v_{NY1} \tag{12}$$

The maximum velocity limit is extended by a factor of $\frac{f_1}{f_2 - f_1}$.

An illustration of how to obtain the unaliasing velocity is in Figure 8. A block diagram of this PW system is in Figure 9. This system has been implemented by Kontron Instruments, Basel, Switzerland [16].

The performance of this method will be degraded when one of the Doppler signals is removed by the wall filter or when the spectrum is broad.

RF Crosscorrelation Method

In PW Doppler system, the conventional autocorrelation estimator is based on phase shift estimation from pulse to pulse. One of its drawbacks is velocity ambiguity. However, when we observe the received RF signal in Figure 10, it is seen that the received signal from pulse to

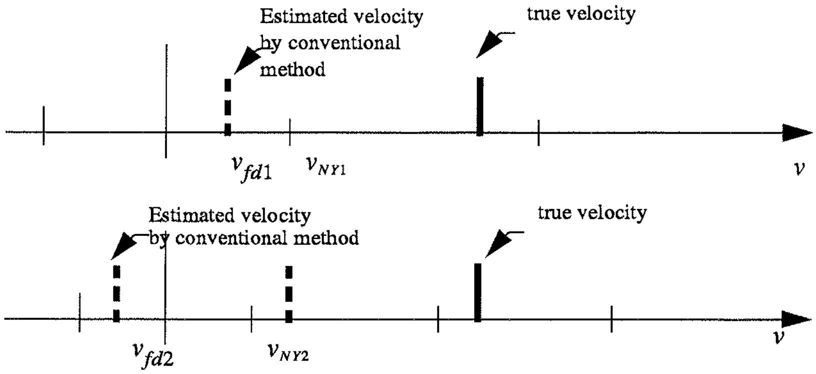

Figure 8 An illustration of unaliasing velocity estimate from dual frequency Doppler.

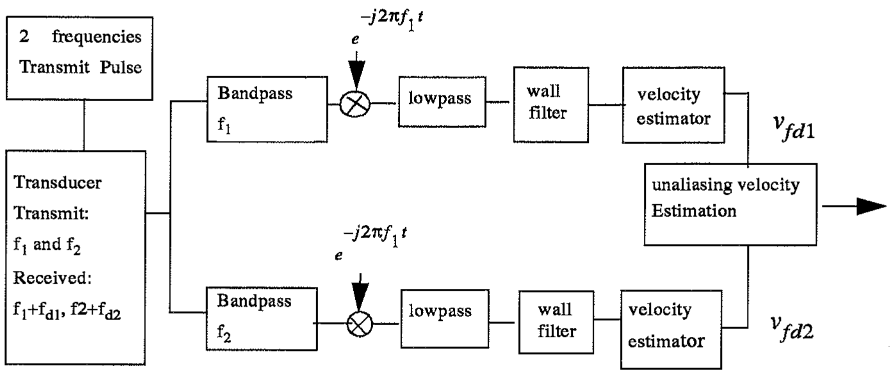

Figure 9 Block diagram for dual frequency Doppler system

pulse is a time delayed version due to the scatterer movement. The time delay τ_v is proportional to the velocity of the scatterer which is:

$$\tau_v = \frac{2Tv\cos\theta}{c} \tag{13}$$

where T is pulse repetition period, v is the blood velocity, c is the ultrasound speed, θ is the angle between the ultrasound beam and blood vessel.

Ideally, by estimating the time delay instead of the phase shift, the velocity can be estimated unambiguously.

For the 2-D data shown in Figure 10, the conventional autocorrelation method estimates the phase shift from pulse to pulse in the same depth (window A). When the blood velocity is high, the phase change is large from pulse to pulse. Velocity aliasing may occur. One solution

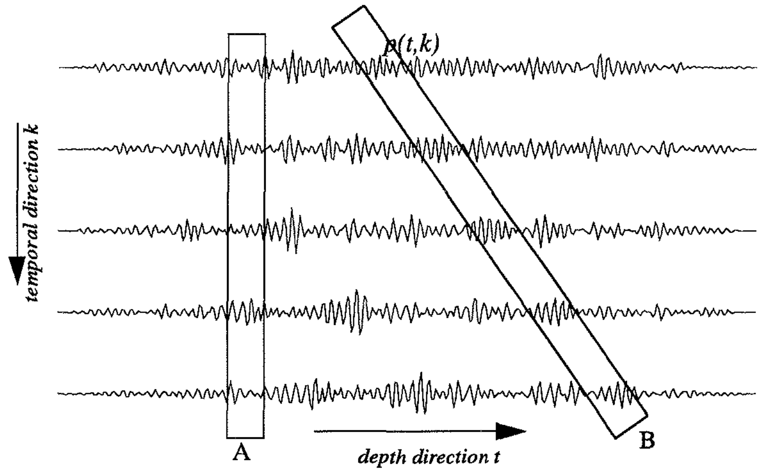

Figure 10 Illustration of 2-D blood signal

to this problem is to use the data in a sloped rectangular window (window B). When the slope is tuned to the time delay τ_v, the phase change for the data from pulse to pulse is minimized, and the mean value of signal power in this window is maximized. Both the 2-D Fourier transform and the maximum likelihood velocity estimator are based on this principle. Alternatively, the signal variance in this sloped window can be set as an objective to minimize. The butterfly search technique uses this concept to get the time delay information. Moreover, the signal in this sloped window is the most highly correlated. The RF crosscorrelation method utilizes this information.

The RF crosscorrelation method was reported in [17] and [18]. In this method, the time delay is estimated by the correlation function. It is calculated by searching for the maximum correlation coefficient between the successive received echoes. If $p(t, k)$ is the k-th received echo, its 2-D correlation function from pulse to pulse is denoted as $R(\tau, m)$.This correlation function has maximum magnitude at the time delay τ_v, i.e, $R(\tau_v, 1) = max_\tau R(\tau, 1)$, where m=1 (Figure 11). This method can estimate high velocities and it has smaller estimation variance in the wideband case. However, its processing load is high. The load is mainly due to the calculation the RF crosscorrelation function. Decimating the sampling rate of the RF signal can reduce the processing load because the data block becomes sparse and the computation for the crosscorrelation function is reduced. However, interpolation has to be performed on the correlation function to estimate the time delay accurately. Some interpolation methods are proposed in Paper B.

2-D Fourier Transform:

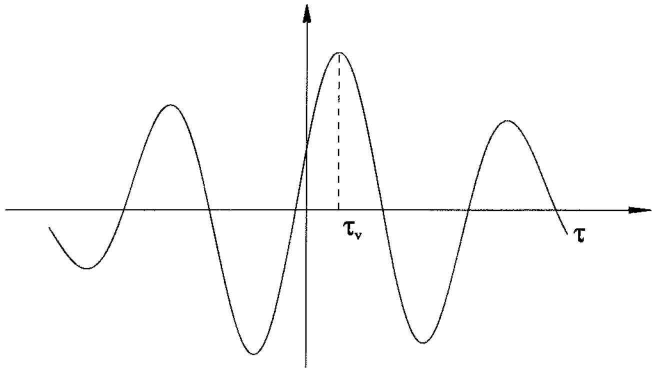

Figure 11 RF correlation function $R(\tau, 1)$

This method was reported in [19] and [20]. The time delay τ_v is found by integrating the data along the rectangular window (window B) with a slope τ:

$$B(\tau) = \int_t \left| \sum_k p(t - k\tau, k) \right|^2 dt \qquad (14)$$

When $\tau = \tau_v$, the integration $B(\tau)$ has the maximum value. In [19], it was shown that an integration along the rectangular window with slope τ in depth/time plane is equivalent to an integration of the magnitude squared of the 2-D Fourier plane along the straight line with slope τ. Thus, this method is called 2-D processing of pulsed Doppler method in [19] and 2-D Fourier transform in [20].

Wideband Maximum Likelihood Velocity Estimator (MLE)

This estimator was developed by Ferrara and Algazi [21] and [22]. It utilizes both the shift in time and the shift in frequency to estimate velocity. An implementation of the likelihood for a point target is shown in Figure 12.

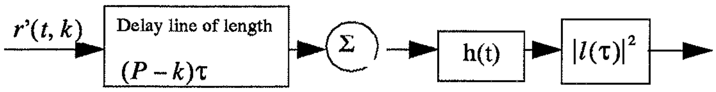

Figure 12 Implementation of the wideband point MLE where signal is matched to $h(t) = s^*(t)\exp\left(j\frac{2\omega_0}{c}vt\right)$ and l is likelihood function

When we ignore the frequency shift and assume the matched filter is a rectangular function, this method is similar to the 2-D Fourier transform method. Because it uses both the frequency and time shift information, the estimation variance is less than for other methods [21]. This estimator has a considerably higher complexity which results in more expensive hardware and longer processing time.

Butterfly Search Technique

This technique was presented in [23]. It utilizes the fact that the variance is minimum to the samples in the line with slope τ_v or in the butterfly line τ_v. This method can be used with either RF received signal or the quadrature signal. Under some assumptions, the butterfly method has the same form as the wideband maximum likelihood velocity estimator.

The key to solving the velocity ambiguity is to use both the phase and the amplitude information. The conventional autocorrelation method utilizes only the phase information, hence, it has velocity aliasing when the velocity exceeds the Nyquist limit. Based on the conventional autocorrelation method, a new extended autocorrelation method which uses both the phase and amplitude of 2-D correlation function is presented in Paper A. It is shown that this new method has similar performance to the crosscorrelation method, but with more computational efficiency than the crosscorrelation method. This new method is ready to be implemented on a commercial system.

4.4 Other Activities and Directions in Doppler Signal Processing

Recently, a nonlinear filter method has been used to differentiate the blood signal from the clutter signal. This method is based on ultrasound contrast agents which are suspensions of gas microbubbles. Due to nonlinear backscattering from these microbubbles, harmonics are generated [24]. If a bandpass filter in a receiver is tuned to the second harmonic, only the blood signal and white noise will be received. The wall signal will be suppressed effectively. This method is very useful when the blood flow velocity is comparable to that of the surrounding tissue and vessel wall. Commercial scanners with harmonic Doppler imaging is currently available. These scanners are transmit at one frequency and receive at its second harmonic. For example, ultrasound could be transmitted at 3-4 *MHz* and echoes detected at 6-8*MHz*.

Traditional Doppler techniques can only estimate the blood flow velocity along axis of the transducer beam. However, most vessels exhibit curvature and branching. Considerable efforts have been devoted to overcoming the angle dependence problem [25] and [26]. The methods for measuring more than one component of blood velocity may be broadly grouped into two categories: one uses multiple conventional Doppler transducers, while the other uses image sequences. Using the first group methods, two or three parallel beams are generated.

The axis velocity components are calculated along each beam the same as the traditional technique. The lateral velocity components are calculated by tracking the signal from beam to beam. With a triple-beam transducer, 3-D blood flow velocity can be measured. The second group methods are based on tracking the speckle pattern in a sequence of successive images [27]. This tracking can be accomplished with a block-matching search algorithm. In this method, we select a target block in the first image and compare blocks within the second frame to find out where the scatterers in the target block have moved to. The similarity between two blocks can be measured with a 2-D correlation coefficient, a sum of absolute difference or by mean square error.

The improvements to spectral estimation techniques for CFI is also a significant area. The maximum blood velocity is an important parameter for diagnosis of heart diseases. The velocity estimators discussed above give only the mean velocity and velocity spread. The spectrum analysis gives the entire velocity distribution in the sample volume and presents accurate quantitative blood velocity information [28]. Spectrum analysis based on the modified periodogram method and parameter spectrum estimation methods have been commonly used [6]. Because the Doppler signal is a moving average process [6], computational efficient spectrum estimators based on Fourier transforms are widely used in clinical practice. Such methods have spectrum aliasing when the blood velocity exceeds the Nyquist velocity. The velocity matched spectrum [28] technique is capable of suppressing the velocity ambiguity. In [16], linear interpolation of the complex Doppler signal is used to reconstruct aliased Doppler spectra.

The center frequency for Doppler measurement is typically between 2MHz and 10MHz range. The choice of frequency is a compromise between penetration and range resolution. However, Doppler ultrasound in this frequency range is unable to detect the low blood velocities in small vessels or in the microcirculation. Estimation of low blood velocity with high frequency PW ultrasound ($38MHz$) is reported in [29] and it is used for mapping blood velocities in small regions near the transducer. A high frequency ($40MHz$) CW Doppler ultrasound system for detecting blood flow in the microcirculation is reported in [30].

4.5 Flow Images from Water-tank Experiments

In this section, we give an experimental example to show the procedures of the signal processing in CFI. It is seen that we are successful in removing the clutter and extracting the parameters of power, bandwidth and velocity. Specially, we are able to estimate high velocities without velocity ambiguity. A water tank model was set up in Appendix A. The illustration of jet stream is featured in Figure 13. The Nyquist limit in this experiment is

0.8867m/s. The received signal is demodulated to baseband.

Figure 14:

(a): Logarithm power grey image of jet stream. The signal from boundaries is too strong to see the jet steam from this image.

(b): Logarithm power grey image after the wall filter (Paper D). The stationary signals from boundaries have been removed and the jet steam can be seen clearly from this image.

(c): Bandwidth grey image of the jet stream. The stream near the hole has high velocity which corresponds to high bandwidth due to the transit time effect.

(d): Velocity grey image of the jet stream. The velocities were estimated by the conventional autocorrelation method. The velocity aliasing has been observed in this example. The velocities which exceed the Nyquist limit 0.8867m/s cannot be estimated correctly.

(e): Velocity grey image of the jet stream using the extended autocorrelation method described in Paper A. This method can resolve the velocity ambiguity. The velocities which exceed the Nuquist limit have been estimated correctly. However, there are still some velocity estimation errors in the image. This kind error is called as "global error". It is caused by the variance of the estimated correlation function. Factors which affect the variance of the estimated correlation function error such as the size of the 2-D data window, the bandwidth of the received signal, the used correlation estimator and the signal to noise ratio are discussed in Paper A. A 2-D tracking method can reduce this kind of global error as described in paper A.

(f): Velocity grey image of the jet stream using the extended autocorrelation method and a 2-D tracking (Paper A). In order to reduce the global errors, a 2-D tracking method can be used. It is based on the knowledge from flow physics that the blood velocity is continuous both in depth and temporal directions.

(g): Color velocity image of the jet stream using the autocorrelation method. The red indicates positive velocities which are defined by the flow moving toward the transducer. The blue indicates the negative velocities which means the flow is moving away from transducer.

(h): Color velocity image of the jet stream using the extended autocorrelation method.

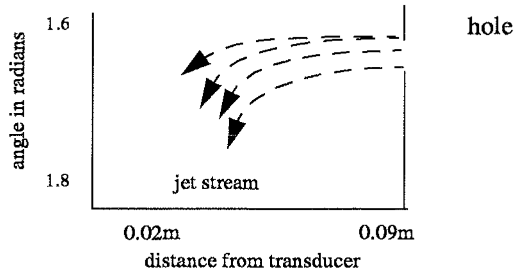

Figure 13 An illustration of jet stream

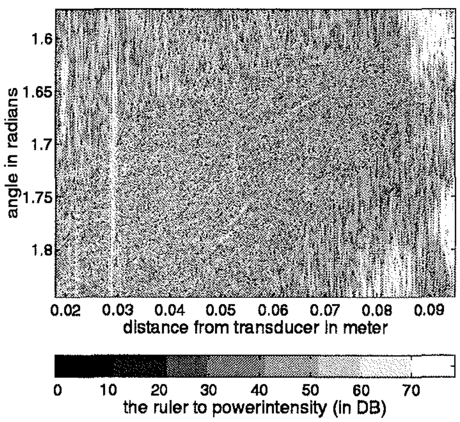

(a) Raw power grey image (in dB) of jet stream (without highpass filter)

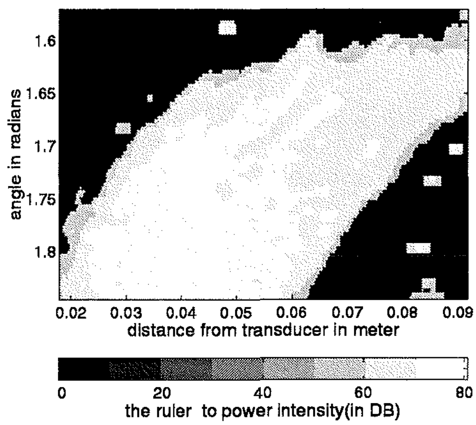

(b) Power grey image (in dB) of jet stream after highpass filtering

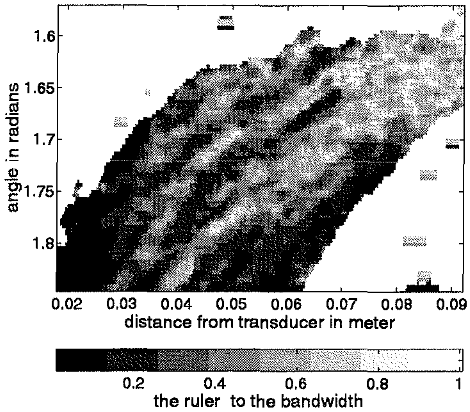

(c) Bandwidth grey image of jet stream.

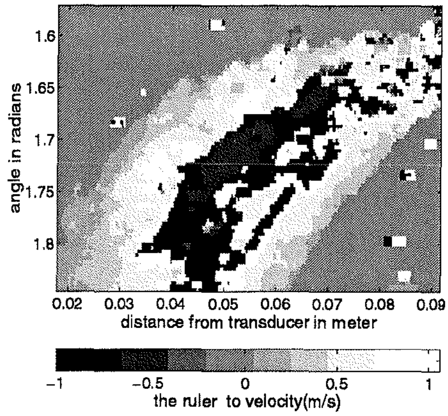

(d) Velocity grey image of the jet stream using the autocorrelation method.

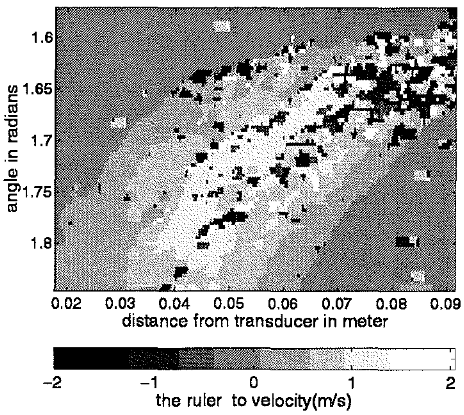

(e) Velocity grey image of the jet stream using the extended autocorrelation method.

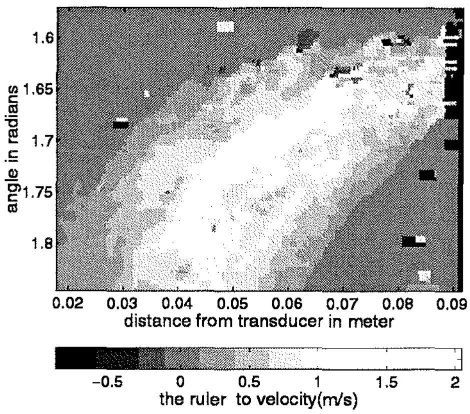

(f) Velocity grey image of the jet stream using the extended autocorrelation method and 2-D tracking

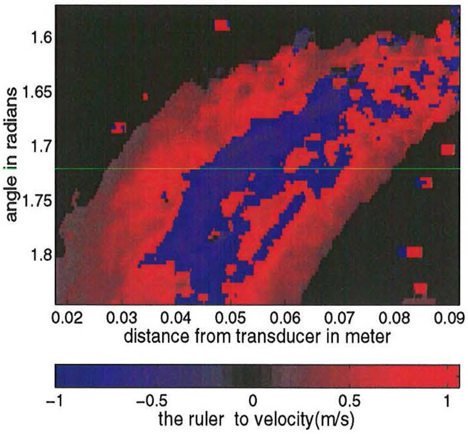

(g) Color velocity image of the jet stream using the autocorrelation method.

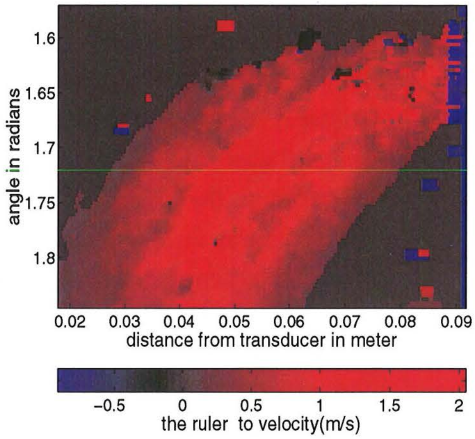

(h) Color velocity image of the jet stream using the extended autocorrelation method.

Figure14 Experimental flow images of jet stream from water-tank. The Nyquist limit in this experiment is 0.8867m/s.

4.6 An overview of the papers in this thesis

Two issues were discussed in this work. One is unaliasing velocity estimators (Paper A and Paper B). The other is clutter filter (Paper C and Paper D). An overview of these papers are presented in this section.

Paper A: The autocorrelation method and the crosscorrelation method are two major techniques used in the color flow imaging. The autocorrelation method is of computational simplicity, but it has some drawbacks such as large estimation variance and the velocity ambiguity. The crosscorrelation method is superior to the autocorrelation method in the aspects of the estimation variance and the velocity ambiguity, but it requires longer processing time. In this paper, a new extended autocorrelation method is presented. It is shown that the EAM has similar performance to the crosscorrelation method. Both of them have smaller estimation variance than the AM and have the ability to estimate velocities beyond the Nyquist limit. However the EAM is more computationally efficient than the CCM.

Paper B: The cross correlation method (CCM) for blood flow velocity measurement is based on time delay estimation of the echoes from pulse-to-pulse. The time delay is estimated by searching for the peak location of the correlation function. The sampling frequency of the received signal is usually kept as low as possible in order to reduce computational complexity, and the peak in the correlation function is found by interpolating the correlation function. The parabolic-fit interpolation method introduces bias at low sampling rate to ultrasound center frequency ratio. In this study, four different methods are suggested to improve the estimation accuracy:

1. Parabolic interpolation with bias-compensation, derived from a theoretical signal model.
2. Parabolic interpolation combined with linear filter interpolation of the correlation function.
3. Parabolic interpolation to the correlation function of the complex signal envelope.
4. Matched filter interpolation applied to the correlation function.

Each of which is useful in reducing the required computation in the RF-signal cross-correlation method. The matched filter interpolation method has improved the performance of the estimator when the signal to noise is low, as is typically the case for the received blood signal.

Paper C: In pulsed wave Doppler ultrasonic measurements, a highpass wall filter is used to suppress the clutter signal prior to the blood velocity estimation. In order to achieve an acceptably high frame rate in CFI, only 4-16 pulses from each beam direction are available for analysis. The conventional highpass filters (IIR and FIR) have a settling time which must be removed prior to the velocity estimation. However, this reduces velocity resolution. In order to reduce the settling time, only low order FIR filters or IIR filters with special initialization can be used. In addition, a regression filter was proposed [3]. In this work, the FIR clutter filter and regression clutter filter have been evaluated using experimental data from the subclavian artery and the mitral region of heart. The results show that when the number of segments is short (less than 16), the regression filter gives better results than the FIR filter. When the number of segments is increased to 30, no significant difference exists between the FIR filter and the regression filter.

Paper D: In pulsed wave Doppler ultrasonic measurements, a highpass clutter filter is used to remove the clutter signal prior to the blood velocity estimation. For high velocity measurements, the clutter filter creates dead zones where the Doppler frequency equals multiples of the pulse repetition frequency. In this work, the effect of the wall filter has been studied for two different blood velocity estimators; the crosscorrelation method and the extended autocorrelation method. When the pulse bandwidth is sufficiently high, the Doppler signal bandwidth will exceed the wall filter cut-off frequency due to the transit-time effect, and the dead zones are partially removed. However, the chance of velocity aliasing is increased in these zones due to the filtering, both for the CCM and EAM method.

References

[1] S. Satomura, "Ultrasonic Doppler Method for The Inspection of Cardiac Functions," *J. Acost. Soc. Am.*, vol. 29, pp.1181-1185, 1957.

[2] P. Atkinson and J. P. Woodcock, "Doppler Ultrasound and its use in Clinical Measurement," *Academic Press,* 1982.

[3] D. W. Baker and D. W. Watkins: "A Phase Coherent Pulse Doppler System for Cardiovascular Measurements," *Proc. 20th Ann. Conf. on Eng. in Med. and Biol.*, vol, 1967.

[4] Bjφrn A. J. Angelsen, "Waves, Signals And Signal Processing In Medical Ultrasonics," *Textbooks*, Trondheim, Norway, April, 1996.

[5] Hans Torp, "Signal Processing in Real-Time, Two-Dimensional Doppler Color Flow Mapping," *Dr., Techn. Dissertation*, the Norwegian University of Science & Technology. 1990

[6] Kjell Kristoffersen, "On the Processing of Doppler Signals in Ultrasonic Blood Velocity Measurements," *Dr., Techn. Dissertation,* the Norwegian University of Science & Technology, 1985.

[7] Jen U. Quistgaard, "Signal Acquisition and Processing in Medical Diagnostic Ultrasound," *IEEE Signal Processing Magazine,* vol.14, No.1. January, 1997.

[8] Charles E. Cook and Marvin Bernfeld, "Radar Signals--An Introduction to Theory and Application," Academic Press, New York, London, 1967.

[9] Bjφrn A. J. Angelsen, Hans Torp, Sverre Holm, Kjell Kristoffersen and T.A. Whittingham, "Review Paper: Which Transducer Array is Best?," *European Journal of Ultrasound* 2. pp.151-164, 1995

[10] A. Kadi and T. Loupas, "On the Performance of Regression and Step-Initialized IIR Clutters for Color Doppler Systems in Diagnosing Medical Ultrasound," *IEEE Trans. On Ultrasound, Ferroelectrics, and Frequency Control,* Vol.42, no.5, pp.927-937, 1995.

[11] R. B. Peterson, L. E. Atlas and K. W. Beach, "A Comparison of IIR Initialization Techniques for Improved Color Doppler Wall Filter Performance," *IEEE Ultrasonics Symposium*, Seattle, WA, 1994.

[12] Hoeks, A. P. G., van de Vorst, J. J. W., Dabekaussen, A. Brands, P. J. and Reneman, R. S., "An Efficient Algorithm to Low Frequency Doppler Signals in Digital Doppler System," *Ultrasonic Imaging* 13, pp.135-144, 1991.

[13] H. Torp, "Clutter Rejection Filters in Color Flow Imaging: A Theoretical Approach," *IEEE Trans. On Ultrasound, Ferroelectrics, and Frequency Control,* Vol.44, no.2, March, 1997.

[14] Bjφrn. A. J. Angelsen, Kjell Kristoffersen, "Discrete Time Estimation of the Mean Doppler Frequency in Ultrasonic Blood Velocity Measurement," *IEEE Trans. on Biomedical Eng. vol. BME-30,* No.4, april, 1983.

[15] C. Kasai, K. Namekawa, A. Koyano, and R. Omoto, "Real-Time Two-Dimensional Blood Flow Imaging Using an Autocorrelation Technique," *IEEE Trans. Sonics Ultras., vol.SU-32,* pp 458-464, 1985.

[16] H. J. Nitzpon, J. C. Rajaonah, C. B. Burckhardt, B. Dousse, and J. J. Meister, "A New Pulse Wave Doppler Ultrasound System to Measure Blood Velocities Beyond the Nyquist Limit," *IEEE Transactions on UFFC.* Vol.42 No.2 March 1995.

[17] O. Bonnefous and Pesquė. "Time Domain Formulation of Pulse-Doppler Ultrasound and Blood Velocity Estimation by Cross-Correlation," *in Ultrasonic Imaging* 8. 1986.

[18] O. Bonnefous and Pesquė. and X. Bernard, "A New Velocity Estimator for Color Flow Mapping," *in Proc. IEEE Ultrason. Symp.,* pp.8185-860, 1986.

[19] W. T. Mayo and P. M. Embree, "Two Dimensional Processing of Pulsed Doppler Signal," *US. Patent* no. 4,930,513.

[20] L. S. Wilson, "Description of Broad-Band Pulsed Doppler Ultrasound Processing Using the Two-Dimensional Fourier Transform," *Ultrasonic Imaging* 13, 301-315, 1991.

[21] K. W. Ferrara and V. Ralph Algazi, "A New Wideband Spread Target Maximum Likelihood Estimator for Blood Velocity Estimation--Part I: Theory," *IEEE Trans.on Ultrasound, Ferroelectrics, and Frequency Control,*vol.38, NO.1.January, 1991.

[22] K. W. Ferrara and V. Ralph Algazi, "A New Wideband Spread Target Maximum Likelihood Estimator for Blood Flow Velocity Estimation -Part II: Evaluation of Estimators," *IEEE Trans. on Ultrasound, Ferroelectrics, and Frequency Control,*vol.38, NO.1. pp.17-26,1991.

[23] S. K. Alam and K. J. Parker, "The Butterfly Search Technique for Estimation of Blood Velocity," *Ultrasound in Med. & Biol.,*Vol 21, No.5, pp.657-670, 1995.

[24] P. N. Burns, "Harmonic Imaging and Doppler Using Microbubble Contrast Agents," *IEEE Ultrasonics Symposium,* Baltimore, MD, 1993.

[25] DY Fei, CT Fu, WH Brewer and KA Kraft "Angle Independent Doppler Color Imaging: Determination of Accuracy and A Method of Display," *Ultrasound in Med. & Biol.*, Vol 20, No.2, pp.147-155, 1994.

[26] I. A. Hein, "Multi-Directional Ultrasonic Blood Flow Measurement with A Triple-Beam Ultrasonic Lens," *IEEE Ultrasonics Symposium*, Baltimore, MD, 1993.

[27] L. S. Wilson and R. W. Gill, "Measurement of Two-Dimensional Blood Velocity Vectors by the Ultrasonic Speckle Projection Technique," *Ultrasonic imaging 15,* 286-303, 1993.

[28] H. Torp and K. Kristoffersen, "Velocity Matched Spectrum Analysis: A New Method for Suppressing Velocity Ambiguity in Pulsed-Wave Doppler," *Ultrasound in Med. & Bio.,* Vol. 21 No.7, pp937-944, 1995.

[29] K. W. Ferraral B. G. Zagar, J. B. Sokil-Melgar, R. H. Silverman, and I. M. Aslanidis, "Estimation of Blood Velocity with High Frequency Ultrasound," *IEEE Transactions on UFFC.* Vol.43 No.1 January, 1996.

[30] D. A. Christopher, P. N. Burns, J. Armstrong and S. F. Foster, "A High-Frequency Continuous-Wave Doppler Ultrasound System for the Detection of Blood Flow in the Microcirculation," *Ultrasound in Med. & Biol.,* Vol.22, No.9, pp.1191-1203, 1996.

[31] Jϕrgen Arendt Jensen, "Estimation of Blood Velocities Using Ultrasound-A Signal Processing Approach," *Cambridge University Press,* 1996.

Paper A

An Extended Autocorrelation Method for Estimation of Blood Velocity

Parts of this paper were published in: Xiaoming Lai, Hans Torp, Kjell Kristoffersen, "Extended Autocorrelation Method for Color Flow Imaging", *Proceedings of 15th International Congress on Acoustics,* Trondheim, Norway, pp.347-350, 1995. (In Appendix A), and in: H. Torp, X. M. Lai and K. Kristoffersen, "Comparison between Cross-Correlation and Auto-Correlation Technique in Color Flow Image", *Proceedings of IEEE International Ultrasonics Symposium, Baltimore, MD,* pp.1039-1042, 1993.

A large part (Except *D* in section *VI*) of this paper was published in: X. Lai, H. Torp and K. Kristoffersen, "An Extended Autocorrelation Method for Estimation of Blood Velocity", *IEEE Trans. on Ultrasound, Ferroelectrics, and Frequency Control,* Vol. 44, No. 6, Nov. 1997.

An Extended Autocorrelation Method for Estimation of Blood Velocity

Abstract

The conventional *autocorrelation method* (AM) [1] to estimate the blood velocity for *color flow imaging* (CFI) is based on the phase estimation of the autocorrelation function. In this paper, a new *extended autocorrelation method* (EAM) that use both phase and magnitude of the two dimensional (depth and temporal direction) autocorrelation function for estimating the blood velocity is presented. It is shown that the EAM has similar performance to the *crosscorrelation method* (CCM). Both of them have smaller estimation variance than the AM and have the ability to estimate velocities beyond the Nyquist velocity. However the EAM is more computationally efficient than the CCM. 2-D blood flow signals with rectilinear velocity including the transit time effect have also been simulated and the results are presented in this paper. For comparison, the EAM and the CCM have been applied to the simulated signals in which the flow velocities are up to 4 times the Nyquist velocity. The EAM has been further verified by experimental RF data from the subclavian artery.

I.Introduction

Doppler ultrasound is an important noninvasive technique for measuring blood velocity in order to diagnose cardiovascular diseases. The pulsed Doppler technique is widely used at present time because it also offers range resolution. With this method, sequential short ultrasound pulses are transmitted into the vessel or heart at a *pulse repetition frequency* (PRF). Returned signals are received sequentially after a certain delay following the pulse transmission. The blood velocity within selected ranges can be estimated from the received signal. Sweeping the beam across the vessel gives a complete measurement of a 2-D flow profile in the vessel which includes velocity and its variance. A color flow image is obtained by coding the velocities. The velocity variance has also been used to modulate the color in some display modes.

Today, two widely used velocity estimation methods are the Doppler technique AM and the time domain technique CCM. The AM technique was first developed for weather radar applications and applied to ultrasound blood velocity measurement later [1]. It is based on the phase estimation for successive pulses from the complex demodulated signal. Due to its computational simplicity, most ultrasound scanners for CFI use this method today. But the AM is regarded as a narrowband estimation method because it has small estimation variance when the bandwidth of the received signal is narrow. Its estimation variance increases greatly when the bandwidth of the received signal is wide. This leads to poor image quality. On the other hand, reduced bandwidth limits the range resolution, so there is a trade-off between velocity estimation variance and range resolution.

The sampled nature of the pulsed Doppler introduces a limit on the maximum velocity which can be measured. The maximum velocity is referred to as the Nyquist limit and is given by

$$v = \frac{c \times PRF}{4 f_0 \cos\theta} \tag{1}$$

where c is the sound velocity, f_0 is the transmitted center frequency, and θ is the angle between the ultrasound beam and the blood vessel. Velocities exceeding this Nyquist limit are often found in various jet flows in heart defects (valve stenoses and regurgitations, ventricular septal defect etc.).

The CCM is an alternative algorithm for blood velocity estimation [2] and [3]. The CCM is based on estimation of the time delays of the received RF echoes from the pulse-to-pulse cross correlation function. It is superior to the AM in some aspects, however its computation is considerable more time consuming. In practical applications, the received signal is sampled along the depth direction with a certain rate. Since the CCM is performed on the RF-signal, the minimum sampling rate is much higher than that in the baseband. In addition, the location of the maximum in the crosscorrelation function is not constrained to discrete increments and hence, the true location of the maximum has to be estimated by means of interpolation methods. The interpolation accuracy depends on the ratio of the sampling rate to the center frequency. In order to improve the estimation accuracy for low ratio of the sampling rate to the center frequency, some time consuming interpolation techniques have to be used. Besides the CCM, there are some other velocity estimation techniques such as the 2-D Fourier transform method [4] and the maximum likelihood estimator [5] and [6] which are superior to the AM, but the computation requirements are higher. These techniques will not be discussed further in this work.

In this paper, the EAM which is developed from the AM is presented and it is compared to the CCM. This paper is organized as follows: In section II, a 2-D correlation function model based on [9] is introduced. From this 2-D correlation function model, a simulation model for 2-D blood signal is obtained. In section III, the EAM technique is described and a theoretical comparison between EAM and CCM is given. In section IV, the EAM is analyzed by simulation. In section V, the EAM is verified by experiment. In section VI, factors which affect the estimation results are discussed.

II The Correlation Function and Blood Signal Model

A. The Correlation Function Model

The correlation function plays an important role in the blood velocity parameters estimation. Most velocity estimators are based on the correlation function. This is because the received blood signal is a Gaussian random signal [7] which is completely characterized by its correlation function [8]. Therefore, the blood velocity parameters are included in the correlation function. In this section, a 2-D correlation function model based on [9] is introduced.

The received 2-D RF signal is denoted as $p(t,k)$ where t is the elapsed time after pulse transmission which corresponds to a certain depth from the transducer and k is the pulse number. Its correlation function is defined by the statistical ensemble average of the signal product:

$$R(\tau, m) \equiv \langle p(t, k)p(t+\tau, k+m)\rangle \tag{2}$$

assuming that $f(t) = r(t)\cos\omega_0 t$ is the transmitted pulse, where $r(t)$ is the envelope of the transmitted signal, ω_0 is transmitted center frequency, and assuming that $s(t) = e(t)\cos\omega_c t$ is the received signal from a single scatterer, where $e(t)$ is the envelope of the received pulse and ω_c is the mean frequency of the received pulse. The function $e(t)$ is determined by the convolution of the envelope of the transmitted pulse, the impulse response of transmission and reception transducer. The mean frequency of the received pulse may be different from the center frequency of transmitted pulse. This is because when there is the effect of the frequency dependent attenuation and frequency random fluctuation, the envelope and the center frequency of the received pulse are altered [10]. The major effect is a shift in the spectral mean. Thus, the effect to the envelope will be neglected. The mean frequency is shifted from ω_0 to ω_c.

When the effect of the beam profile is taken into account and $b(d)$ is the transverse beam sensitivity function, where d is the distance from the ultrasonic beam center axis, the received pulse is: $s(t)b(d)$. This is based on the assumption of separability of the radial and transverse impulse response [9]. In [11], with the stationary and uniform velocity field assumption, the RF correlation function is given by:

$$R(\tau, k) = R_e(\tau - k\tau_v)\cos(\omega_c(\tau - k\tau_v))R_B(kTv\sin\theta) \tag{3}$$

$R_e(\tau)$ is the correlation function of $e(t)$ and $R_B(kTv\sin\theta)$ is the correlation function of lateral sensitivity function $B(d)$.

$$\tau_v = -\frac{2Tv\cos\theta}{c} \tag{4}$$

τ_v is the delay between echoes from two subsequent pulses caused by the scatterer movement.

$v\cos\theta$ and $v\sin\theta$ are the velocity components in the radial (along the ultrasonic beam) and the lateral (transversal to the ultrasonic beam) direction. T is the pulse repetition period. The radial velocity towards to the transducer is defined as positive velocity. Note that the autocorrelation model in (3) includes decorrelation caused by lateral velocity components. Decorrelation caused by velocity gradients may be included by integrating (3) over the corresponding velocity distribution.

B. Simulation Model for the Blood Signal

Assuming the echo response of a single moving scatterer is defined by:

$$h(t, k) = s(t - k\tau_v)b(kTv\sin\theta) \tag{5}$$

The 2-D blood signal can be written as a 2-D convolution between the echo response and the 2-D Gaussian random signal $n(t,k)$, i.e.

$$p(t, k) = h(t, k) \otimes n(t, k). \tag{6}$$

Then the correlation function of the blood signal in (6) equals $R(\tau,k)$ in (3).

Figure 1 is an illustration of the simulation model for the blood signal, including additive white noise to account for the thermal noise from the transducer and receiver amplifier. Figure 2 shows the echo response $h(t,k)$ from a scatterer and the simulated RF blood signal $p(t,k)$.

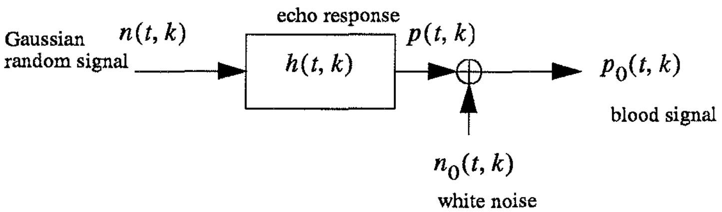

Figure 1 The 2-D blood signal model

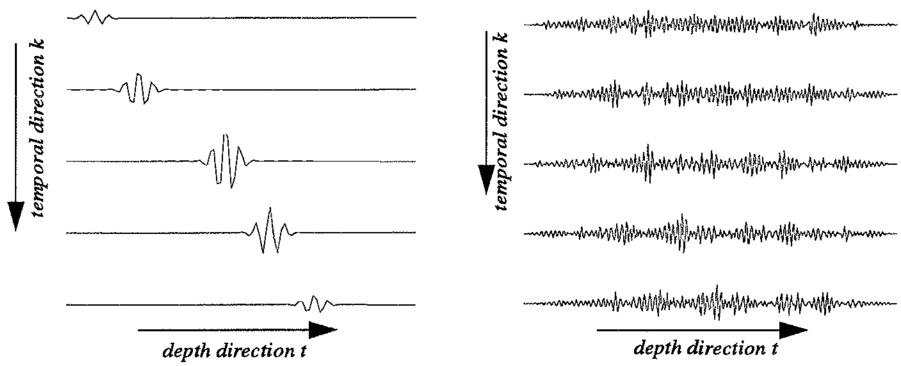

Figure 2 Left plot is the illustration of the echo response $h(t, k)$ from a single scatterer. Right plot is the simulated blood signal $p(t, k)$

III. The Extended Autocorrelation Method

A. The Conventional Autocorrelation Method with Frequency Compensation

In the conventional autocorrelation method (AM), the complex correlation function with lag one in the temporal direction is used to calculate the normalized mean frequency [1]. Using the notation for the 2-D correlation function, the normalized mean frequency in the temporal direction is estimated as [12]:

$$\varpi = phase(R_x(0, 1)). \tag{7}$$

From the Doppler equation, the velocity estimate is calculated, assuming that the center frequency of the received signal is constant and equal to the transmitted frequency f_0

$$v = \frac{c\varpi PRF}{4\pi f_0 \cos\theta}. \tag{8}$$

Frequency dependent attenuation and frequency random fluctuation effects cause variations in the received signal center frequency. This results in velocity bias and estimation variance. The effect of the frequency dependent attenuation becomes significant especially in the wideband signals. This effect can be reduced by estimating the center frequency of the received signal f_c and using it for the estimation, i.e.

$$v = \frac{c\varpi PRF}{4\pi f_c \cos\theta}. \tag{9}$$

The deviation of the received signal center frequency $\Delta f = f_c - f_0$ is estimated from the autocorrelation function with lag in the depth range direction:

$$\Delta f = \frac{phase(R_x(\tau, 0))}{2\pi\tau} \tag{10}$$

This method is referred to as "AM with frequency compensation" and is also described in [12] and [13].

B. The Extended Autocorrelation Method

From (3), it is seen that both the envelope and the phase of the correlation function include velocity information. The AM uses only the phase to estimate the velocity. Due to the periodicity of the phase, aliasing will occur for velocities exceeding the Nyquist limit.

A new method, the extended autocorrelation method (EAM), which uses both the phase and the magnitude of the correlation function to estimate the velocity has been developed. The phase information is used for accurate velocity estimation and the magnitude is used to solve the ambiguity. As in the correlation function model, the time delay τ_v and the phase $-\omega_c\tau_v$ which account for the Doppler shift, both include velocity information. The phase $-\omega_c\tau_v$ is proportional to the time delay, however, due to the periodicity of the phase, the phase estimation wraps the time delay information. When the time delay increases and $-\omega_c\tau_v$ is beyond $|\pi|$, the phase estimation still lies within $|\pi|$ and aliasing occurs. Because the time domain method CCM directly estimates the time delay, there is no velocity ambiguity. The time delay estimation in the CCM is found by maximizing the RF correlation function, $R(\tau,1)$. The maximum magnitude of $R(\tau,1)$ occurs when $\tau = \tau_v$. It is seen from (3) that the envelope correlation function $R_e(\tau - \tau_v)$ attains its maximum and the phase equals $-\omega_c\tau_v$. Thus, the CCM combines the envelope and the phase information which leads to no velocity ambiguity. If the envelope information was discarded, there would be the same velocity ambiguity problem as in the AM.

The relation between the phase and the time delay is

$$\varpi = phase(R_x(0, 1)) = ((-2\pi f_c\tau_v + sign(-2\pi f_c\tau_v)\pi))_{2\pi} \tag{11}$$

where $((\ ))_{2\pi}$ denotes modulo 2π operation, *sign* is for the sign function.

The time delay τ_v will not be estimated correctly when $|-2\pi f_c\tau_v| > |\pi|$.

The phase estimate results in a number of possible time delay candidates

$$phase(R_x(0, 1)) + 2n\pi = -2\pi f_c \times \tau_n \qquad n = 0, \pm1, \pm2\ldots, \tag{12}$$

where τ_n denotes delay candidates. When n=0, the velocity is below the Nyquist limit. Rearranging (12) gives

$$\tau_n = -\frac{\varpi}{2\pi f_c} - \frac{n}{f_c} \qquad n = 0, \pm1, \pm2\ldots. \tag{13}$$

Because the peak of the envelope is located in τ_v, the true delay candidate is found by maximizing the envelope of the correlation function, $n' = max_n(R(\tau_n, 1))$. This is the basic idea for the EAM method.

In its simplest form, the time delay candidates are found from the phase of $R_x(0,1)$. In the appendix, a complete relation between the phase of the 2-D correlation function and the mean frequency in both directions is given, and the normalized mean frequency in the temporal direction can be estimated by:

$$\varpi = phase(R_x(\tau, 1)) - \Delta\omega\tau. \tag{14}$$

It means that the normalized mean frequency in the temporal direction can be estimated by the phase $R_x(\tau,1)$ for any τ in addition to the phase of $R_x(0,1)$ for $\tau = 0$. It is also seen that the phase $R_x(\tau,1)$ is independent of τ when there is no frequency shift of the received blood signal from ω_0, i.e. $\Delta\omega = 0$.

For real signals, the envelope of the correlation function is discrete for the sampled echo signal, but the delay candidates can be at any position and it is necessary to reconstruct the envelope for all τ's by interpolation techniques. Unlike in the CCM where a high performance interpolation technique is needed to locate the precise delay, the interpolation technique is not so crucial in the EAM; a parabolic interpolation usually results in good performance, even with low depth sampling rate.

In the EAM, several delay candidates, τ_n, are found by extending the phase estimation result ϖ periodically. Then the n which gives the maximum amplitude of $R_x(\tau_n, 1)$ is determined. The EAM algorithm is illustrated in Figure 3.

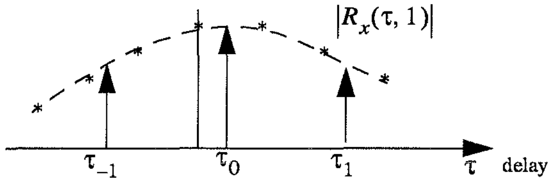

Figure 3 An illustration of the EAM. * represents the amplitude of correlation function $R_x(\tau, 1)$ in sampling points. The dash curve represents the reconstructed envelope of $R_x(\tau, 1)$. $\tau_{-1}, \tau_0, \tau_1$ are the three candidates for the velocity. τ_0 is the candidate for the true velocity in this example because it corresponds to maximum amplitude.

C. Comparison Between the EAM and the CCM

At present, the AM and the CCM are the two most commonly used techniques for estimating blood flow velocity. The CCM is usually referred to as a time domain technique, whereas the AM is referred to as a frequency domain Doppler technique. The advantages of the time domain method over the Doppler technique are discussed in [14] and [15]. The EAM is developed from the AM and, therefore, it is performed on the baseband complex signals. In contrast, the CCM is performed on the real valued RF signals. It is worthwhile to compare the EAM with the time domain method CCM and it is interesting to see in the following discussion that those two methods essentially estimate the same parameter. We will first briefly discuss the CCM algorithm.

1. The CCM

In the cross correlation method, the object is to find the time delay τ_v by searching for the location of the maximum of the RF correlation function $R(\tau, 1)$ i.e.

$$\tau_v = max_\tau(R(\tau, 1)).$$

A typical example of a RF correlation function is given in Figure 4. The RF correlation function is the product of the envelope and the modulating signal $\cos 2\pi f_c(\tau - \tau_v)$. The modulating signal is a periodic function with multiple peaks at $2\pi f_c(\tau - \tau_v) = 2n\pi$, which can be reformulated to

$$\tau = ((\tau_v + sign(\tau_v)f_c))_{2f_c} + \frac{n}{f_c} \qquad n = 0, \pm 1, \pm 2 \ldots \tag{15}$$

When the envelope of the correlation function is constant, several peaks will have the same magnitude. For a shaped envelope, differences in the magnitude of the peaks appear and this makes it possible to pick out the true peak.

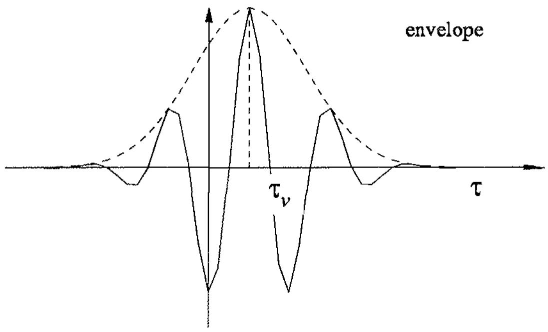

Figure 4 An illustration of a RF correlation function which is the product of the modulation function and the envelope. The modulation function determines the precise delay locations, the envelope determines the true delay τ_v from delay locations.

In a practical implementation, the RF correlation function $R(\tau, 1)$ is discrete and interpolation is necessary in order to estimate precise time delays. The interpolation is used in order to locate the peak in the RF correlation function, therefore, the interpolation technique is crucial in order to obtain good estimation accuracy.

2. A Theoretical Comparison of the EAM and the CCM

The relation between the complex demodulated signal $x(t,k)$ and the RF signal $p(t,k)$ is:

$$p(t, k) = Re(x(t, k)e^{j\omega_0 t}) \tag{16}$$

The complex correlation function is defined as:

$$R_x(\tau, m) = \langle x^*(t, k)x(t + \tau, k + m)\rangle$$

and RF real correlation function is

$$R(\tau, m) = \langle p(t, k)p(t + \tau, k + m)\rangle$$

By some algebraic manipulations, the following relation is obtained

$$R(\tau, m) = \frac{1}{2}Re(e^{j\omega_0\tau}R_x(\tau, m)) + \frac{1}{2}Re(e^{j\omega_0\tau}\langle x^*(t, k)x(t + \tau, k + m)e^{j2\omega_0 t}\rangle) \tag{17}$$

The second term has zero mean and will approach zero when the smoothing in depth direction extends to more than one period of the transmitted signal. This is usually the case due to the high frequency of the transmitted signal. So (17) can be approximated to:

$$R(\tau, m) \approx \frac{1}{2} Re(e^{j\omega_0\tau} R_x(\tau, m)) \tag{18}$$

Usually, only the correlation function with temporal lag one (m=1) is used in both the CCM and the EAM.

If the magnitude of the complex correlation function $|R_x(\tau, 1)|$ is sufficiently smooth compared to the modulation function $\cos(\omega_0\tau)$, then the peak $\tau = \tau_v$ in the RF correlation function $R(\tau, 1)$ occurs when

$$phase(R_x(\tau_v, 1)) + \omega_0\tau_v + 2n\pi = 0 \qquad n = 0, \pm1, \pm2\ldots \tag{19}$$

By combining the equations (14) and (19), the following relation between the time delay τ_v and the mean frequency estimate ϖ is obtained:

$$\Delta w\tau_v + \varpi + \omega_0\tau_v + 2n\pi = 0 \tag{20}$$

The time delay τ_v is:

$$\tau_v = \frac{-\varpi - 2\pi n}{\omega_0 + \Delta w} \tag{21}$$

Observe that τ_v is the same as the delay candidates - τ_n in the EAM. The time delay τ_v in (21) is not unique, but the true velocity corresponds to the delay which maximize the envelope.

3. Comparison of the Processing Time

The processing time is mainly spent on calculating the correlation function in the CCM and in the EAM. Although the interpolation step also requires substantial processing time, especially when the sampling frequency in the depth direction is low, the computational efficiency is comparable to that of the correlation function. The processing time depends on the number of data samples. The EAM operates on the complex signal where the sampling rate can be decreased substantially compared to the CCM. This reduces the computational requirement. By calculation, one depth sample delay corresponds to $2f_0/f_s$ times the Nyquist velocity. In order to estimate velocities up to 4 times the Nyquist velocity, $2f_s/f_0$ samples are required in the depth direction.

For instance, if the sampling frequency of the demodulated signal *fsd,* equals the transmitted frequency, five correlation coefficients are required to estimate a velocity range of four times the Nyquist limit.

In the EAM, the calculations are: five complex correlation coefficients from the data block $N \times K$, where N is the depth averaging samples and K is the temporal averaging samples.

In the CCM, the calculations are: $5f_s/fsd$ correlation coefficients from the data block $N \times \left(\frac{fs}{fsd}\right)K$.

Assuming that the calculation of the correlation function is proportional to the data size, the ratio of the calculation of the correlation coefficients of the CCM to the EAM is

$$\frac{1}{2}\left(\frac{fs}{fsd}\right)^2 \tag{22}$$

When $f_s = 10MHz$, $fsd = 2.5MHz$, the ratio is 8, but in this case, the interpolation method in the CCM is time consuming. The total computation in the EAM is much less than the CCM. When $f_s = 20MHz$, a parabolic interpolation method to the CCM works well, the interpolation step will not take too much time, but the ratio of the calculation of the correlation function in (22) is 32.

IV. Analysis of the EAM and the CCM by Simulations

A. Simulation Signal and Parameters

A 2-D Gaussian random signal based on the blood signal model in section II is simulated. The length of the wideband transmitted pulse is approximately two cycle periods. Typically, a wideband transmitted pulse is minimum phase with a rapid rise and more gradual fall of the pulse envelope. However, a Gaussian shape envelope of the received signal was used in our simulations. What is important for the performance is the envelope of the correlation function, which will approach a Gaussian form, also for the minimum phase pulse. The received signal from a scatterer is then

$$s(t)b(d) = \exp\left(\frac{-t^2}{\sigma^2}\right)\cos(2\pi f_0 t)b(kTv\sin\theta)$$

The standard deviation is set to $\sigma = 1/f_0$, giving a pulse length of approximately two cycle periods. The pulse bandwidth BW is defined as $1/\sigma$ which the magnitude of the envelope decreases 8.69dB. The transverse beam profile b is assumed to Gaussian function [9] and $b(d) = \exp(-3d^2/2B^2)$ is used in our simulation, where B is the Beam width.

The other parameters for all the simulations in the paper are given in Table I. The Nyquist velocity is determined by (1) and equals 1.0265 m/s with the given parameters.

Table 1: PARAMETERS FOR SIMULATIONS

Center frequency f_0	2.5MHz
Pulse bandwidth BW	2.5MHz
Pulse repetition frequency PRF	6564Hz
Speed of sound c	1540m/s
Measurement angle θ	10 degree
Temporal averaging	1.8ms or 12 samples for the signal of prf 6564Hz
Depth averaging	3 *0.8μs or 24 samples for the signal of f_s =10MHz and f_0 =2.5MHz
Beam width B	2 mm

B. Signal to Noise Ratio

White noise is added to the final RF signal as shown in Figure 1. The signal to noise ratio for the blood signal is defined as:

$$SNR = 10\log\frac{\sum_n\sum_k p^2(n, k)}{\sum_n\sum_k n_0^2(n, k)} \tag{23}$$

$$p_0(n, k) = p(n, k) + n_0(n, k) \tag{24}$$

The complex signal $x(n, k)$ is obtained by demodulating the RF-signal $p_0(n, k)$. Signals with SNR=30dB and SNR=0dB are used for the simulations in this work.

C. Simulation Results

The estimation Results for the CCM and the EAM are shown in Figure 5. The sampling rate f_s is $10MHz$ for both methods

The blood signal is a random signal. Because the mean frequency estimate based on the correlation function has a distribution close to Gaussian [5], the estimation variance possesses a chi-square distribution. To evaluate the estimator of the CCM and the EAM, the estimation results in this work were based on 50 independent simulations. A confidence interval for the variance of a normal random variable can be obtained from the statistic [19] which is: $[0.84s, 1.25s]$, where s is the estimated standard derivation. This parameter gives the reliability of this simulation. The 95% confidence interval of the standard deviation for the CCM is plotted in Figure 5. The simulation results in Figure 5 show that the CCM and the EAM have similar performance, especially when the signal to noise ratio is high. They can estimate velocities up to four times Nyquist velocity and give similar variance. The estimation variance depends on the correlation length of the signal. For the highest velocities, the correlation length decreases due to the transit time through the ultrasound beam, giving increased estimation variance.

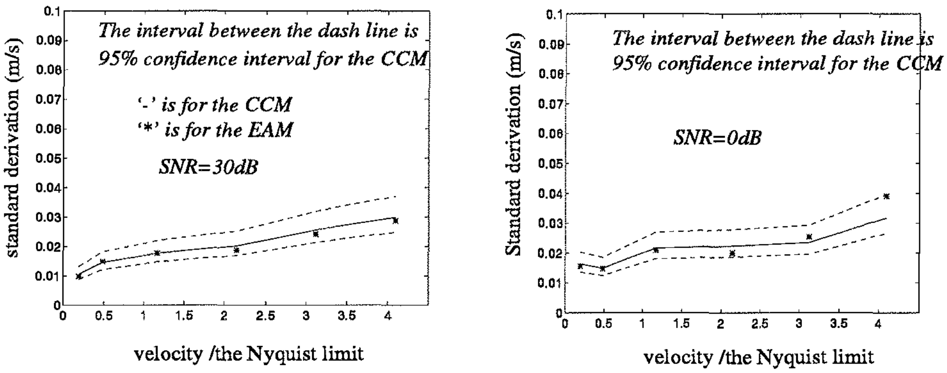

Figure 5 Standard deviation of velocity estimation by the CCM and the EAM. Solid line is for the CCM. '*' is for the EAM, dash lines indicate the 95% confidence interval based on the standard deviation of the CCM.

Since the EAM operates on the complex demodulated signals, the sampling rate f_s can be reduced down to the bandwidth of the signal, which was BW=2.5 *MHz*. However, the CCM perform on the RF signal, which requires a sampling rate of $2f_0 + BW$. In the simulations f_s=2.5 *MHz*, 5 *MHz*, and 10 *MHz* was used for EAM, and f_s=10 *MHz* was used for CCM. The estimation results for the EAM with sampling rate 10*MHz*, 5*MHz* and 2.5*MHz* are shown in Figure 6. 95% confidence interval of the standard deviation for this simulation is:, $[0.84s, 1.25s]$ where s is the estimated standard derivation. 95% confidence interval of the standard deviation for the EAM in the sampling rate 10*MHz* is shown in Figure 6.

The results for the EAM with sampling rate 10*MHz*, 5*MHz* and 2.5*MHz* have no significant difference when the signal to noise ratio is high. When the signal to noise ratio is low, the standard derivation in the case of sampling rate 2.5*MHz* is slightly higher than for sampling rate 10*MHz* and 5*MHz*.

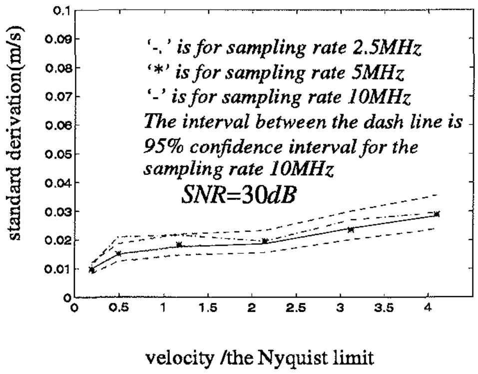

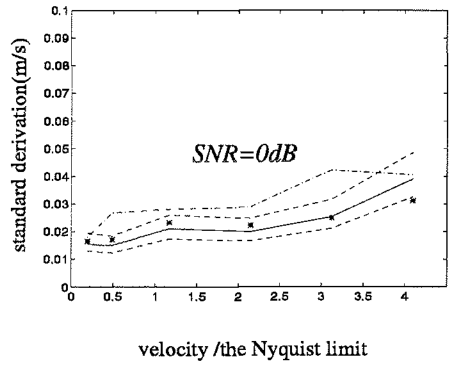

Figure 6 Standard deviation of the velocity estimator EAM in sampling rate 10*MHz*, 5*MHz* and 2.5*MHz*.Solid line is for the sampling rate 10*MHz*, '*' is for the sampling rate 5*MHz* and '-.' is for the sampling rate 2.5*MHz*.

V. Experiment Verification

The EAM was verified by experimental data from the subclavian artery. The CCM was also applied to the experimental data for comparison. The RF data from a ultrasound scanner (Vingmed CFM 800) was collected in real-time via a custom data grabbing system. The slow tissue movement signal in the raw data was removed by a 4 order IIR butterworth high pass filter with normalized cutoff frequency 0.155. Then the data was demodulated with the center frequency 2.5*MHz*.

A. The AM with frequency compensation is applied to the experimental data from the subclavian artery. The quality improvement achieved by the frequency compensation is shown in Figure 7. Left plot is the estimation result by the AM. Right plot is the estimation result by the AM with frequency compensation. The curve in the right plot is smoother than the left, indicating lower estimation variance.

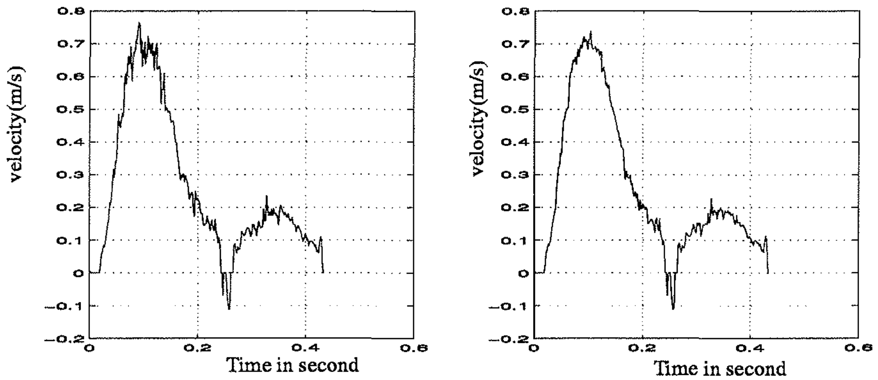

Figure 7 Comparing the AM to the AM with frequency compensation method. Left plot is the results of the AM, right plot is the results of the AM with frequency compensation

B. Comparison between the EAM and the CCM when the velocities are within the Nyquist limit

The depth averaging in this experiment was $0.8\mu s$, i.e. 8 samples in depth direction for f_s=10*MHz*, f_0=2.5*MHz*. The other parameters in the upper plots Figure 8 (a), (b) were the same as in the simulation in this paper. They show no difference between the two methods. Both of them give good results.

C. Comparison between the EAM and the CCM when there are velocities beyond the Nyquist velocity but within 2 times the Nyquist limits

In the middle plots (c), (d) in Figure 8 are the results from another set of experimental data from the subclavian artery. The pulse repetition frequency was reduced to 4*kHz*, so the Nyquist velocity has been reduced. The depth averaging is $1.2\mu s$, i.e. 12 samples for f_s=10*MHz*, f_0=2.5*MHz*. The temporal averaging is 6ms, i.e. 24 samples. The overlap is 3ms between temporal averaging. The performance of the two methods are similar.

D. Comparison between the EAM and the CCM when there are velocities up to 4 times Nyquist limits

The data in this experiment was acquired by decimating the RF data in experiment B to reduce the pulse repetition frequency, so a lower Nyquist limit was obtained. This decimation was done before the wall motion filter. The depth averaging in this experiment is $1.2\mu s$, i.e. 12 samples for f_s=10*MHz*, f_0=2.5*MHz*. The temporal averaging is 6ms, i.e. 12 pulses by

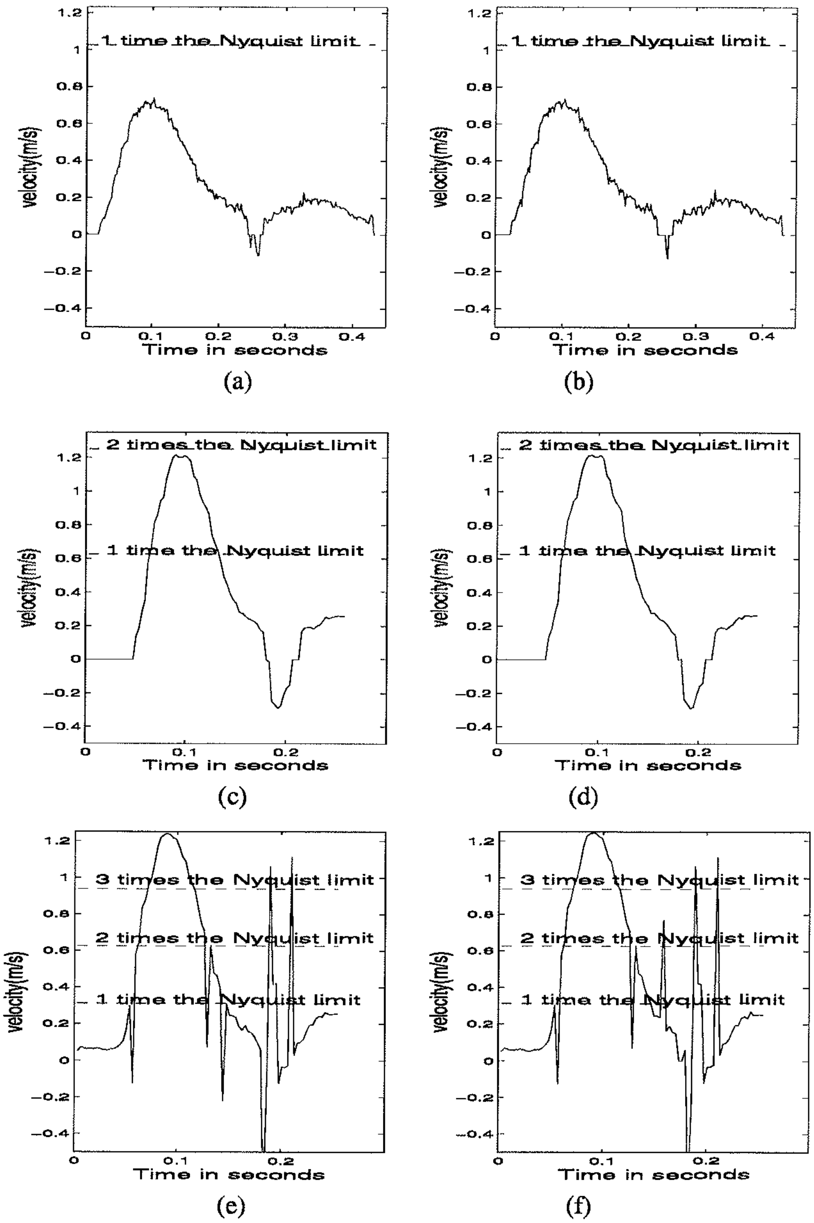

Figure 8 Experimental data from subclavian artery analyzed by the EAM and the CCM. Left plots (a), (c) and (e) are the results by the EAM. Right plots (b), (d) and (f) are the results by the CCM. Upper plots (a) and (b): The Nyquist limit is 1.0265m/s and the velocities are within the Nyquist limit. Middle plots (c) and (d): The Nyquist limit is 0.6255m/s and the velocities are within twice the Nyquist limit. Lower plot (e) and (f): The Nyquist limit is 0.3128m/s and the velocities are within 4 times the Nyquist limit.

repetition frequency $2kHz$. The overlap is 3ms between temporal averaging. The results in the lower plots (e), (f) in Figure 8 show that both the EAM and the CCM can estimate the velocities up to 4 times the Nyquist limit. But there were global errors in the results.

Two gray scale velocity images in the upper (a) and middle (b) in Figure 9 are by the EAM and the CCM. The experimental data is the same as in the experiment B. The depth averaging was 1.2μs, the temporal averaging was 3ms. No overlap between temporal averaging. Velocities within two times the Nyquist limits have been estimated. There was no significant difference between the two images. Global errors can be seen in both images. In order to reduce the global errors, a 2-D tracking method has been used. It is based on the knowledge from flow physics that the blood velocity is continuous both in depth and temporal directions. The global error is always twice the Nyquist limit, which makes the velocity discontinues. The tracking method is to compare the present point to the previous neighboring points, if the velocity varies beyond the Nyquist limit, then the present point is taken to have global error. Then the velocity in the present point should be added or subtracted twice the Nyquist velocity until the difference between its velocity and the velocity of previous neighboring points is within the Nyquist limit. The lower image (c) in Figure 9 is the results of the upper image (a) of Figure 9 by 2-D tracking method. It is seen that the quality of the velocity image has been improved. It should be mentioned that the velocity in the previous neighboring points is important for tracking. If the velocity of the reference points --neighboring points is not correct, it may cause velocity images with large errors.

In Figure 10, there are three gray scale velocity images in which velocities within four times the Nyquist limits have been estimated by the EAM and the CCM, respectively. The experimental data is the same as in the experiment C. The depth averaging was $1.2\mu s$, the temporal averaging was 6ms with 3ms overlap between temporal averaging. There was no significant difference between the two images Figure 14 (a) and (b). The global errors can be seen in both images. The global errors can be reduced by 2-D tracking. This is shown in the lower image (c) in Figure 10.

VI. Discussing factors which affect the Estimation Results

A. The Effects of the Pulse Bandwidth and Signal to Noise Ratio to the EAM

The velocity estimation variance and sensitivity versus the pulse bandwidth and signal to noise ratio was discussed in [17]. The velocity estimation variance decreases and the sensitivity increases with increasing pulse bandwidth as long as the signal to noise ratio is sufficiently high. Under poor SNR condition, the pulse bandwidth should be reduced in order to increase the sensitivity. To global error which is caused by choosing the wrong peak in the

(a)

(b)

(c)

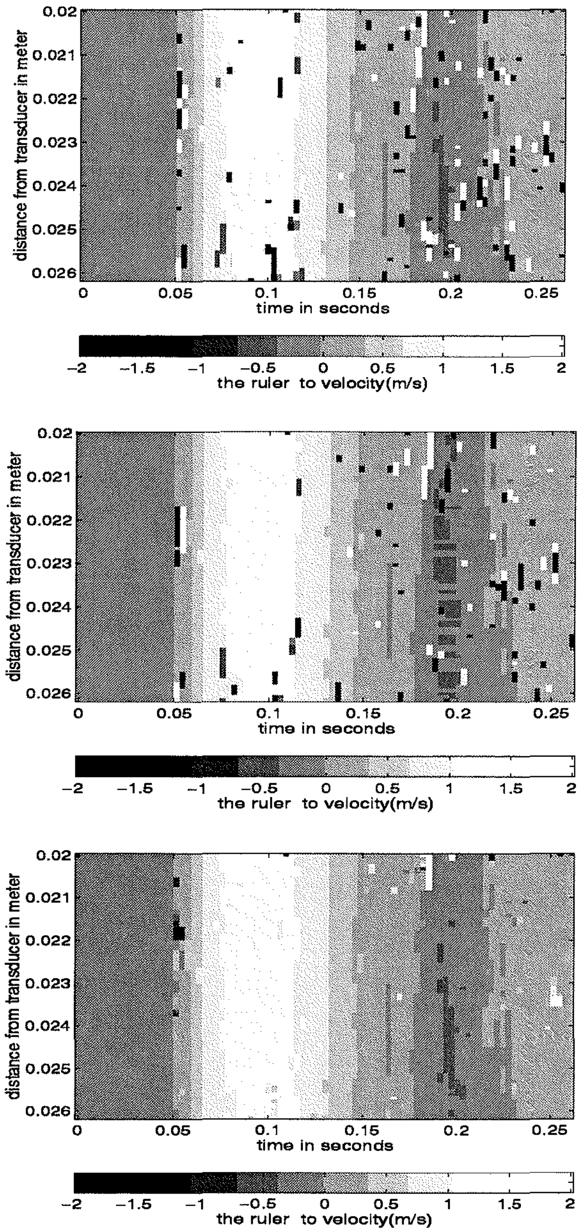

Figure 9 Velocity image from subclavian artery analyzed by the EAM and the CCM. The Nyquist limit is 0.6255m/s and the velocities are within 2 times the Nyquist limit. Upper image (a) is the results by the EAM. Middle image (b) is the results by the CCM. Lower image (c) is obtained from the upper image with 2-D tracking.

(a)

(b)

(c)

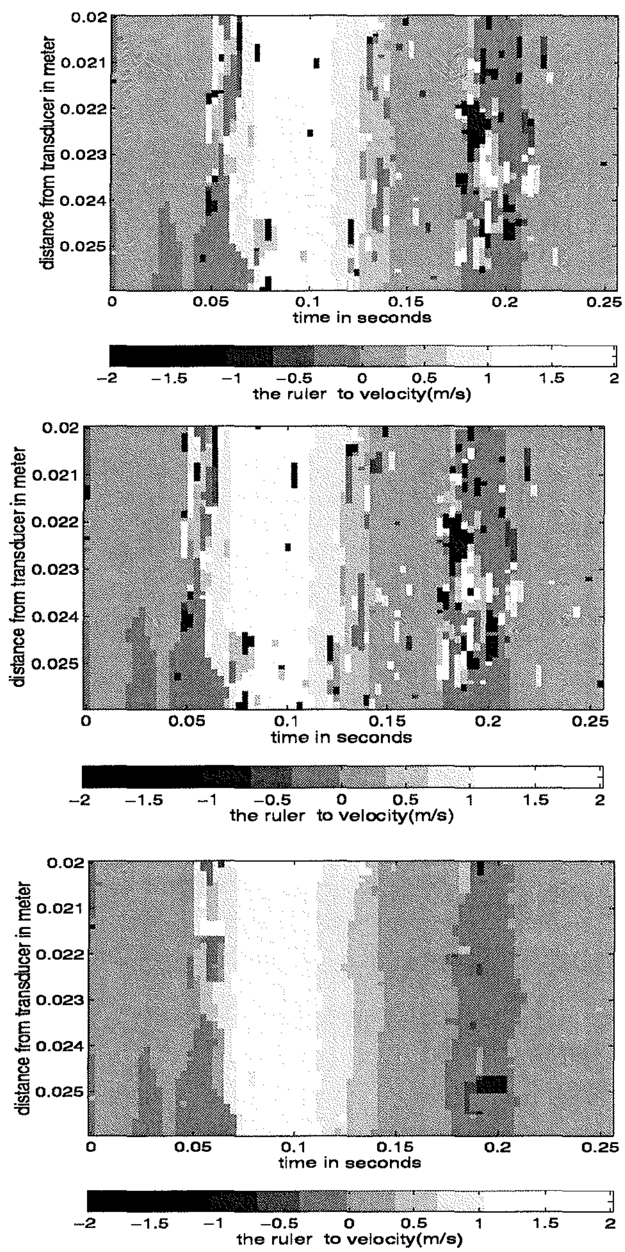

Figure 10 Velocity image from subclavian artery analyzed by the EAM and the CCM. The Nyquist limit is 0.3128m/s and the velocities are within 4 times the Nyquist limit. Upper image (a) is the results by the EAM. Middle image (b) is the results by the CCM. Lower image(c) is obtained from the upper image(a) with 2-D tracking.

correlation function, it decreases with the pulse bandwidth [21]. It is because that the shape of the envelope affects the searching of the maximum. A sharp envelope makes it easy to tell the main peak from subsidiary peaks. A flatter envelope makes it difficult to find the main peak. Sometimes it can choose the wrong peak and the ambiguity associated with aliasing occurs. The shape of the correlation function envelope is determined by the pulse bandwidth. High pulse bandwidth signal corresponds to a sharp envelope. Narrow pulse bandwidth signal correspond to a flat envelope.

Thus, there is trade-off between the wideband pulse and narrow band pulse since the optimization for the velocity estimation variance and sensitivity are contradictory. When SNR is low, the aliasing errors occur easily. This is because the correlation function for poor SNR conditions is flat compared to high SNR conditions. The estimation variance of the correlation function has heavy influence on the detection of the true peak in the correlation function, and aliasing error can occur.

B. The Effect of the Depth Averaging Time and the Temporal Averaging Time to the EAM

Increasing the depth averaging time and temporal averaging time, the estimation variance is decreased [22]. The depth averaging determines the range resolution. To get a high range resolution, the depth averaging can not be too long. The temporal averaging time affects the frame rate. To keep a high frame rate in color flow imaging, the temporal averaging time can not be too long. The temporal samples are typically 6 to 16. With a pulse repetition frequency of 5 *kHz*, this corresponds to 1.2 - 3.2 msec averaging time.

C. The Effect of Measurement Angle and Velocity of Scatterers to the EAM

When increasing the measurement angle, the transversal velocity increases. This increases the estimation variance due to the decorrelation caused by the beam profile. For the higher velocities, the transversal velocities are higher. This increases estimation variance the same as the results for increasing the measurement angle.

D. The Effects of the Correlation Estimator

The correlation estimator affects the estimate of the velocity. Several estimators are available such as the biased estimator, the unbiased estimator [20] and the normalized estimator [22]. Given $M \times L$ 2-D sequence $x(n,k)$, an unbiased estimator of the 2-D correlation function is defined as:

$$c_u(m, l) = \frac{1}{M-|m|}\frac{1}{L-|l|}\sum_{n=0}^{M-|m|-1}\sum_{k=0}^{L-|l|-1} x(n, k)x^*(n+m, k+l)$$

A biased estimator of the 2-D correlation function is defined as:

$$c_b(m, l) = \frac{1}{ML} \sum_{n=0}^{M-|m|-1} \sum_{k=0}^{L-|l|-1} x(n, k)x^*(n+m, k+l)$$

A normalized estimator of the 2-D correlation function is defined as:

$$c_n(m, l) = \frac{\sum_{n=0}^{M-|m|-1} \sum_{k=0}^{L-|l|-1} x(n, k)x^*(n+m, k+l)}{\sqrt{\sum_{n=0}^{M-|m|-1} \sum_{k=0}^{L-|l|-1} x(n, k)x^*(n, k) \sum_{n=0}^{M-|m|-1} \sum_{k=0}^{L-|l|-1} x(n+m, k+l)x^*(n+m, k+l)}}$$

Among those, the biased and unbiased correlation function estimators were used in our simulation due to calculation requirements. The biased estimator has smaller estimation variance than the unbiased estimator, but its estimated amplitude does not approach the expected value of the autocorrelation function coefficient. The estimated amplitude of the correlation function is weighted by a triangular function window. The larger τ in $R(\tau,1)$, the larger bias. When there is a high velocity, the maximum amplitude of the correlation function corresponds to a large τ. However, due to the effect of the triangular window, the maximum amplitude is easily located for small τ. So the high velocity can't be estimated by using the biased autocorrelation estimator. The unbiased estimator has to be used to estimate the high velocities because its estimated amplitude of the correlation function is unbiased to the expected correlation function. The estimated amplitude is regarded as weighted by rectangular function window, the amplitude in large τ is not attenuated. Unfortunately, it yields a much higher variance than the biased estimator for large τ.

The unbiased estimator is suitable to use for signal with high velocities, the biased estimator is suitable to use for signal with low velocities. If the unbiased estimator is used for the signal with low velocity, global error easily occurs and the estimation value is usually higher than the true value. If the biased estimator is used for the signal with high velocity, global error easily occurs and the estimation value is usually lower than the true value. Several correlation estimators have been investigated and that there is not a particular correlation estimator that can give good results in the whole velocity range from zero to four times the Nyquist limit for either the EAM or the CCM.

The effects of the correlation estimator to the velocity estimation can be verified by the simulation and experiment. In this simulation, all the parameters are the same as in section IV except the depth averaging is $10\mu s$. The simulation results are obtained by applying the biased correlation estimator and unbiased correlation estimator with respect to low velocity case (0.2 m/s) and high velocity case. For each case, we have 50 simulation results which is presented by the histgram in Figure 11 and Figure 12.

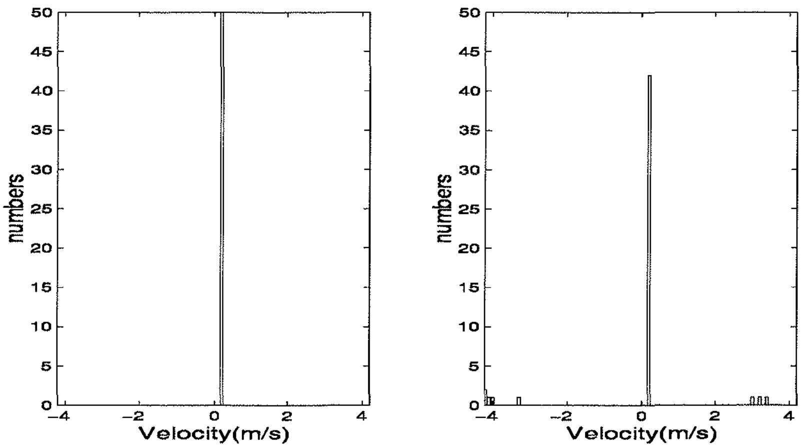

Figure 11 Histgram for velocity estimation results (from 50 simulations) when velocity is 0.2m/s. The results by using the biased correlation estimator is in the left plot. The results by using the unbiased correlation estimator is in the right plot.

From Figure 11, there are global errors in the right plot where the unbiased correlation estimator is used. No global errors in the left plot and the mean value is around 0.2m/s. That means the estimation results is better by using the biased correlation estimator than by the unbiased correlation estimator when the velocities are low. It is seen that for the same data, using different correlation estimator, we get different estimation results.
From Figure 12, there are global errors in the left plot where the biased correlation estimator is used.

In the right plot where the unbiased correlation estimator is used, no global errors have been observed and the mean value is around 3.2m/s. That means the estimation results is better by using the unbiased correlation estimator than by the biased correlation estimate when the velocities are high.

In practice, the velocity range may be large. Whether the biased or the unbiased correlation estimator should be used depends on the velocity. However, the velocity is unknown until it is estimated by using the correlation estimator. Methods to choose the biased or the unbiased estimator are recommended by means of the bandwidth parameter. Because a high velocity scatterer of wide bandwidth has small correlation coefficient, the bandwidth can be represented approximately by the correlation coefficient as discussed in the correlation function model.

The effect of the correlation estimator to the bandwidth parameter is not so crucial as to the

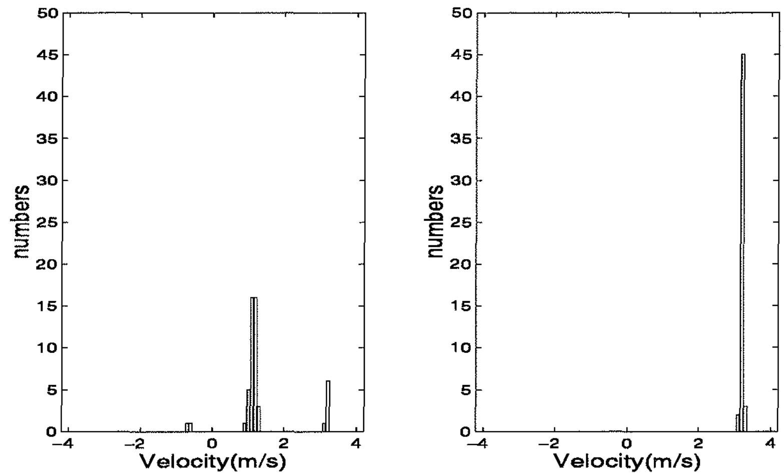

Figure 12 Histgram for velocity estimation results (from 50 simulations) wher velocity is 3.2m/s. The results by using the biased correlation estimator is in the left plot. The results by using the unbiased correlation estimator is in the right plot

velocity. It is feasible to use to the bandwidth parameter to determine the type of estimator. Figure 13 is a block diagram of blood velocity estimation.

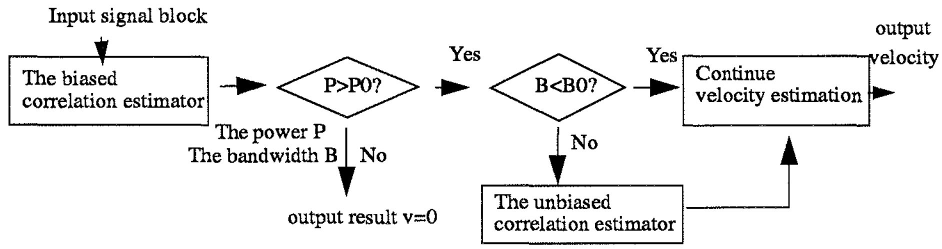

Figure 13 Velocity estimation diagram using the biased or the unbiased estimator automatically by the bandwidth parameter. P0 is the power threshold, B0 is the bandwidth threshold.

P0 and the B0 are the thresholds of the signal power and the bandwidth. If the power is below the power threshold, it means no blood signals have been detected or only noise is present, so the velocity is set to zero. If the signal has enough power, then test the bandwidth. If the signal has high bandwidth, then high velocities are possible. Then the unbiased estimator is chosen. Otherwise, the biased estimator is used. The velocity estimation refers to the EAM or the CCM. Figure 14 is an example for switching from the biased to the unbiased estimator automatically by using the bandwidth parameter. For comparison, we give the estimation results using either biased correlation estimator or the unbiased correlation estimator in Figure 15.

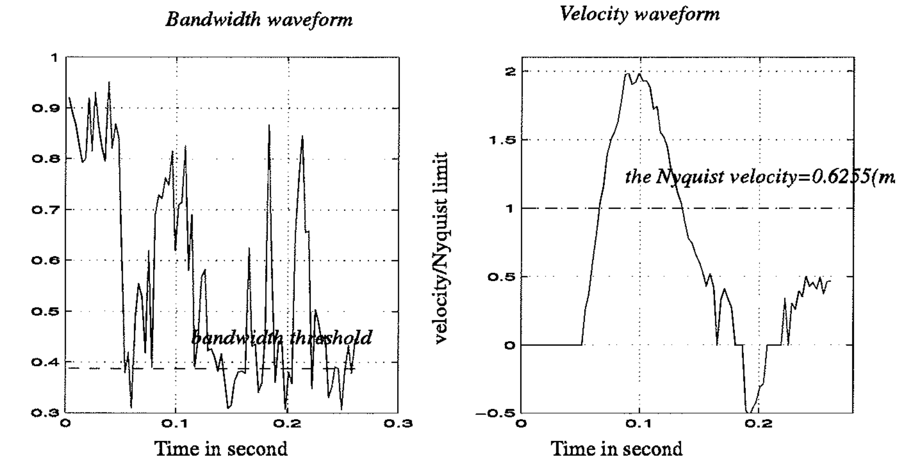

Figure 14 An example for switching the biased to the unbiased correlation estimator by means of the bandwidth parameter.

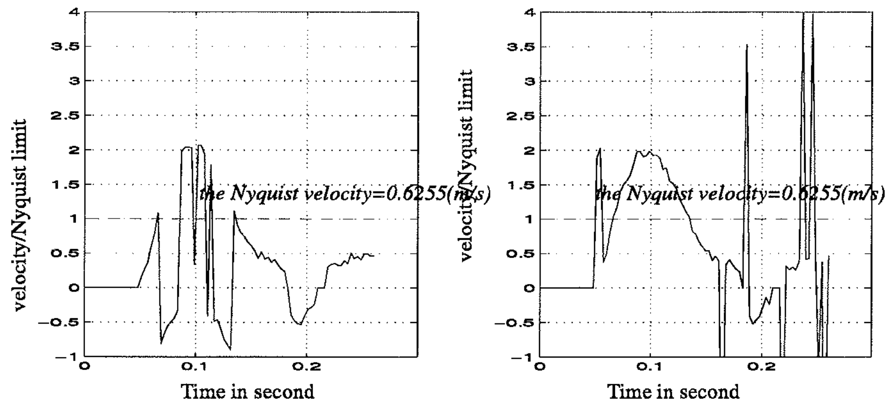

Figure 15 The results comparison by using either biased correlation estimator or unbiased correlation estimator. Left plot is the results for using the biased estimator. Right plot is the results for using the unbiased estimator.

Another velocity estimation diagram shown in Figure 16 can also be used. It uses only the unbiased estimator, but uses the bandwidth parameter to limit the velocity range. The velocity range processing means that the estimated velocity adds or subtracts twice the Nyquist limit until the velocity is within the defined velocity limit. When the bandwidth is low, the velocity is low. Then the velocity range can be defined, for instance, within the Nyquist limit.

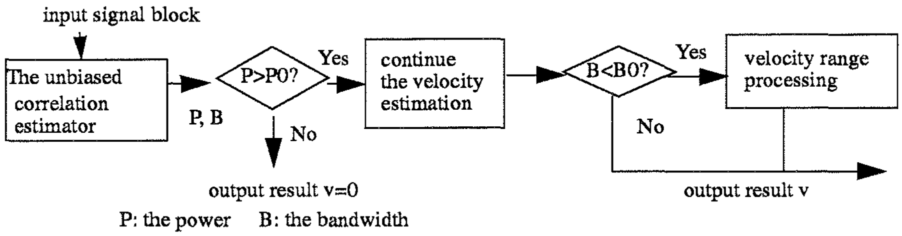

Figure 16 Velocity estimation diagram using only the unbiased estimator. The low velocities are found by limiting the velocity range by means of the bandwidth parameter. P0 is the power threshold, B0 is the bandwidth threshold.

The rectilinear velocity flow is only considered in the paper, so the bandwidth can be used to distinguish between high velocities and the low velocities. In practice, the turbulent flow is possible for the patient which signal components distribute all over the frequency range in the power spectrum and it has a broadband Doppler signal. The broadband implies two types of flow. To distinguish between these two types of flow, some prior knowledge about flow is needed.

E. Effects of the Prior Knowledge of Flow to the Estimation

The more the prior information, the better the estimation results. The prior information of flow includes the type of flow, the flow velocity range and the flow direction. The type could be rectilinear or turbulence flow. The flow velocity range, for example, is within the Nyquist limit, twice the Nyquist limit or multiple times the Nyquist limit. The flow direction is whether the flow is unidirectional or it has the positive or negative flow.

In summary, the parameters which affect the estimation result in the CCM can also affect the estimation results in the EAM.

Conclusions

A new extended autocorrelation method to estimate the velocity in color flow imaging is presented. Compared to the autocorrelation method, it has small estimation variance and the capability to estimate high velocities beyond the Nyquist limit. The performance improvement can be explained by the depth information added in the estimation. The small estimation variance is due to the frequency compensation by using several samples of the signal in the depth range. The capability to estimate high velocities beyond the Nyquist limit is because the envelope of the correlation function in depth is used. The frequency dependent attenuation and random fluctuation has not affected the EAM velocity estimation due to the frequency compensation. It is shown that the EAM and the CCM have similar performance.

The processing time is mainly spent in the calculation of the complex correlation function in the EAM. In the CCM, the processing time is spent on the calculation of the RF correlation function in addition to the interpolation method. Because the EAM performs on the demodulated complex data in contrast to the RF data in the CCM, the computation requirement has been reduced greatly in the EAM.

The estimate result to the EAM, as to the CCM, can be affected by many factors such as the SNR, the pulse bandwidth, measurement angle, scatterer velocities and the data block size. The global errors can be observed when estimating the velocity exceeding the Nyquist limit. By applying a 2-D tracking method, the amount of global errors can be reduced.

The EAM has been verified by simulations and experimental RF data with velocities up to 4 times the Nyquist limit. The CCM has also been applied to the simulation and experimental RF data for comparison.

Appendix

Mean Frequency Estimator

It is shown that the complex Doppler signal is a complex Gaussian process. Therefore, the autocorrelation function $R_x(\tau, n)$ and the power spectrum density $G(\omega_1, \omega_2)$ is a Fourier transform pair. The autocorrelation function can be written as

$$R_x(\tau, n) = \int_{-\infty}^{\infty} \int_{-\pi}^{\pi} G(\omega_1, \omega_2) e^{j\omega_1\tau + j\omega_2 n} d\omega_1 d\omega_2 \tag{25}$$

Let $\Delta\omega$ denote mean frequency in depth direction, ϖ is the mean frequency in the temporal direction. They are defined by

$$\varpi = \int_{-\infty}^{\infty} \int_{-\pi}^{\pi} \omega_2 G(\omega_1, \omega_2) d\omega_1 d\omega_2 \Big/ \int_{-\infty}^{\infty} \int_{-\pi}^{\pi} G(\omega_1, \omega_2) d\omega_1 d\omega_2 \tag{26}$$

$$\Delta\omega = \int_{-\infty}^{\infty} \int_{-\pi}^{\pi} \omega_1 G(\omega_1, \omega_2) d\omega_1 d\omega_2 \Big/ \int_{-\infty}^{\infty} \int_{-\pi}^{\pi} G(\omega_1, \omega_2) d\omega_1 d\omega_2 \tag{27}$$

Expanding $e^{j\omega_1\tau + j\omega_2 n}$ in (25) by a power series in the points $\Delta\omega$, ϖ

$$R_x(\tau, n) = e^{j\Delta\omega\tau + j\varpi n}\left(\int_{-\infty}^{\infty}\int_{-\pi}^{\pi} d\omega_1 d\omega_2 G(\omega_1, \omega_2) e^{j(\omega_1 - \Delta\omega)\tau + j(\omega_2 - \varpi)n}\right) \quad (28)$$

$$= e^{j\Delta\omega\tau + j\varpi n}\int_{-\infty}^{\infty}\int_{-\pi}^{\pi} d\omega_1 d\omega_2 G(\omega_1, \omega_2)\Big(1 + j(\omega_1 - \Delta\omega)\tau + j(\omega_2 - \varpi)n$$

$$-\frac{1}{2}(\omega_1 - \Delta\omega)^2 - \frac{1}{2}(\omega_2 - \varpi)^2 + \ldots\Big)$$

$$R_x(\tau, n) \approx e^{j\Delta\omega\tau + j\varpi n}\int_{-\infty}^{\infty}\int_{-\pi}^{\pi} d\omega_1 d\omega_2 G(\omega_1, \omega_2)\left(1 - \frac{1}{2}(\omega_1 - \Delta\omega)^2 - \frac{1}{2}(\omega_2 - \varpi)^2 + \ldots\right) \quad (29)$$

The first power term in (28) is zero. The approximation in (29) is valid when $G(\omega_1, \omega_2)$ vanishes outside a small area around $\omega_1 = \Delta\omega$, $\omega_2 = \varpi$, the third and higher term approach zero. That implies $G(\omega_1, \omega_2)$ should have a narrow 2-D bandwidth. Thus, (29) is a good approximation to the higher sampling rate signal both in the depth and temporal direction because this signal has a narrow bandwidth.

From (29), the relation between the phase and the mean frequencies is:

$$phase(R_x(\tau, n)) = \Delta\omega\tau + \varpi n \quad (30)$$

The mean frequencies in the 2-D sampled signal is given by:

$$\Delta\omega = \frac{phase(R_x(1, 0))}{Ts} \quad (31)$$

$$\varpi = \frac{phase(R_x(0, 1))}{T} \quad (32)$$

Ts is the sampling period in depth direction. T is the pulse repetition period

References

[1] C. Kasai, K. Namekawa, A. Koyano, and R. Omoto, "Real-time Two-Dimensional Blood Flow Imaging Using an Autocorrelation Technique," *IEEE Trans.Sonics Ultras.*, vol.SU-32, pp.458-464, 1985

[2] O. Bonnefous and Pesquė, "Time Domain formulation of Pulse-Doppler Ultrasound and Blood VelocityEstimation by Cross-Correlation," *in Ultrasonic Imaging 8.* 1986

[3] O. Bonnefous and Pesquė., and X. Bernard, "A New Velocity Estimator for Color Flow Mapping," *in Proc. IEEE Ultrason. Symp.*, pp.885-860, 1986.

[4] L. S. Wilson, "Description of Broad-Band Pulsed Doppler Ultrasound Processing Using the Two-Dimensional Fourier Transform," *Ultrasonic Imaging* 13, 301-315, 1991.

[5] K. W. Ferrara, V. Ralph Algazi, "A New Wideband Spread Target Maximum Likelihood Estimator for Blood Velocity Estimation--Part I: Theory," *IEEE Trans.on Ultrasound, Ferroelectrics, and Frequency Control,* vol.38, NO.1. January, 1991.

[6] K. W. Ferrara, V. Ralph Algazi, "A New Wideband Spread Target Maximum Likelihood Estimator for Blood Flow Velocity Estimation--Part II: Evaluation of Estimators," *IEEE Trans.on Ultrasound, Ferroelectrics, and Frequency Control,* vol.38, NO.1. pp.17-26, 1991.

[7] B. A. J. Angelsen and K. Kristoffersen, "On Ultrasonic MTI Measurement of Velocity Profiles in Blood Flow," IEEE Trans. Biomed. Eng., vol. BME-26, pp.665-671, 1979.

[8] A. Papoulis, "Probability, Random Variables and Stochastic Processes," McGraw-Hill, 1965

[9] H. Torp, K. Kristoffersen and B. Angelsen, "Autocorrelation Technique in Color Flow Imaging, Signal Model and Statistical Properties of the Autocorrelation Estimates," *IEEE Trans.on Ultrasound, Ferroelectrics, and Frequency Control,* vol 41. N0.5 Sep.1994.

[10] K. W. Ferrara, V. Ralph Algaz & et.al, "The Effect of Frequency Dependent Scattering and Attenuation on the Estimation of Blood Velocity Using Ultrasound," *IEEE Trans.on Ultrasound,Ferroelectrics,and Frequency Control,* vol.39, No.6 November, 1992

[11] H. Torp, K. Kristoffersen, "Velocity Matched Spectrum Analysis: A New Method for Suppressing Velocity Ambiguity in Pulsed-Wave Doppler," *Ultrasound in Med. & Biol.,* Vol. 21 No.7, pp.937-944, 1995

[12] Thanasis Loupas, J.T. Powers and Robert W. Gill, "An Axial Velocity Estimator for Ultrasound Blood Flow imaging, Based on a Full Evaluation of the Doppler Equation by Means of a Two-Dimensional Autocorrelation Approach," *IEEE Trans.on Ultrasound, Ferroelectrics, and Frequency Control,* vol.42, NO.4. July, 1995.

[13] H. Torp, K. Kristoffersen, "Method for Calculation of Blood Velocity and Blood Velocity Spread From Multigated Doppler Signal," *US Patent* No. 5.560.363, Oct.1, 1996.

[14] I. A. Hein, William D. O'Brien, "Current Time-Domain Methods for Assessing Tissue Motion by Analysis from Reflected Ultrasound Echoes--A Review," *IEEE Trans. on Ultrasound, Ferroelectrics, and Frequency Control,* vol.40, NO.2. March, 1993.

[15] A. Herment, P. Dumee, "Comparison of blood flow imaging methods," *European Journal of Ultrasound, pp.*345--353, 1994

[16] P. G. M. de Jong, T. Arts, A. P. G. Hoeks and R. S. Reneman, "Determination of Tissue Motion Velocity by Correlation Interpolation of Pulsed Ultrasonic Echo Signals," *Ultrasonic Imaging* 12, pp.84-98, 1990.

[17] H. Torp, X. M. Lai and K. Kristoffersen. "Comparison Between Cross-Correlation and Auto-Correlation Technique in Color Flow Image," *Proceedings of IEEE International Ultrasonics Symposium,* Baltimore, MD, pp.1039-1042, 1993.

[18] A. P. G. Hoeks, T. G. J. Arts, P. J. Brands and R. S. Reneman, "Comparison of the Performance of the RF Crosscorrelation and Doppler Autocorrelation Technique to Estimate the Mean Velocity of Simulated Ultrasound Signals," *Ultrasound Med. Biol.,* vol.19, pp 727-740, 1993.

[19] Edward R. Dougherty, "Probability and Statistics for the Engineering, Computing and Physical Sciences," Chapter 7, Prentice Hall International, Inc., 1990.

[20] A. V. Oppenheim, R. W. Schafer, "Digital Signal Processing," Prentice Hall INC, Chapter 11, 1975.

[21] J. A. Jensen, "Range/Velocity limitations for Time-Domain Blood Velocity Estimation", *Ultrasound in Med. & Biol.*, Vol. 19 No.9, pp.741-749, 1993.

[22] S. G. Foster, P. M. Embree, and W. D. O'Brien, "Flow Velocity Profile Via Time-Domain Correlation Error Analysis and Computer Simulation," *IEEE Trans. on Ultrasound, Ferroelectrics, and Frequency Control,* vol.37, NO.2. May, 1990.

Paper B

Interpolation Methods for Time Delay Estimation Using Crosscorrelation Method for Blood Velocity Measurement

This is a revised version in accordance with reviewer's comments of paper: X. Lai, H. Torp, "Interpolation Methods for Time Delay Estimation in the RF-Signal Crosscorrelation Technique for Blood Velocity Measurement", which was submitted to *IEEE Trans. on Ultrasound, Ferroelectrics, and Frequency Control.*

A part of this paper was published in: X. Lai, H. Torp, "Interpolation Methods for Time Delay Estimation in the RF-Signal Crosscorrelation Technique for Blood Velocity Measurement", *Proceedings of IEEE International Ultrasonics Symposium,* San Antonio, Texas, pp.1211-1216, 1996. (In Appendix B)

Interpolation Methods for Time Delay Estimation Using Crosscorrelation Method for Blood Velocity Measurement

Abstract

The cross correlation method (CCM) for blood flow velocity measurement is based on time delay estimation of the echoes from pulse-to-pulse. The sampling frequency of the received signal is usually kept as low as possible in order to reduce computational complexity, and the peak in the correlation function is found by interpolating the correlation function. The parabolic-fit interpolation method introduces bias at low sampling rate to ultrasound center frequency ratio. In this study, four different methods are suggested to improve the estimation accuracy:

1. Parabolic interpolation with bias-compensation, derived from a theoretical signal model.
2. Parabolic interpolation combined with linear filter interpolation of the correlation function.
3. Parabolic interpolation to the correlation function of the complex signal envelope.
4. Matched filter interpolation applied to the correlation function.

The new interpolation methods are analyzed both by computer simulated signals and RF-signals recorded from a patient with time delay up to $2/f_0$, where f_0 is the center frequency. The simulation results show that these methods are more accurate than the parabolic-fit method. From the simulation, the worst estimation accuracy is about 1.25% of $1/f_0$ for the parabolic-fit interpolation and it is improved by the above methods to less than 0.5% of $1/f_0$ when the sampling rate is 10 *MHz*, the center frequency is 2.5 *MHz* and the bandwidth is 1 *MHz*. These improvement can also be observed in the experimental data. Furthermore, the matched filter interpolation gives the best performance when signal to noise ratio (*SNR*) is low. This is verified both by simulation and experimentation.

I. Introduction

Blood velocity is an important parameter for the clinical diagnosis of vascular disease. Ultrasound has become an indispensable noninvasive tool for blood velocity measurement. The pulse Doppler technique is widely used, because it can provide range resolution. With this method, sequential short ultrasound pulses are transmitted into the vessel or heart at a *pulse repetition frequency* (PRF). Return signals are received sequentially after a certain delay following the pulse transmission. Due to the movement of the scatterers, the received echo is a time delayed version of the echo from the previous pulse if the time transit effects are not considered. In the conventional autocorrelation method [1] this time shift is estimated from the pulse to pulse phase shift of the complex signal envelope. In the cross correlation method (CCM) [2] and [3], the time shift of the echoes is estimated directly from the RF-signal. It has advantages over the Doppler method [4] in some circumstances. The main advantages are that CCM is a wideband estimator and it does not suffer from the Nyquist limit. The main drawback is the computational load due to RF-signal processing.

In the CCM, the time delay is estimated by searching for the maximum correlation coefficient between the successive received echoes. If the received echoes are denoted as $p(t, k)$, where t is the elapsed time after pulse transmission which corresponds to a certain depth from the transducer, k is the pulse number, its two dimension (2-D) correlation function is denoted $R(\tau, m)$ which is defined as:

$$R(\tau, m) = \int_t \left(\sum_k p(t, k) p(t+\tau, k+m) \right) dt$$

In the CCM, we use $R(\tau, m)$ in the lag one, i.e. m=1 for estimating the time delay. Then the correlation function has maximum magnitude in the time delay τ_v, i.e. $R(\tau_v, 1) = max_\tau R(\tau, 1)$.

A 2-D correlation function model was given in [5]. The magnitude of the correlation function has a shape close to the Gaussian function [5]. With the approximated Gaussian envelope and without lateral transit time effect, a theoretical 2-D RF correlation model is:

$$R(\tau, 1) = \exp\left(-\frac{(\tau-\tau_v)^2}{2\sigma^2}\right)\cos(2\pi f_0(\tau-\tau_v)) \qquad \tau_v = -\frac{2Tv\cos\theta}{c} \tag{1}$$

In which σ is the standard derivation which is related to the transmitted signal bandwidth B by B=2/σ. T is pulse repetition period, v is the blood velocity, c is the ultrasound speed, θ is the angle between the ultrasound beam and blood vessel. Figure 1 is an illustration of the RF correlation function.

In practice, the echo signal is discrete due to the sampling in time. The true location of the maximum correlation coefficient is not constrained to discrete increments, and may fall between the discrete sampling points which results in estimation inaccuracy. An interpolation technique is usually used to improved the time delay estimation accuracy [9]. Special interests

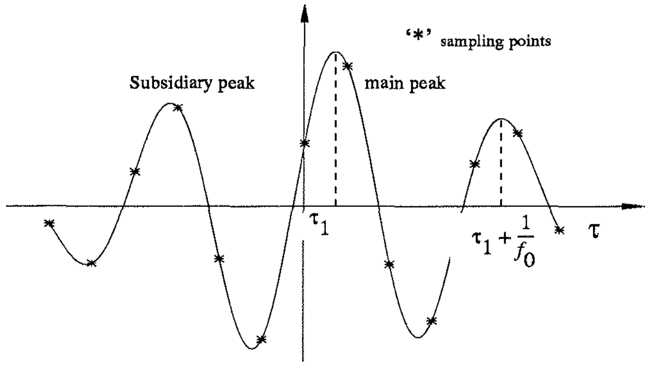

Figure 1 RF correlation function $R(\tau,m)$ when m=1

to discuss the interpolation methods in the low sampling rate are: firstly, the computation to calculate the correlation function and to filter the wall signal. can be reduced. The received signal is usually composed of not only the blood signal but also the clutter signals or wall signal from the boundary and wall vessel, therefore, it is necessary to remove the wall signal prior to the time delay estimation. This is generally implemented by a highpass filter or a wall filter. This filtering is operated on the signal from the same depth. When the sampling rate in is lower, the wall filtering becomes simple. Secondly, most scanners use the Doppler method which is based on the baseband complex signal. The sampling rate is usually low in those systems. In order to implement the crosscorrelation technique in those systems, the interpolation methods are investigated.

The most widely used interpolation method is the parabolic-fit which is simple but its estimation bias is high when the sampling rate to the center frequency ratio (f_s/f_0) is low (in the order of 4) [9]. In addition to the parabolic-fit, the cosine-fit [6], [7], [8] and [9] and the reconstructive interpolation methods [9] are also used. The cosine-fit interpolation can be used at f_s/f_0 =4 with high estimation accuracy, but as mentioned in [7] it has velocity aliasing for velocities exceeding the Nyquist limit. The reconstructive interpolation method [9] and [10] is based on the Nyquist sampling theorem, that is, a bandlimited continuous-time signal can be reconstructed from its digital samples. The key component in the reconstruction is the ideal lowpass filter. It cannot be implemented in practical system, a reasonable approximated lowpass filter is used. Therefore, an approximated continuous-time signal is reconstructed. Its computational time is usually longer than the other interpolation methods.

In this work, four other interpolation methods are proposed and evaluated. The paper is organized as follows: In part II, the four interpolation methods are described. In part III, the performance of the cosine-fitting interpolation method, the reconstruction filter interpolation method and the other four interpolation methods described in part II are compared by simulations. In part IV, the four interpolation methods are evaluated by the experiments.

II. Interpolation Methods description

A. Parabolic Interpolation with Bias-compensation

It is seen from Figure 1 that the interpolation is necessary to get good time delay estimation. One simple interpolation method is parabolic-fitting, which has been used in many applications. In our application, the parabolic-fitting is performed near the peak and only requires a few operations. An illustration of parabolic-fit is shown in Figure 2. The parabola has the form $y(x) = ax^2 + bx + c$. The location of the maximum coefficient:

$$\delta = -b/2a = (y(-1)-y(1))/2(y(-1)-y(0)+y(1)) \tag{2}$$

The parabolic-fit works well at high sampling rate RF correlation function, but it has substantial bias when the sampling rate is low. Specially, it induces high bias to low Q-factor ($Q = f_0/B$) signal which corresponds to narrow correlation function curve. The parabolic interpolation bias also depends on the location of the time delay, or blood velocity v.

To a given velocity v, the parabolic interpolation bias b is:

$$b = f\left(v, \frac{f_s}{f_0}, Q\right) = v - \hat{v}\left(v, \frac{f_s}{f_0}, Q\right) \tag{3}$$

where f means a function of argument v, *fs/f0,* and Q. $\hat{v}$ is the estimated velocity and $\hat{v}\left(v, \frac{f_s}{f_0}, Q\right)$ means $\hat{v}$ is a function of argument v, *fs/f0,* and Q.

If we can predict the bias b, it should able be possible to compensate for it by using this *priori* knowledge. A theoretical prediction of the bias b can be obtained from correlation function model described in (1) when oversampling f_s/f_0 and Q-factor are given. In order to obtained bias b, (1) should be written as a discrete form. Then we interpolate the discrete correlation function by parabolic-fit and search for the time delay $\hat{\tau}$ which maximized correlation magnitude. The difference of $\tau_v - \hat{\tau}$ is the bias. Because the time delay corresponds to the velocity, we also get the velocity bias b. Varying τ_v in (1), the bias b for different velocity is obtained as plotted in Figure 3.

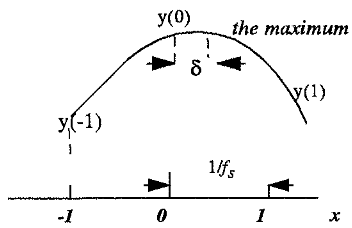

Figure 2 An illustration of the parabolic fitting

It is shown in Appendix 1 that in most applications, the $\ddot{v}$ and the v is uniquely determined when f_s/f_0 and Q are given. We can use a zero order approximation:

$$f\left(v, \frac{f_s}{f_0}, Q\right) \approx f\left(\hat{v}, \frac{f_s}{f_0}, Q\right) \tag{4}$$

Rewrite (3) as:

$$v = \hat{v} + b = \hat{v} + f\left(\hat{v}, \frac{f_s}{f_0}, Q\right) \tag{5}$$

The blood velocity estimated by (5) is the parabolic-fit with bias-compensation. Bias b is obtained from theoretical correction function model. The bias-compensation may be implemented by a lookup table.

De Jong, et al.in [7] and [8] developed a correlation interpolation algorithm that approximates the correlation function by a cosine model. By using a few correlation coefficients, the parameter values in the model are solved and the location of the maximum of correlation function is estimated. Both the parabolic-fit with the bias-compensation and the cosine-fit interpolation methods use correlation function models. The difference between them is the envelope shape; the envelope to the model of the parabolic-fit with bias-compensation method is a Gaussian shape, the envelope to the model of cosine-fit interpolation is constant amplitude or it is a rectangular function for the truncated the correlation function. Thus, the cosine-fitting method uses an approximation correlation function model. The location (or time delay) of the maximum of the cosine function is solved from a few correlation coefficients. If Gaussian envelope is used, more correlation coefficients are required.

The bandwidth B has been included in the parabolic-fit with bias compensation model, so it

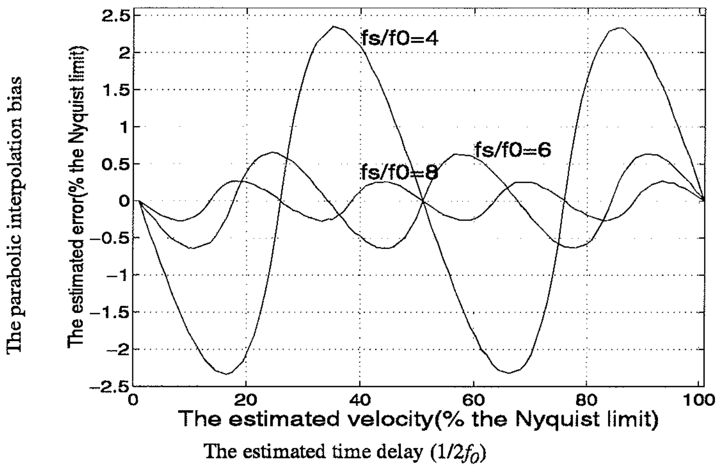

Figure 3 The velocity estimation bias by parabolic interpolation for the signal with Q=1 which is calculated from the theoretical correlation function model.

can be applied to both narrow band signal and wideband signal. Nevertheless, the rectangular shape envelope is only a good approximation to the narrow band blood signal. Therefore, the cosine-fit can work well with the narrowband signal, however, there may have large estimation bias to the wideband signal.

False peaks and aliasing.

In the CCM, the velocity is estimated by the time delay which has the maximum correlation magnitude. In practice, there may be peak hopping or false peak errors, that is, the main peak may be mistaken from main peak to subsidiary peak due to the estimation variance of the correlation function. In the Doppler method [4], there is velocity aliasing when the true velocity is beyond the Nyquist limit. The aliasing appears at multiple of two times the Nyquist limit velocity. As discussed in [17], the false peaks in the CCM appear at time delays which are equivalent to the multiple of two times Nyquist velocity in the Doppler method, therefore, they are same kind of errors in the sense of aliasing. Thus, the peak hopping or false peak detection is also called aliasing in this paper and the velocity which corresponds to the time delay $1/2f_0$ is called the Nyquist limit.

The parabolic-fit can only be applied locally around the peak. As a result, the first step in the parabolic-fit is to select the peak from the discrete correlation coefficients. Therefore, it can only improve accuracy when the global peak is correctly selected from the discrete samples. When f_s/f_0 is low, the false maximum from the subsidiary peak is selected. As a result, aliasing occurs. This occurs more frequently with the narrowband signal because its envelope of the correlation function is flat. An aliasing example from practical blood signal is shown in Figure 4.

The cosine-fit interpolation uses the center ultrasound frequency and not the envelope of the correlation function. It discards the valuable envelope information, the velocity aliasing is inherent.

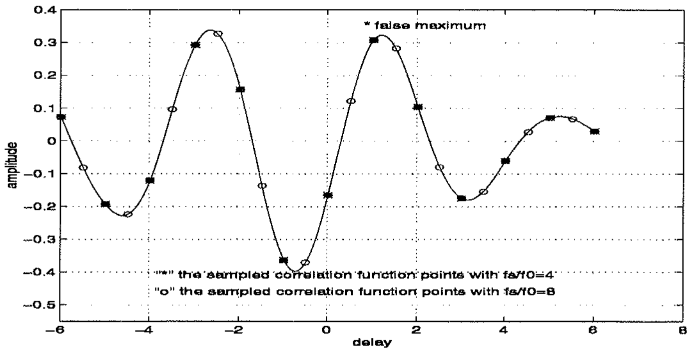

Figure 4 An illustration that the false maximum in the discrete correlation function is occurred when the ratio of the sampling rate to the center frequency is low.

Effect of the Frequency Dependent Attenuation.

The cosine-fit and the parabolic-fit for delay estimation both depends on the parameters of their own correlation function model, however, the cosine-fit uses more correlation coefficients than the parabolic-fit with bias compensation, the additional parameters are used to estimate the center frequency of the received signal. Hence, the frequency dependent attenuation does not degrade the cosine-fit interpolation method.

In the parabolic-fit with bias-compensation, the frequency dependent attenuation may cause performance degradation. However, it is impractical to use the center frequency of the received signal and in this method the center frequency of the received signal is assumed to be equal to the center frequency of the transmitted signal. Nevertheless, this does not significantly affect the estimation results because the estimated velocity bias in the parabolic-fit with bias-compensation is related to oversampling f_s/f_0 instead of f_0. When f_0 has a shift Δf, $f_s/(f_0+\Delta f)$ has little difference to f_s/f_0.

Effect of signal decorrelation.

The correlation function model in (1) does not include the effect of signal decorrelation. When there is serious signal decorrelation, the bias-compensation method may increase estimation bias and variance. However, in our experimentation and simulation signal which the lateral time transit effect has been included, the bias-compensation method still works well. No significant difference has been observed, as compared to the results of other methods.

B. Parabolic-fit Interpolation Combined with Linear Filter Interpolation

The parabolic-fit interpolation uses a few correlation coefficients in the vicinity of the maximum discrete point. According to Appendix 2, the requirement for oversampling to reduce the chance of aliasing is:

$$\frac{f_s}{f_0} > \frac{\pi}{\mathrm{acos}[\exp(-2Q^2)]} \tag{6}$$

In many cases, this requirement is not satisfied. Increasing f_s/f_0 to Lf_s/f_0 can reduce the chance of aliasing; where L is the interpolation rate. It also reduces interpolation error by using parabolic-fitting. According to (6), the required L depends on the Q-factor of the signal. For Q=1 signal, if Lf_s/f_0>6.42, there will be no aliasing induced by peak hopping error. Therefore, for a transmitted signal with a approximated two cycle period pulse (the central frequency is 2.5*MHz* in our simulations later), an interpolation rate L=2 is sufficient to reduce the aliasing error induced due to low oversampling $f_s/f_0=4$. Furthermore, the estimation bias introduced by the parabolic-fitting is small when L=2. From Figure 3, the estimation bias has been reduced from 1% to less than 0.25% of $1/f_0$ when $f_s/f_0=4$ is increased to $f_s/f_0=8$.

The digital approach of the linear filter interpolation is usually used to increase the sampling rate from f_s/f_0 to Lf_s/f_0 by using lowpass filter [10]. The process of increasing the sampling rate is introduced in [10] and a diagram for linear filter interpolation is plotted in Figure 5.

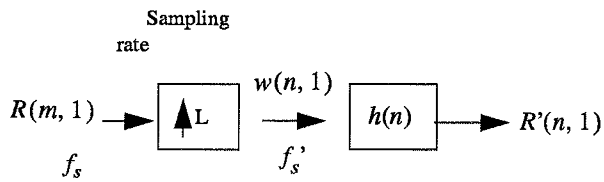

Figure 5 Block diagram of the linear filter interpolation

If the sampling rate f_s of the RF correlation function $R(m, 1)$ is interpolated to sampling rate f_s', $L = f_s'/f_s$, then there are L-1 new sample points between each pair of points of $R(m, 1)$. Initially, we set these interpolation point to zero, creating the signal:

$$w(n,1) = \begin{cases} R\left(\frac{n}{L}, 1\right) & n = 0, \pm L, \pm 2L\ldots \\ 0 & otherwise \end{cases} \tag{7}$$

The spectrum of $w(n, 1)$ contains not only baseband frequencies (i.e. $-\pi/L \ \ to \ \ \pi/L$) of interest, but also the images of the baseband frequencies centered at harmonics of the original sampling frequency $(\pm 2\pi/L, \pm 4\pi/L, \ldots)$. Normally, to recover the baseband signal of interest and to eliminate the unwanted image components, it is necessary to use a digital anti-aliasing filter with near ideal lowpass characteristic:

$$H(\omega) = \begin{cases} 1 & |\omega| < \frac{\pi}{L} \\ 0 & otherwise \end{cases} \tag{8}$$

A simple filter design, for the case L=2, is by window design method:

$$h(n) = \frac{\sin\left(\frac{\pi n}{2}\right)}{\frac{\pi n}{2}}, \qquad n = 0, \pm 1, \pm 2, \ldots M \tag{9}$$

Where M is the length of the window and $h(n)$ has the coefficient with

$$h(n) = \begin{cases} 1 & n = 0 \\ 0 & n = \pm 2, \pm 4, \ldots \end{cases} \tag{10}$$

It satisfies the zero-crossing criterion of ideal filters and is an efficient design where every other coefficient is zero and need not be computed in a practical implementation.

In addition to the filter in (14), other halfband filters [10] are also of interest for interpolation by a factor of “two”. They have a spectrum symmetric property where

$$H(\omega) = 1 - H(\pi - \omega)$$

This also improves computation efficiency.

In this interpolation method, the sampling rate of the correlation coefficients is increased by a small factor before the parabolic-fit. This is more efficient than the reconstruct filter interpolation [9] in which the interpolation rate L has to be very high (L=50) to get similar estimation accuracy.

C. Parabolic Interpolation to the Correlation Function of the Complex Signal Envelope

Most existing ultrasound scanners are already equipped to demodulate RF signal to the baseband signal. The sampling rate is lower in the baseband than that in RF-data. The minimum sampling rate is determined by the sampling theorem. To realize crosscorrelation technique on these scanners, in this method, the cross correlation function is calculated and interpolate in the baseband, and then remodulated to the RF domain. It is easier to interpolate the baseband signal since it is slowly varying compared to the RF signal.

The modulation formula from baseband correlation function $R_x(\tau,k)$ to RF-band correlation function $R(\tau,k)$ [11] is:

$$R(\tau, k) = 0.5Re(R_x(\tau, k)\exp(j2\pi f_0\tau)) \tag{11}$$

From (1), the expected shape of the correlation function R_x is Gaussian shape. It is conceivable that a simple way is parabolic-fit to the Gaussian function locally, that is, using several samples of the correlation function centered around its magnitude peak. An illustration of parabolic interpolation in the complex envelope is shown in the Figure 6.

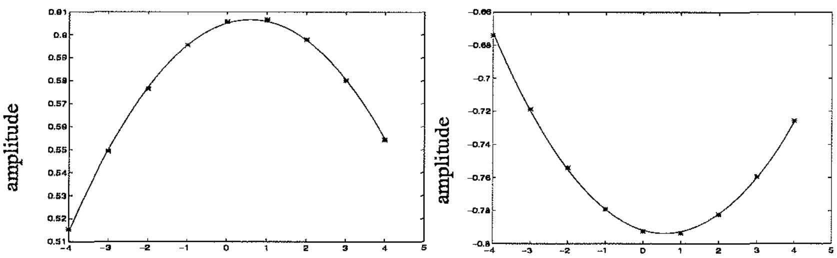

(a) Parabolic-fit in real part

(b) Parabolic-fit in imaginary part

Modulation from the complex envelope to the RF correlation signal is the most costly step in term of computation. One way to reduce computation is to modulate iteratively around magnitude peak [9]. At each iteration, only a few points are modulated to the RF band, and the RF magnitude is compared among those points.

D. Matched Filtering for Interpolation

Time delay estimation is used in many applications. A generalized crosscorrelation method was developed in the classical work [14]. The block diagram is in Figure 7.

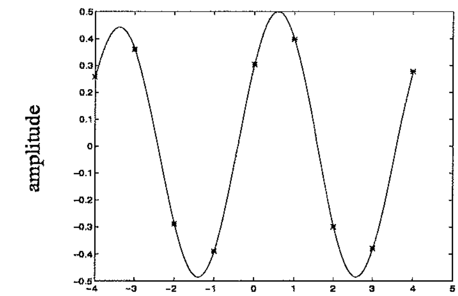

A RF correlation function which is obtained from complex correlation function (a) and (b)

Figure 6 An illustration of the parabolic interpolation to the correlation function of complex envelope. '*' is for sampled points. '-' is for interpolated curve.

Figure 7 Diagram of time delay estimate

Due to the deteriorating effect of the noise on the time delay detection, a false peak may be produced and cause a false estimate of the time delay. The purpose of the optimum linear filter is to minimize the occurrence of false peaks.

The optimum filter obtained in [14] was based on two conditions. One is that only two pulses have been transmitted and the other is no decorrelation between two received echoes. This is not the case here since more than two pulses have been transmitted and transversal velocity components are present. However, for simplicity, we still use the optimum filter of [14].

According to the criterion of maximizing the expected signal peak at τ relative to the background noise, an optimum filter was given in [14] in term of signal and noise spectral density. However, it is certainly difficult to design the true optimum filter, since it has a complicated relationship to signal and noise spectral characteristics. Thus an Eckart filter [14] is used. It uses the criterion that maximizes the ratio of the mean correlator output due to the signal present to the variance of the correlator output due to noise alone. The Eckart filter is an approximation of the optimum filter when *SNR* is low. This Eckart filter is also referred to as a matched filter. This was also discussed in Appendix B. The matched filter for estimating time delay is

$$m(\tau) = \int(\hat{R}(t, 1))R(\tau - t, 1)d\tau_1 \tag{12}$$

where $\ddot{R}(t, 1)$ is the estimated correlation function from the signal, and $R(\tau, 1)$ is the correlation function model. A correlation function model in which transit time effect is not taken into account is used and it is:

$$R(\tau, 1) = \exp\left(-\frac{\tau^2}{2\sigma^2}\right)\cos(2\pi f_0 \tau) \tag{13}$$

The peak detector is performed on filtered signal $m(\tau)$.

Matched Filter Interpolation.

The matched filter can also be used in the interpolation for estimation time delay when the RF-signal is sampled with a low sampling rate. The matched filter is the expected correlation function as in (18). Thus, it can be sampled according to our requirements.

In this application, the matched filter is sampled by f_s', which is rather higher than f_s and where $1/f_s$' satisfies the resolution of the time delay estimation. This densely sampled matched filter can also be used as an anti-aliasing filter in the linear interpolation, where it is unnecessary to use an additional narrowband anti-aliasing filter. Thus, the matched filter has two functions: one is that it is a suboptimal linear filter which maximizes the signal peak to output noise, and the other is that it replaces the narrowband anti-aliasing filter which eliminates the image spectra produced in the zero padding. An implementation of the matched filter interpolation is illustrated in Figure 8.

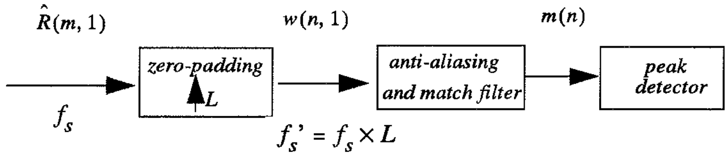

Figure 8 Block of the match filtering and interpolation

The correlation function is sampled by f_s. L is interpolation rate. $w(n, 1)$ is a function after L-1 new zero values between each pair of sample values of $\ddot{R}(m, 1)$ has been padded. It has the same sampling rate f_s' as matched filter $\ddot{R}(n, 1)$. The typical spectra is illustrated in Figure 9.

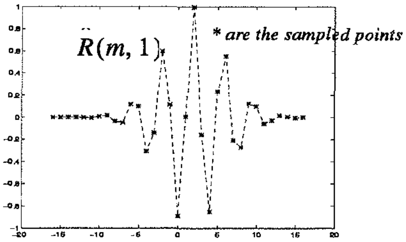

(a)The correlation function with low sampling rate

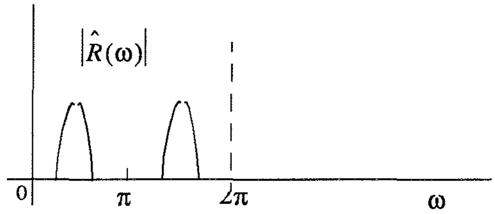

The baseband frequencies of (a)

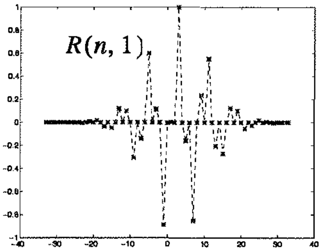

(b)The correlation function with zero padding, the sampling rate is increased from fs to fs'

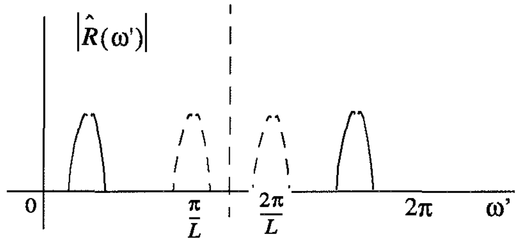

The spectrum after zero-padding which includes the baseband frequencies and their images centered at harmonics of the original sampling frequency

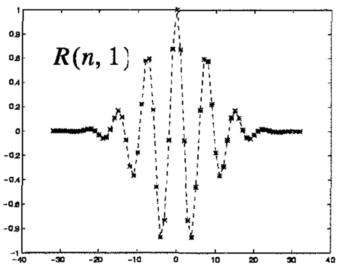

(c) The match filter with sampling rate fs'

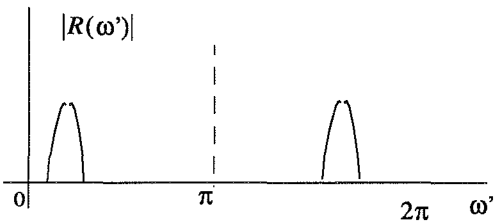

The spectra of the matched filter

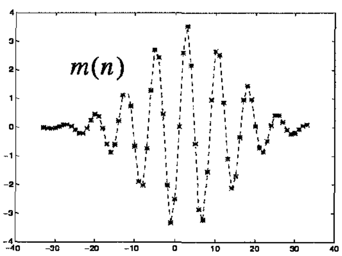

(d) The interpolated and matched correlation function

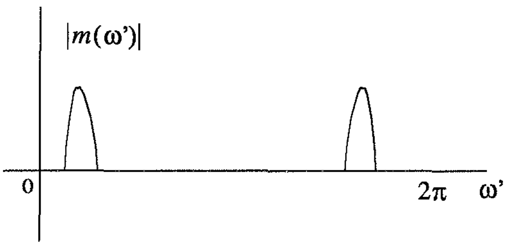

The spectra of the interpolated and matched correlation function

Figure 9 Typical correlation function waveforms and theirs spectra for matched filter interpolation

Comparing Matched Filter Interpolation with Reconstruction Filter Interpolation to Find Time Delay

A reconstructive linear filter interpolation method is used to reconstruct a sampled signal. The purpose of matched filtering for detecting the time delay is to maximize the expected signal peak relative to output noise, rather than the reproduction of the crosscorrelation function signal. In frequency domain, the difference of these two method is the anti-aliasing filter. The matched filter interpolation method uses a *priori* information about the correlation function. It has similar spectral shape and bandwidth that is similar to the correlation function spectrum. For the reconstruction method, an ideal anti-aliasing lowpass filter is used. When the SNR is high, the two methods perform similarly. However, when the SNR is low, the matched filter interpolation method perform better because it has a narrower bandwidth than the lowpass filter, which is used in the reconstructive linear interpolation method. The difference in performance becomes most significant when the received signal has narrow bandwidth. The computational complexity is similar for both the reconstruction interpolation and matched filter interpolation method. Using FIR lowpass filter can reduce the computation. Using multistage implementation of the interpolation [10] and iterative implementation approach [9] can reduce the computation further for both the matched filter and the reconstructive interpolation.

III. Evaluation the Interpolation Methods by Simulation

Simulation signal

The blood signal model used here is the same as in [17], where the 2-D blood signal is generated by a 2-D convolution between the echo response *h(t,k)* from a single scatterer and a 2-D Gaussian random signal *n(t,k)*. In this model, the transit time effect in the lateral beam profile direction is included. The echo response in this simulation is:

$$h(t,k) = \exp\left(\frac{-t^2}{\sigma^2}\right)\cos(2\pi f_0 t)b(kTv\sin\theta)$$

where b is the transverse beam profile and it is assumed to be a Gaussian function [5]. $b(d) = \exp(-3d^2/2B^2)$ is used in our simulation, where B is the beam width. A Gaussian shape envelope in the echo response was used, as discussed in [17]. With a wideband signal, the standard deviation is set to $\sigma = 1/f_0$, giving a pulse length of approximately two cycle periods. The pulse bandwidth BW is defined as $1/\sigma$ which the magnitude of the envelope decreases by 8.69dB.

The used parameters are given as follows.

Pulse repetition frequency *prf*	6564Hz	Ultrasonic measurement angle θ	10degree

Speed of sound c	1540m/s	Temporal averaging ta	1.8ms
Beamwidth	2mm	Depth averaging ra	2.4μ s
Center frequency f_0	2.5MHz	Bandwidth for transmitted signal	2.5MHz

From above parameters, the Nyquist velocity is 1.0265(m/s).

If the blood signal is given by $z(t, k) = y(t, k) + n_1(t, k)$, where y is the signal and n_1 is the noise, the signal to noise ratio for the sampled blood signals is defined as

$$SNR = 10\log\frac{\sum_n\sum_k y^2(n, k)}{\sum_n\sum_k n_1^2(n, k)} \tag{14}$$

A. Velocity Estimation Bias and Standard Deviation by Using Different Interpolation Methods

In [16], it was indicated that the mean frequency estimate based on the correlation function has a distribution close to Gaussian function, and that the estimation variance possesses a chi-square distribution. In [17], it was shown that the CCM method and the mean frequency estimate method have the similar estimation results. Therefore, the estimation variance of the CCM method possesses a chi-square distribution. Reliability of the simulation is indicated by the 95% confidence interval. It can be obtained from the statistic [15] which is: $[0.84SD, 1.25SD]$ where SD is the estimated standard derivation.

Table 1 lists the results of velocity estimation bias and standard deviation (SD) by using different interpolation method from 50 independent simulations. **A** is parabolic-fit without bias compensation, **B** is the cosine-fit interpolation, **Method 1** is the parabolic-fit with bias-compensation. **Method 2** is the parabolic-fit combined with linear filter interpolation. **Method 3** is the parabolic interpolation to the correlation function of the complex signal envelope. **Method 4** is the matched filter interpolation.

Table 1: Velocity estimation bias and standard deviation (*SD*)(% Nyquist velocity) SNR=30dB, f_s/f_0=4.

		0.2m/s	0.5m/s	1.2m/s	2.2m/s	3.2m/s	4.2m/s
bias	A	-2.1919	0.3215	--	--	--	--
	B	-0.6332	-0.0779	--	--	--	--
	Method 1	-0.0585	-0.0560	--	--	--	--
	Method 2	-0.3082	-0.5832	0.4834	0.5210	0.7866	0.3295
	Method 3	-0.093	-0.049	0.097	0.010	0.195	0.023
	Method 4	0.434	0.591	0.818	0.880	0.721	0.418
SD	A	1.2859	1.1593	--	--	--	--
	B	1.0619	1.4126	--	--	--	--
	Method 1	1.0326	1.4189	--	--	--	--
	Method 2	1.1412	1.4588	1.8770	1.9351	2.5188	3.0802
	Method 3	0.922	1.442	1.724	1.812	2.289	2.871
	Method 4	1.007	1.474	1.841	1.938	2.565	3.079

The results show that method 1 reduces velocity estimation bias significantly. Cosine-fit interpolation gives similar results. Because the parabolic-fit method suffers from aliasing, it is usually limited by the Nyquist limit (the time delay is within $1/2f_0$). Thus, only the estimation results to the velocities within the Nyquist limit are given in those methods.

For **Method 2, 3,** and **4**, velocities up to 4 times the Nyquist limit, or the time delay up to $2/f_0$ have been estimated. The results for velocities which are within the Nyquist limit are similar to the results of **Method 1**. It should be mentioned that **Method 3** operates with the demodulated signals, the sampling rate can also be reduced from 10 *MHz* ($f_s/f_0=4$) to 5*MHz* ($f_s/f_0=2$) or even 2.5 *MHz* ($f_s/f_0=1$) as illustrated in Table 2.

Table 2: Velocity estimation bias and standard deviation for method 3 in different f_s/f_0 rate, SNR=30dB

		0.2m/s	0.5m/s	1.2m/s	2.2m/s	3.2m/s	4.2m/s
fs/f0=4	bias	-0.093	-0.049	0.097	0.010	0.195	0.023
	SD	0.922	1.442	1.724	1.812	2.289	2.871
fs/f0=2	bias	-1.042	-0.164	-0.906	-0.619	-0.380	-0.277
	SD	1.111	1.564	1.783	2.026	2.192	3.124
fs/f0=1	bias	-0.978	-0.833	-0.710	-0.713	-0.083	-0.287
	SD	1.171	1.662	1.848	1.936	2.519	2.943

The sampling rate for the matched filter is 50 times higher than that of the signal, i.e. 500MHz. The theoretical velocity accuracy is about 0.5% of $1/f_0$ in this case. The results show that there is no significant difference to the results of **Method 2** and **3**.

B. Performance Comparison between the Interpolation Methods in the Low Signal to Noise Ratio Circumstance

As mentioned above, due to the deteriorating effect of the noise on the time delay detection, a false peak in the correlation function may be appeared. This leads to a wrong estimation. The simulation in this section shows that the probability for wrong peak detection is reduced by using matched filter method.

Four interpolation methods mentioned in this paper plus the reconstructive interpolation method [9] are applied to the simulation signal for Q=3 and SNR=-6dB for comparison. The length of transmitted pulse is approximately six cycle periods. In this case, the required interpolation rate L for method 2 is 5 according to (11).

The results are from 900 simulations. The velocities vary from 0.1m/s to 0.9m/s by interval 0.1m/s (The Nyquist limit is 1.0265m/s). In this simulation, the velocity estimation range has not been limited for method 1. The purpose is to display the aliasing error due to the low oversampling.

Histogram for velocity estimation bias are plotted as in Figure 10. The distribution of the bias around zero shows the velocity estimation variance. Due to the aliasing, some estimates were distributed around twice the Nyquist limit which corresponds the time delay $1/f_0$.

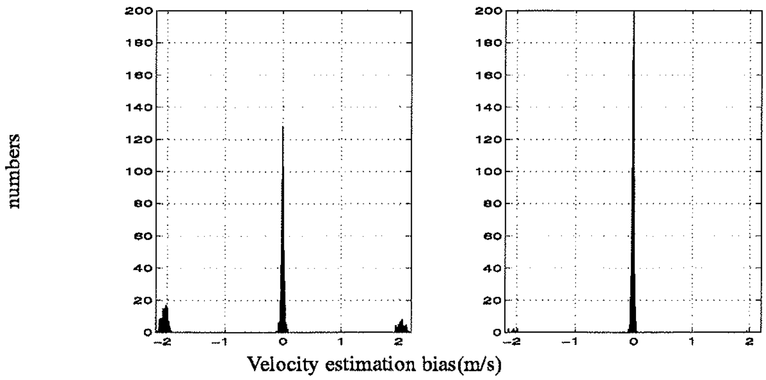

(a) Parabolic-fit with bias compensation

b) Matched filter interpolation

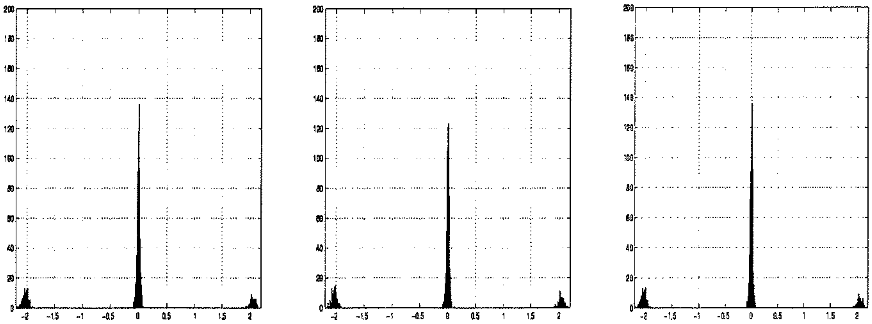

(c) Parabolic-fit combined linear filter interpolation

(d) Parabolic-fit to the complex correlation envelope.

(e) The reconstructive filter interpolation.

Figure 10 Histogram (from 900 simulations) for velocity estimation bias with simulation signal Q=3 and SNR=-6dB.

The interpolation rate is 50 in the reconstructive interpolation. The lowpass filter used in this case is FIR filter designed by window method with a Blackman tapering window. The length of filter is 801 samples.

From the simulation results, it is seen that the matched filter gives best performance at low SNR. This improvement is even more significant for narrow bandwidth signal since the matched filter is more efficient to removed noise in narrow band case.

C. Computation comparison

To implement the CCM method, the received RF data is necessary to pass a highpass filter prior to the correlation function calculation. The computation is usually high when the sampling rate is high, due to filtering and correlation function calculation. Table 3 gave approximated amount of multiplication operations for f_s/f_0=8 with parabolic interpolation method and f_s/f_0=4 with four new interpolation methods. All the methods listed in Table 3 gives similar estimation accuracy, however, the number of operations required for the case f_s/f_0=4 is reduced.

In Table 3, we assume that a regression filter is used as a high pass filter [18] and the number of operation needed for the high pass filter is $2(p+1)K$ [19] where p is the order of regression filter and K is samples in temporal direction. The number of operations required for the correlation function calculation is assumed to be proportional to data block size $N*K$, where N is samples in depth direction.

When f_s/f_0=8, the parabolic interpolation method is used, and only one division is required as in (2). When f_s/f_0=4, interpolation method 1 uses the parabolic-fitting and then looking for table for compensation. Only one division is needed in this interpolation method.

In the interpolation method 2, we interpolate the correlation function $R(n,1)$ by a small rate using linear filter interpolation method. In our simulation, we used a halfband filter and the number of operation for this linear filter interpolation is 51.

In interpolation method 3, we have to modulate the complex signal to RF domain. This is a time-consuming process. In order to save the computation time, we modulate some samples and choose the global maximum. Then we use iteration around the maximum samples. At each iteration, only two samples are modulated. In our simulation, total number of operations for this interpolation method is 88.

In interpolation 4, the computation is usually high for high interpolation rate. To save the computation time, we used a method similar to the interpolation method 3. In our simulation, the number of operations is 748. A summary of the number of operations is in Table 3. The histogram in Figure 11 shows the difference of the number of operations for the case when N=48 (f_s/f_0=8), K=32 and p=3.

It is shown that the amount of operations is reduced when f_s/f_0 is reduced to 4. Furthermore, the amount of operations can be reduced significantly when the original f_s/f_0 is higher than 8.

Table 3: A comparison of the number of operations for different interpolation methods

	f_s/f_0=8	f_s/f_0=4			
	Parabolic-fitting	method 1	method 2	method 3	method 4
Wall filter	$N(p+1)K$	$N(p+1)K/2$			
Correlation function	$N*K$	$NK/2$			
Interpolation	1	1	51	88	748
Total for case N=48, K=32 and p=3	7681	3841	3891	3928	4588

Figure 11 A comparison of the amount of operations for different interpolation methods

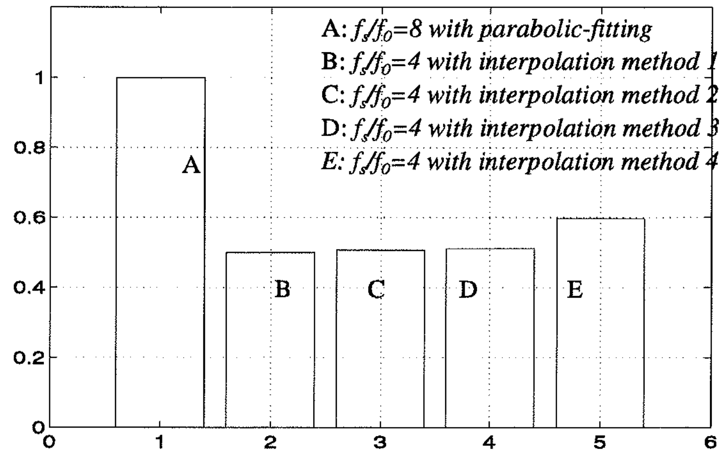

D. Summary the Simulation Results

From simulation results, it is seen when the true velocity is within the Nyquist limit, method 1 gives similar performance to other interpolation methods and it has shortest computation time. Methods 2, 3 and 4 give good results up to 4 times the Nyquist limit. Method 4 gives the best performance when the signal to noise ratio is low. Table 4 summarizes the characteristics of the interpolation methods. The choice of the interpolation method depends mainly on the specific application.

Table 4: Summarizes the characteristics of the interpolation methods
Method 1: Parabolic-fit with bias-compensation
Method 2: Parabolic-fit combined linear filter interpolation
Method 3. Parabolic-fit to the complex correlation envelope
Method 4: Matched filter interpolation

	Method 1	Method 2	Method 3	Method 4
Perform on RF or baseband signal	RF-band	RF-band	Baseband	RF-band
Ovesampling f_s/f_0	f_s/f_0=4	f_s/f_0=4	f_s/f_0=1,2,4	f_s/f_0=4
Estimation Error	small	small	small	small
Velocity estimation range	within the Nyquist limit	excess the Nyquist limit	excess the Nyquist limit	excess the Nyquist limit
Computation time	short	medium	medium	long
Using *a priori* information of the theoretical correlation model	yes	no	no	yes
Performance for low SNR	Not good	Not good	Not good	Best

IV Experimental Evaluation

The interpolation methods are verified by experimental data from human subclavian artery. The RF data from a ultrasound scanner (Vingmed CFM 800) was collected in real time via a custom data acquisition system. The slow tissue movement signal in the raw data was removed by a 4th order IIR butterworth high pass filter with normalized cutoff frequency 0.155. Then the data was demodulated with center frequency 2.5 *MHz*.

A. The Parabolic Interpolation with Bias-compensation Applied to Experimental Data with the Velocities within the Nyquist Limit

The parameters in this experiment were the same as in the simulations. When method 1 is applied to the signal with f_s/f_0 =4, aliasing is easy to be occurred. Thus, we only applied this method to a set experimental data with velocities within the Nyquist limit. The experimental results from the subclavian artery are shown in Figure 12. The cosine-fit method is also applied to the same experimental data for comparison.

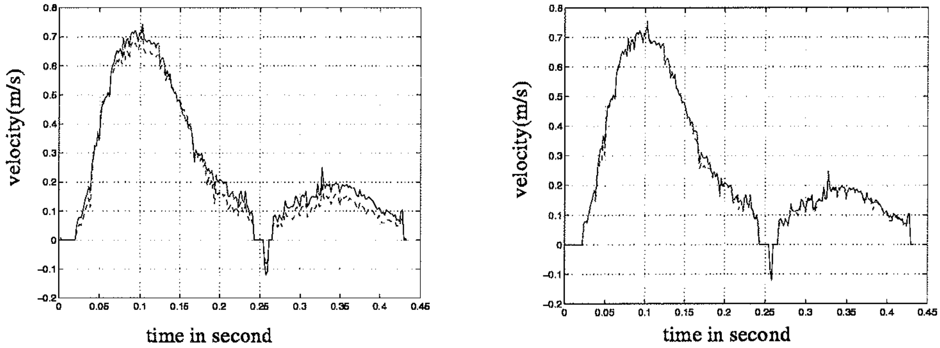

'-' parabolic-fit with bias compensation,
'--' the parabolic-fit without compensation.

'-' cosine-fit interpolation,
'--' parabolic-fit with bias-compensation.

Figure 12 Experimental evaluation of Parabolic-fit with bias-compensation, parabolic-fit and cosine-fit interpolation

It is seen that method 1 has significantly improved the result. There is no significant difference between method 1 and the cosine-fit interpolation method.

B.The interpolation methods applied to the experimental data with velocities up to 2 times the Nyquist limit

The Experimental data from the subclavian artery with the velocities up to twice the Nyquist limit was obtained. In the experiment, the center frequency is 2.5 MHz, the sampling rate in depth is 10 MHz, the pulse repetition frequency is $4kHz$. The depth averaging is 1.0μ s. The temporal averaging is 3ms. The results in Figure 13 and Figure 14 show that method 2, 3 and 4 can interpolate the correlation function with the velocities beyond the Nyquist limit. From (a), (b) and (c) in Figure 14, (c) has fewest velocity aliasing errors. Since the Q-factor in this experiment data is only 1, the performance improvement of the matched filter interpolation is not as significant as that in the simulation where Q is 3.

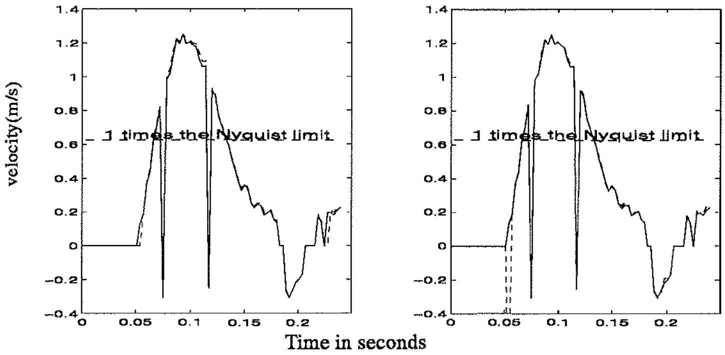

(a) (b)

'--' in (a) parabolic-fit to the complex correlation envelope

'-' in (a) and (b) matched filter interpolation.

'--' in (b) parabolic-fit combined with linear filter interpolation.

Figure 13. Experimental evaluation: Method 2, method 3 and method 4 applied to the experimental data with velocities up to twice the Nyquist limit.

In Figure 14, velocity aliasing errors can be seen. This is due to the fact that factors such as depth averaging time and temporal averaging time, correlation function estimator and signal to noise ratio all can affect the estimation variance of the correlation function. The matched filter method can only reduce the velocity aliasing error caused by low signal to noise ratio. Aliasing can be further reduced by a 2-D tracking method. It is based on the knowledge from flow physics that the blood velocity is continuous both in depth and temporal directions, while aliasing makes the velocity discontinuous. When a velocity discontinuity in the velocity image is detected, then twice the Nyquist velocity should be added or subtracted until the difference between its velocity and the velocity of neighboring points is within the Nyquist limit. The velocity image after 2-D tracking is shown in Figure 14 (d).

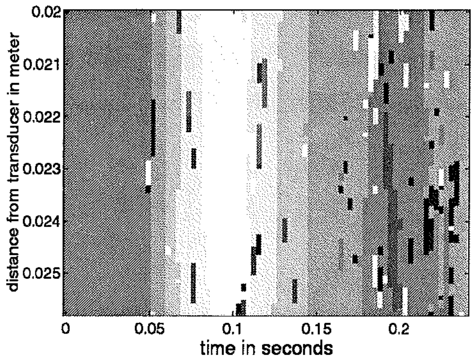

(a)Velocity image obtained with method 2 parabolic-fit combined with linear filter interpolation.

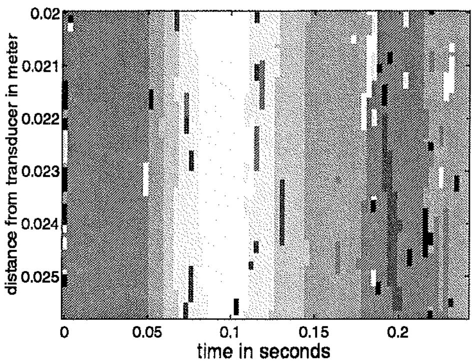

(b)Velocity image obtained with method 3 parabolic-fit to the complex correlation envelope.

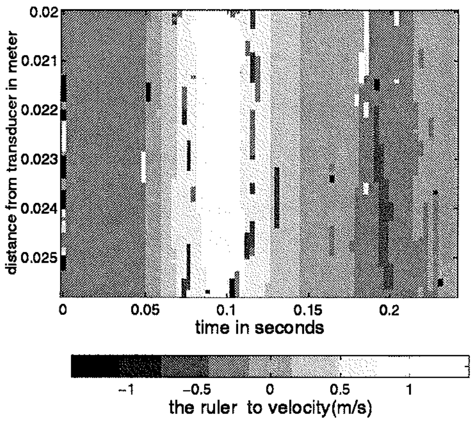

(c) Velocity image obtained with method 4 matched filter interpolation to the correlation function

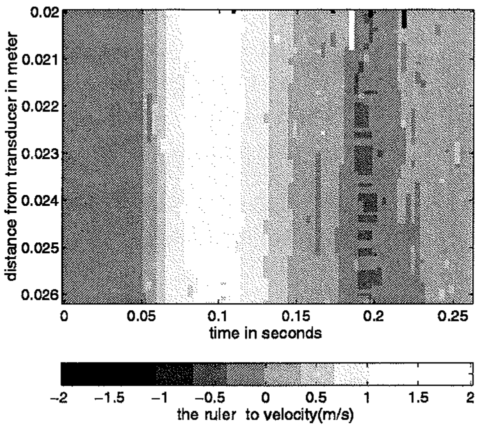

(d) 2-D tracking method applied to the velocity image in (a).

Figure 14 Velocity image of the Subclavian artery with the velocities up to twice the Nyquist limit.

C. The methods applied to the experimental data with velocities up to 4 times the Nyquist limit

The experimental data with velocities up to 4 times the Nyquist limit was obtained by decimating above the RF data to reduce the pulse repetition frequency, so a lower Nyquist velocity was obtained. This decimation was performed prior to the wall motion filter. The depth averring is 1.2μ s, i.e 12 samples. The temporal averaging is 6ms, i.e. 12 pulses by the repetition frequency 2 *kHz*. The estimation results are in Figure 15 and Figure 16. The aliasing can be reduced by 2-D tracking in the velocity as shown in Figure 16.

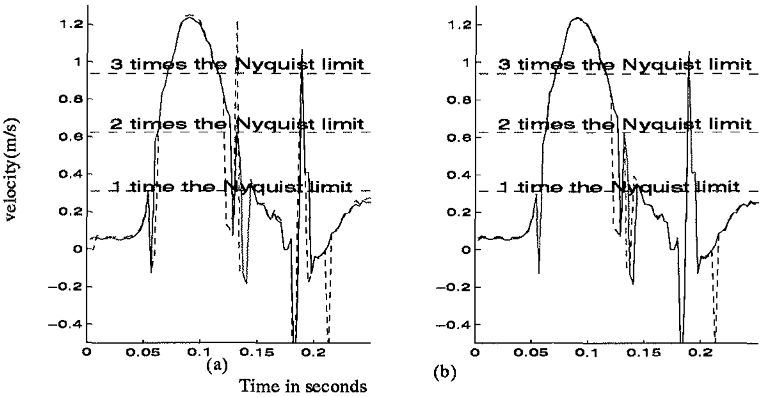

'--' in (a) parabolic-fit to the complex correlation envelope

'-' in (a) and (b) matched filter interpolation.

'--' in (b) parabolic-fit combined with linear filter interpolation.

Figure 15 Experimental evaluation: Method 2, method 3 and method 4 applied to the experimental data with velocities up to 4 times the Nyquist limit.

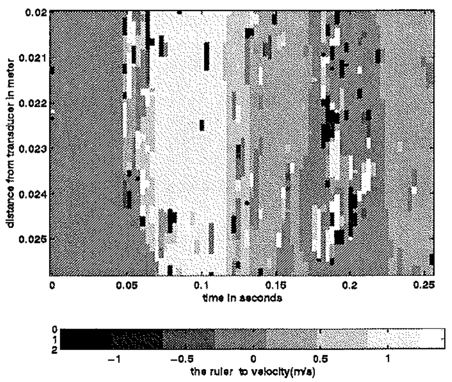

(a) Velocity image obtained with method 2 parabolic-fit combined with linear filter interpolation.

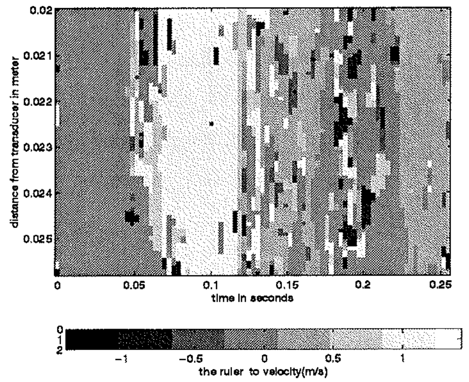

(b)Velocity image obtained with method 3 parabolic-fit to the complex correlation envelope.

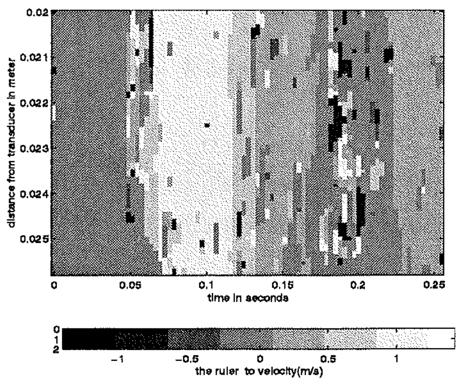

(c) Velocity image obtained with method 4 matched filter interpolation to the correlation function.

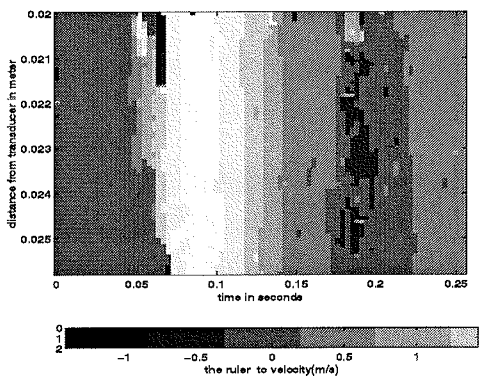

(d) Velocity image obtained with 2-D tracking applied to image (a)

Figure 16 Velocity image of the Subclavian artery with the velocities up to 4 times the Nyquist limit.

V. Conclusions

Four interpolation methods for time delay estimation in the RF-Signal crosscorrelation technique for blood velocity measurement are presented. All the methods have higher velocity estimation accuracy than the parabolic-fit when f_s/f_0 is 4. The estimation accuracy is improved from 1.25% to 0.5% of $1/f_0$ compared to the parabolic-fit interpolation method when f_s/f_0=4 and Q=1.

The first method, parabolic-fit with bias-compensation, has shortest computation time, but suffers from aliasing at low oversampling. It works well if the velocity range is limited within the Nyquist limit which corresponds to the time delay $1/2f_0$. This interpolation method was compared to the cosine-fitting interpolation in this work. It is shown that while both methods suffer from aliasing, parabolic-fit with compensation produces a smaller variance when applied to wideband signal.

The second method, parabolic-fit combined with linear filter interpolation, avoids much aliasing by interpolating the correlation function to a higher sampling rate. Its computation time is between method 1, methods 3 and 4.

The third method, parabolic-fit to the complex correlation function envelope, performs as well as method 2, but requires intensive computations modulating baseband signal to RF-band. An iterative approach can reduce computation time greatly.

The fourth method, matched filter interpolation, maximizes the expected peak value relative to noise. This method was compared to reconstructive filter interpolation, which reconstructs the crosscorrelation function. It is shown the matched filter interpolation method performs better than the reconstructive filter method when SNR is low. Since the matched filter was designed to remove noise power, the matched filter interpolation method gives best performance when SNR is low. This performance improvement is more significant for narrow band signal.

The interpolation methods were verified by simulations with velocities up to 4 times the Nyquist limit corresponding to the time delay $2/f_0$. Further verification was provided by *in vivo* measurements in a subclavian artery with velocities up to 4 times the Nyquist limit. Velocity images have been obtained using method 2, 3 and 4. Most pixels seem to display the correct velocities but a small number of pixels still demonstrate aliasing. A 2-D tracking was used to further reduce aliasing.

Appendix 1

The explanation for the unique determined relation of v and v

From Figure 3, the predicted velocity bias b can be approximated by;

$$\hat{v} = v - b = v - p\sin\frac{N}{200}\pi v \tag{15}$$

where p is the maximum magnitude of the estimation bias. $N=f_s/f_0$ is oversampling, v is the true velocity in terms of percent of the Nyquist limit.

The first order derivative with respect to v is:

$$\hat{v}' = 1 - p\frac{N}{200}\pi\cos\frac{N}{200}\pi v \tag{16}$$

when $p\frac{N}{200}\pi < 1$, i.e.

$$pN < \frac{200}{\pi} \tag{17}$$

then $\hat{v}'$ is strictly positive and it is a monotonic function of v. (17) is usually true, for instance, $pN = 2.5 \times 4 < \frac{200}{\pi}$ for the signal with Q=1 shown in Figure 3.

Appendix 2

Requirement of the oversampling to reduce likelihood of aliasing in the curving-fitting

Considering the correlation function $R(\tau, 1)$ and its sampled version $R\left(\frac{n}{f_s}, 1\right)$, if the true time delay τ_v happens to lie midway between two sampled points and a subsidiary peak lies on a sampled point, then the possibility exists that the sample point of the subsidiary peak has a high value than the point of the true peak, causing aliasing (refer to Figure 1 and Figure 4). In the worst case, we have sample points at $\tau_v \pm \frac{1}{2f_s}$ (half sampling period on both sides of τ_v) and at $\tau_v \pm \frac{1}{f_0}$ (the two nearest subsidiary peaks on the both sides of τ_v), Aliasing occurs when

$$R\left(\tau_v + \frac{1}{2f_s}, 1\right) \le R\left(\tau_v + \frac{1}{f_0}, 1\right) \tag{18}$$

Assuming the correlation function model (1), then (18) becomes:

$$\exp\left(-\frac{\left(\frac{1}{2f_s}\right)^2}{2\sigma^2}\right)\cos\left(\frac{2\pi f_0}{2f_s}\right) \le \exp\left(-\frac{\left(\frac{1}{f_0}\right)^2}{2\sigma^2}\right) \tag{19}$$

Since f_s is usually high compared to $\frac{1}{\sigma}$, we use the approximation

$$\exp\left(-\frac{\left(\frac{1}{2f_s}\right)^2}{2\sigma^2}\right) \approx 1$$

Then (19) can be written as:

$$\cos\left(\frac{\pi f_0}{f_s}\right) \le \exp(-1/2(\sigma f_0)^2) \tag{20}$$

The required oversampling to reduce likelihood of aliasing is:

$$\frac{f_s}{f_0} > \frac{\pi}{\operatorname{acos}[\exp(-1/2(\sigma f_0)^2)]} = \frac{\pi}{\operatorname{acos}[\exp(-2Q^2)]} \tag{21}$$

References

[1] C. Kasai, K. Namekawa, A. Koyano, and R. Omoto. "Real-time Two-Dimensional Blood Flow Imaging Using an Autocorrelation Technique," *IEEE Trans.Sonics Ultras.*, vol. SU-32, pp458-464,1985

[2] O. Bonnefous and Pesquė. "Time Domain formulation of Pulse-Doppler Ultrasound and blood velocity Estimation by Cross-Correlation," *in Ultrasonic Imaging 8. 1986*

[3] O. Bonnefous, Pesquė, and X. Bernard, "A new velocity estimator for color flow mapping," *in Proc. IEEE Ultrason. Symp.*, pp.885-860, 1986

[4] I. A. Hein, William D. O'Brien, "Current Time-Domain Methods for Assessing Tissue Motion by Analysis from Reflected Ultrasound Echoes--A Review," *IEEE Trans.on Ultrasound, Ferroelectrics, and Frequency control,* vol.40, NO.2. March, 1993

[5] H. Torp, K. Kristoffersen, and B. Angelsen, "Autocorrelation Technique in color Flow Imaging, Signal Model and Statistical Properties of the Autocorrelation Estimates," *IEEE Trans.on Ultrasound, Ferroelectrics, and Frequency control,* vol.41. N0.5 Sep. 1994

[6] Foster, GT.C., Embree, M.P. and O' Brien, W.D., "Flow velocity profile via time-domain correlation: error analysis and computer simulation," *IEEE Trans. on Ultrasound, Ferroelectrics, and Frequency control,* vol.37, 164-174, 1990

[7] P. G. M de Jong T. Arts, A. P. G. Hoeks, and R. S Reneman, "Determination of Tissue Motion Velocity by Correlation Interpolation of Pulsed Ultrasonic Echo Signals," *Ultrasonic Imaging* 12, 84-98 (1990)

[8] P. G. M de Jong T. Arts, A. P. G. Hoeks, and R.S Reneman, "Experiment Evaluation of the Correlation Interpolation technique to Measure Regional Tissue velocity," *Ultrasonic Imaging* 13, 145-161 (1991)

[9] I. Cespedes, Y. Huang, J. Ophir and S. Spratt, "Method For Estimation of Subsample Time Delays of Digitized Echo Signals," *Ultrasonic Imaging* 17, pp.142-171, 1995

[10] Jae S. Lim, Alan V. Oppenheim, "Advanced Topics in Signal Processing," Prentice Hall, Englewood Cliffs, NJ, 1988

[11] H. Torp, X. M. Lai and K. Kristoffersen, "Comparison Between Cross-Correlation and Auto-Correlation technique in Color Flow Image," in *Proceedings of IEEE international ultrasonics symposium, Baltimore, MD,* pp.1039-1042, 1993

[12] H. Torp, K. Kristoffersen, "Velocity Matched Spectrum Analysis: A New Method for Suppressing Velocity Ambiguity in Pulsed-Wave Doppler," *Ultrasound in Med. & Bio.*, Vol. 21 No.7, pp 937-944, 1995

[13] K. W. Ferrara, V. Ralph Algaz and J. Liu, "The effect of frequency Dependent Scattering and Attenuation on the Estimation of Blood Velocity Using Ultrasound," *IEEE Trans.on Ultrasound, Ferroelectrics, and Frequency control,* vol. 39, No.6, November, 1992

[14] J. C. Hassab and R.E. Bouchek, "Optimum estimation of time delay by a Generalized Corrector," *IEEE Trans. Acoust, Speech, Signal processing,* vol ASSP-27 pp. 373-380, Aug, 1979

[15] Edward R. Dougherty, "Probability and statistics for the engineering, computing and physical sciences," Prentice hall international, Inc.,1990, chapter 7

[16] K.W. Ferrara, V. Ralph Algazi, "A New Wideband Spread Target Maximum Likelihood Estimator for Blood Velocity Estimation--Part I: Theory," *IEEE Trans.on Ultrasound, Ferroelectrics, and Frequency control,* vol.38, NO.1, January, 1991

[17] X. Lai, H. Torp and K. Kristoffersen, "An extended autocorrelation method for estimation of blood velocity" *IEEE Trans. on Ultrasound, Ferroelectrics, and Frequency control,* Nov. 1997

[18] Hans Torp, "Clutter rejection filters in color flow imaging: A theoretical approach," *IEEE Trans. On Ultrasound, Ferroelectrics, and Frequency control,* Vol.44, No.2, March, 1997.

[19] A. Kadi and T. Loupas, "On the performance of Regression and Step-initialized IIR Clutters for colour Doppler systems in diagnosing medical ultrasound," *IEEE Trans. On Ultrasound, Ferroelectrics, and Frequency control,* Vol.42, No.5, pp.927-937, 1995

Paper C

Experimental Evaluation of Regression and Finite Impulse Response Clutter Filter in Colour Flow Imaging

Experimental Evaluation of Regression and Finite Impulse Response Clutter Filter in Colour Flow Imaging

Abstract

In pulsed wave Doppler ultrasonic measurements, a highpass wall filter is used to suppress the clutter signal prior to the blood velocity estimation. In order to achieve an acceptably high frame rate in CFI, only several pulses from each beam direction are available for analysis. The conventional highpass filters (IIR and FIR) have a settling time which must be removed prior to the velocity estimation. However, this reduces velocity resolution. In order to reduce the settling time, only low order FIR filters or IIR filters with special initialization can be used. In addition, a regression filter was proposed [3].

In this work, the FIR clutter filter and regression clutter filter have been evaluated using experimental data from the subclavian artery and the mitral region of heart. The results show that when the number of segments is short (less than 16), the regression filter gives better results than the FIR filter. When the number of segments is increased to 30, no significant difference exists between the FIR filter and the regression filter.

I. Introduction

In continuous waved Doppler (CW), pulsed wave Doppler (PW) and color flow imaging (CFI) systems, the received Doppler signal not only includes the blood flow signal, but also includes noise and echoes from boundaries and slowly moving solid tissue, which is commonly referred to as the clutter or wall signal. This clutter signal is usually 60-100dB higher than the blood signal. A highpass filter must be used to remove the unwanted clutter signal prior to velocity estimation. This clutter filtering is one of the most critical components for high quality colour flow imaging. An optimal highpass filter is one that can remove high magnitude clutter signals and pass the blood velocity signal. In CW, an analog highpass filter can be used [1]. In PW Doppler, either a combined highpass and lowpass analog filter or conventional digital IIR (infinite impulse response) and FIR (finite impulse response) highpass filter can be exploited to suppress the clutter signal [1]. The IIR filter is often preferred, because it has a steep transition band with low order. In CFI, in order to achieve an acceptably high frame rate to measure fast varying of flow phenomena, only 4-16 pulses are available for analysis from a line of sight. This requires the filter to have a short transient response. A number of different approaches has been proposed for this purpose. IIR filters usually exhibit a long transient response. Therefore, in this case, special precaution should be taken to initialize filters to reduce the transient time [4] [5]. FIR filters with short impulse response can also be used, however, some output samples which equals to the filter order must be discarded. Furthermore, a low order FIR filters limits the clutter capability of suppression. A regression filter was proposed in [3]: the slowly varying wall signals is fitted to a curve which is then subtracted from the Doppler signal. The advantage of this technique is that the number of output samples is not reduced.

In this work, we compared experimentally the performance of FIR clutter filter and the regression clutter filter.

II. FIR clutter and Regression Filters

A. FIR clutter Filter

In order to remove high amplitude low frequency wall signals, the filter should have sufficiently high stop-band damping. In addition, in order to prevent the filter from removing the blood signal, the filter should have a steep transition band. Thus, a high order FIR filter is required. Inadequate clutter filtering will introduce bias into the velocity estimation. Clutter artifacts pulls the estimated velocity towards the clutter velocity (negative bias). A filter with a broad transition band may remove the blood signals and limit their detectability. As a result, the estimated velocity has a positive bias.

The long settling time of the high order FIR filter means that some sample points must be discarded prior to estimation. For a long signal segment, the estimation would not be significantly affected by discarding several samples. However, for a short signal segment, the estimation variance will be increased greatly by the reduction of sample points. Therefore, there is trade-off between the FIR filter order and the performance of the filter. In this work, a first and a second order FIR filters, as well as a high order (8th order) FIR filter were studied.

In radar and sonar system as mentioned in [1] and [6], a simple first order FIR filter is usually used to remove the stationary signal. Using this technique, the received signal from two consecutive ultrasound pulses are subtracted. e.g.,

$$z(k) = y(k) - y(k-1) \tag{1}$$

where $z(k)$ is the filtered data, $y(k)$ is received Doppler signal. Its performance is described by its frequency transfer function, as shown in Figure 1.

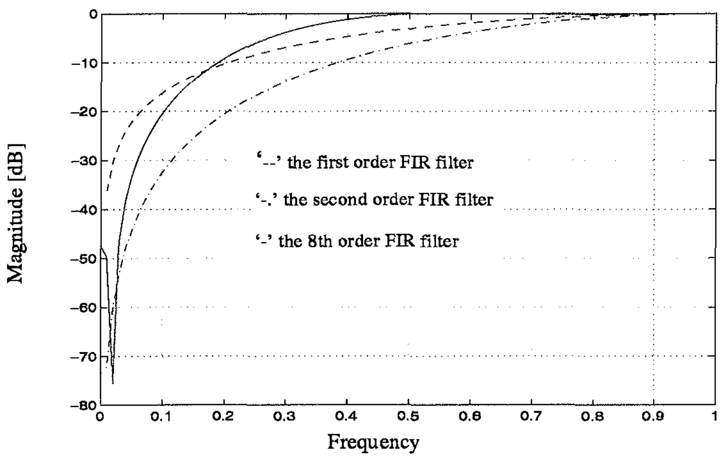

Figure 1 Frequency response of FIR filter

This filter is limited to be removal of small magnitude wall signals. Furthermore, its cut-off frequency is high (for example, to remove a 40 dB wall signal, the cut-off frequency is over 0.5π) which means it may also removes blood signal and the velocities lower than half the Nyquist limit will not be estimated correctly.

The advantage of this filter is that it has the shortest settling time of all the FIR type filters and is easy to implement in real time.

A second order filter which is also used in radar systems can be described by

$$z(k) = 0.5y(k) - y(k-1) + 0.5y(k-2) \tag{2}$$

It is also easy to implement in real time because no multiplication is required. Its frequency transfer function is also shown in Figure 1. Compared to the first order filter, the performance of the second order filter has been improved. In order to remove a 60dB wall signal, the cut-off frequency is about 0.3π. However, the setting time is longer than the first order FIR filter.

Although the second order filter has better performance than the first order filter, its transition band is still wide. For cardiac examinations, the simple FIR filter is not adequate for removing the tissue signals, since the heart walls are moving rapidly and produce quite large Doppler shifts. Thus, other high order FIR filters must be used. In Figure 1, a frequency response for a 8th order FIR filter is plotted. This filter is obtained by using the window design method: Kaiser window with a beta-value of 2.5.

B. Regression filter

The regression filter, or polynomial fitting is based on the fact that the short signal segment can be assumed as the sum of a curve (or straight line) for which reflects a slowly varying, low frequency clutter signal and a fluctuation around this curve for which reflects a quickly varying high frequency blood signal. By subtracting the curve from the Doppler signal, the clutter signal can be suppressed. An example of regression filtering is shown in Figure 2. In the left side, the solid curve is the Doppler signal, the dashed line is the clutter signal. By subtracting the clutter signal from the Doppler signal, the blood signal is obtained (Figure 2).

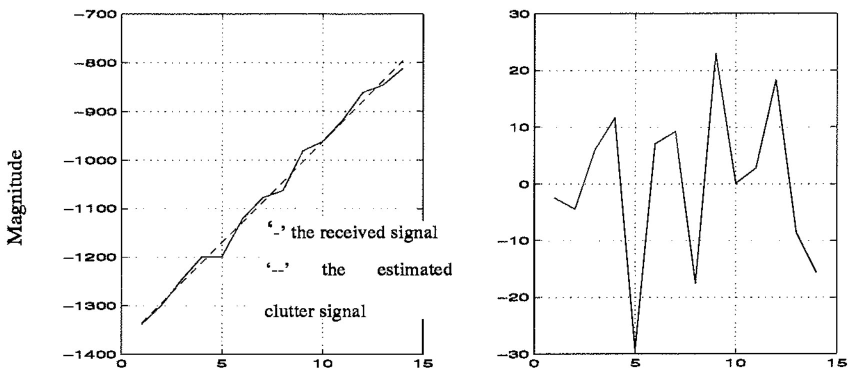

Figure 2 An example of regression filtering. (a) The Doppler signal and estimated clutter signal. (b) The filtered segment (The Doppler signal minus the estimated clutter signal).

If input Doppler signal is denoted as a vector:

$$\underline{x} = (x(1), \ldots, x(N)),$$

output filtered signal as a vector

$$\underline{y} = (y(1), \ldots, y(N)).$$

From [2], we have $\underline{y} = A\underline{x}$, where $A = \{a(n, m)\}$ is a filter matrix and

$$y(k) = \sum_{n=1}^{N} a(n, k)x(n) \qquad k = 1, 2, \ldots K \tag{3}$$

If we assume that the clutter signal is contained in a subspace κ of $\mathbf{C}^N$, the projection transform P_κ from $\mathbf{C}^N$ onto κ gives the least square fit to the clutter component. If we have an orthonormal basis for $\mathbf{C}^N$, the filter operation can be performed by calculating the projection along each basis vector, and subtract the projection from the original signal. i.e.

$$\underline{y} = A\underline{x} = (I - P_\kappa)\underline{x} \tag{4}$$

where I is the identity matrix. One of the most frequently used set of orthogonal polynomials is the Legendre polynomials $\{b_n\}$, which are orthogonal on [-1 1] with respect to the weigh function $w(k)=1$. The b_n are given by:

$$b_0(k) = 1\,,\ b_1(k) = k\,,\ b_2(k) = k^2 - 1/3\,,\ b_3(k) = k^3 - \frac{3}{5}k$$

The Legendre polynomials $\{b_n\}$ can also be obtained by applying the Gram-Schmidt orthonormalization process to the algebraic polynomials $\{1, k, k^2, k^3 \ldots\}$.

In fact, the filtering results remains the same by using the equal order algebraic polynomial [4] and orthogonal polynomials. The advantage of using orthogonal polynomials is that this technique minimizes the operations needed to find the coefficients. From [4], the number of operations (add/multiply) for matrix implementation of regression filtering is $2(P+1)K$, where P is the basis order, N is the segment length. Due to the symmetry of the basis vectors, the number of operations required to find the coefficients by using orthogonal polynomials is $(P+1)K$. Furthermore, the projected coefficients are independent due to the orthogonal property of the basis function. This makes the higher order regression results can employ the lower order regression results. This fact is extremely useful for adaptive filtering. However, by using algebraic polynomials, a new equation has to be solved for different order regressions.

The performance of time invariant IIR and FIR filters can be evaluated from their frequency response. The filtered output signal is the convolution in the time domain of the filter and the input signal. For the regression filter, the filtered signal is the difference between the input signal and the estimated clutter signal. However, a frequency response function $H(\omega)$ was defined in [2] to evaluate the quality of the regression filter. It was defined as the power of the output signal when the input is a complex harmonic signal. i.e.,

$$x(k) = e^{jk\omega} \qquad k = 1, \ldots K \tag{5}$$

$$y(k) = \sum_{n=1}^{N} a(n, k)e^{jn\omega} \tag{6}$$

$$H(\omega) = \frac{1}{N}\sum_{k=1}^{N} |A_k(\omega)|^2 \tag{7}$$

The quantity $A_k(\omega)$ is the Fourier transform of row number k in the filter matrix. From this frequency response of the regression filter, the cut-off frequency decreases by increasing the signal segment. However, the cut-off frequency of the regression filter increases with filter

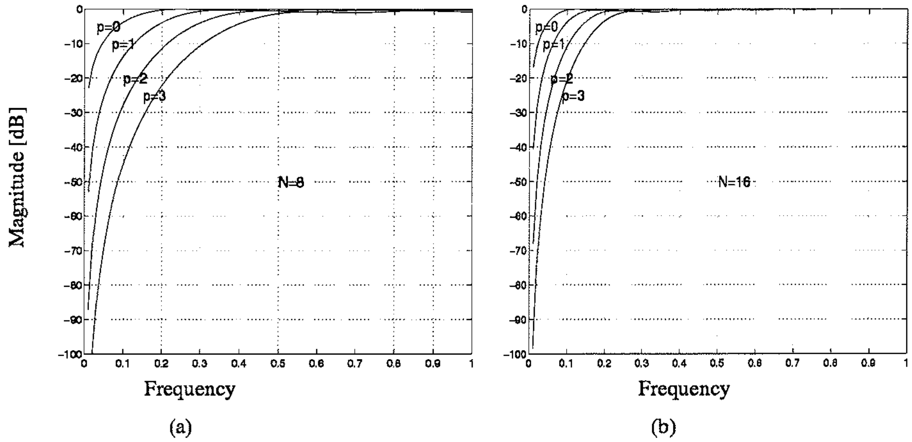

Figure 3 Frequency response for the regression filter. (a) N=8 samples per segment. (b) N=16 samples per segment.

order. The slope of the transition band is related to the segment length and filter order. If a high magnitude clutter signal has to be removed, the lowest velocity that can be estimated increases, while the velocity estimation range decreases. In the regression filter, there is a trade-off between the removable clutter magnitude and the velocity estimation range. Due to the fact that the clutter amplitude may vary considerably from one area to another area, an adaptive regression filter can be used to give optimum filtering results.

III. Experimental Verification

A. Experiment Setting and Referenced Velocity Estimation Results

An experimental evaluation of the regression filters and FIR filters was performed in this section. The RF data was collected by an ultrasound scanner (Vingmed CFM 800) via a custom data acquisition system. The experimental data was from the subclavian artery. The experimental parameters were as follows:

Pulse repetition frequency (PRF)	Center frequency (f_0)	Pulse length	Depth averaging
2.5kHz	2.5MHz	1μs	0.312mm

The sound velocity used was 1540m/s and the Nyquist limit with these parameters was 0.385m/s.

A typical power spectrum from this experiment data is shown in Figure 4. The clutter signal is about 40dB higher than the blood signal. Our first goal is to remove this clutter signal. Due to the fact that mechanical scanning was used in this experiment and this scanning system has a continuous movement of the beam, the data from each range gate can be regarded as continuous. Thus, a conventional clutter filter may be used. We used an IIR filter to give the referenced velocity estimation results. The data from each range gate is continuous, therefore, any length N can be used. Usually N must be small enough so that the signal remains stationary. In this work, we used N=8, 16 and 30. Then, we apply regression filters and FIR filters to data. The results are compared to the referenced results.

The used IIR highpass filter was a 4th order butterworth filter. Its normalized cut-off frequency was 0.155. Its frequency response is plotted in Figure 5. After high pass filtering, some samples at the beginning and the end of the filtered data were dropped in order to reduce the transient effects. Following that, we used a conventional autocorrelation method to estimate the velocity. The temporal averaging was 3.2ms (N=8), 6.4ms (N=16) and 12ms (N=30), respectively. The results were shown in Figure 6. In this experiment, some velocities have exceeded the Nyquist limit. In order to prevent aliasing, another velocity estimator should be used, such as the extended autocorrelation estimator [paper A] and the correlation estimator [paper B]. However, the unambiguous velocity estimate is not our main concern in this work. A further discussion on the effect of the clutter filter on the extended autocorrelation estimator and the correlation estimator is in paper D.

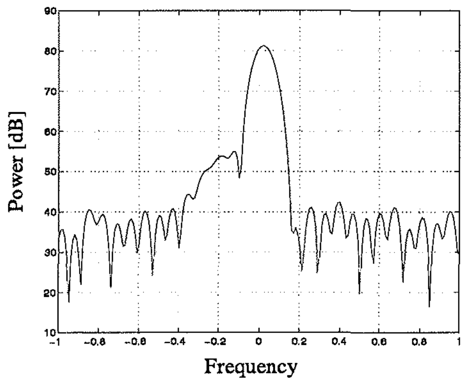

Figure 4 The power spectrum of the Doppler signal calculated for N=12.

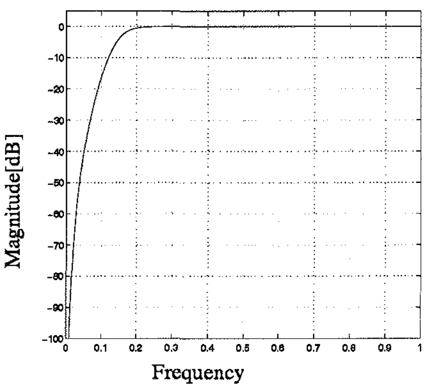

Figure 5 Frequency response of 4 order IIR butterworth filter

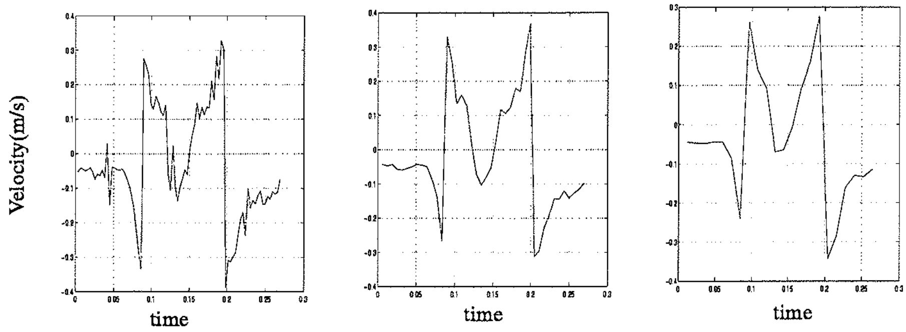

(a) N=8 (b) N=16 (c) N=30

Figure 6 Referenced velocity estimation results. 4th order IIR butterworth filter is applied to the data from each range prior to velocity estimation which was based on segment length (a) N=8, (b) N=16, (c) N=30.

B. The Velocity Estimation Results When the regression filter is Applied to the Experiment Signal

The velocity estimation results are in Figure 7 to Figure 9. Table 1 gives a guide of the velocity estimation figures.

Table 1: A list of velocity estimation results using regression filter

Filter order	N=8	N=16	N=30
1	Figure 7 (a)	Figure 8 (a)	Figure 9 (a)
2	Figure 7 (b)	Figure 8 (b)	Figure 9 (b)
3	Figure 7 (c)	Figure 8 (c)	Figure 9 (c)

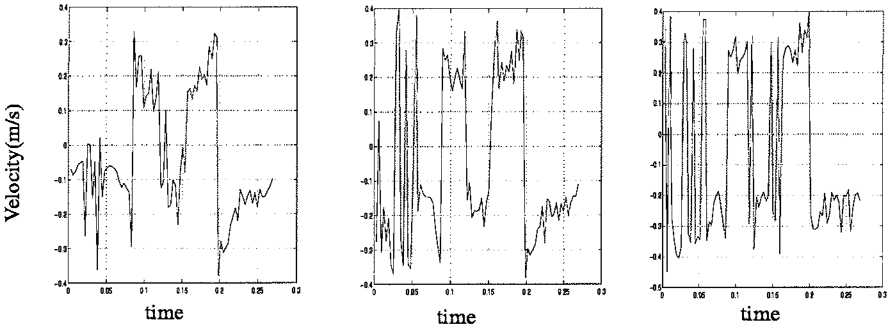

(a) first order filter (b) second order filter (c) third order filter

Figure 7 The velocity estimation results when the regression filter is applied to ***N*=8** segment length. The regression filter order (a) One, (b) Two, (c) Three.

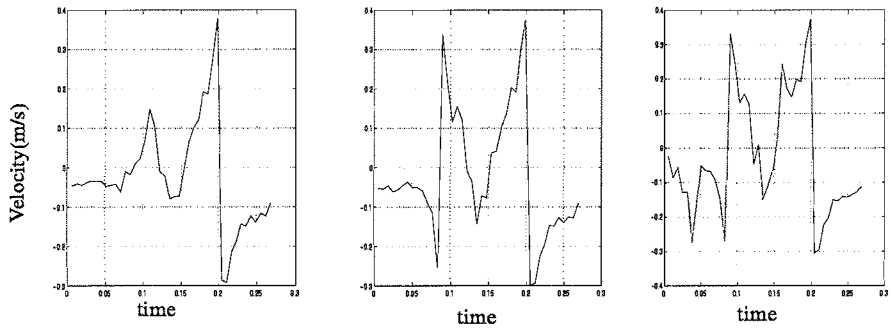

(a) first order filter (b) second order filter (c) third order filter

Figure 8 The velocity estimation results when the regression filter is applied to ***N*=16** segment length. The regression filter order (a) One, (b) Two, (c) Three.

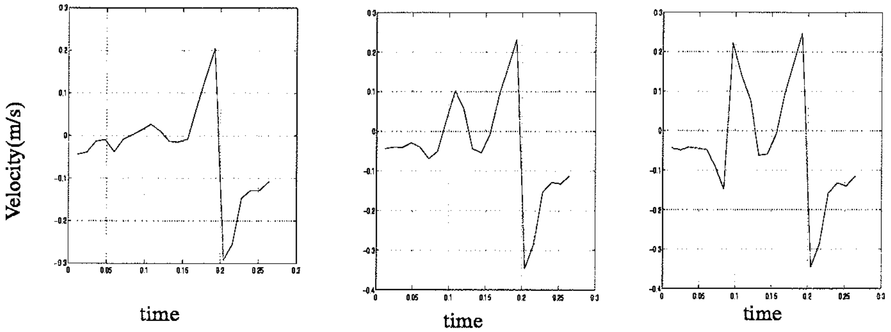

(a) first order filter (b) second order filter (c) third order filter

Figure 9 The velocity estimation results when the regression filter is applied to ***N*=30** segment length. The regression filter order (a) One, (b) Two, (c) Three.

C. The Velocity Estimation Results when FIR Clutter Filter Applied to the Experimental Signal

The velocity estimation results are in Figure 10 to Figure 12. In order to reduce the transit response effect, some points were discarded prior to the velocity estimation. Table 2 gives a guide of the velocity estimation figures.

Table 2: A list of velocity estimation results using FIR filter

Filter order	N=8	N=16	N=30
1	Figure 10 (a)	Figure 11 (a)	Figure 12 (a)
2	Figure 10 (b)	Figure 12 (b)	Figure 12 (b)
8	Figure 10 (c)	Figure 13 (c)	Figure 12 (c)

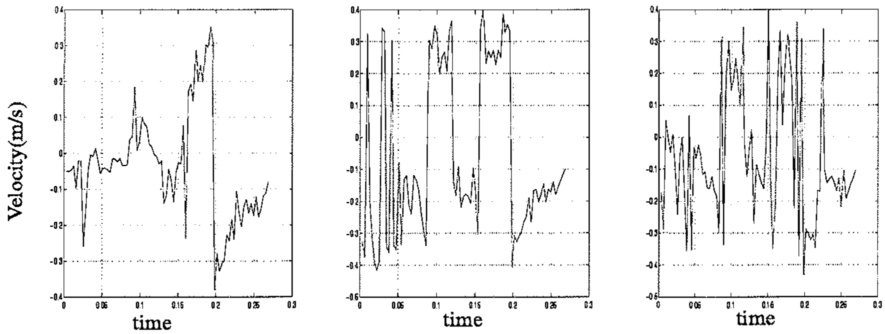

(a) the first order FIR (b) the second order FIR (c) the 8th order FIR

Figure 10 The velocity estimation results when the FIR highpass filter applied to N=**8** segment length. The FIR filter order (a) One, (b) Two, (c) Eight.

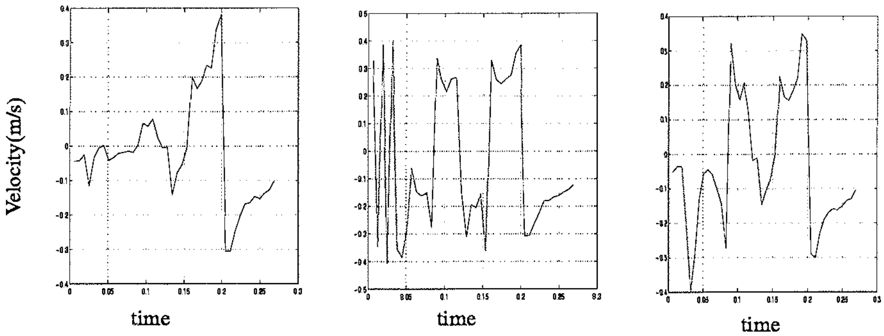

(a) first order FIR filter (b) second order FIR filter (c) 8th order FIR filter

Figure 11 The velocity estimation results when the FIR highpass filter applied to N=**16** segment length. The FIR filter order (a) One, (b) Two, (c) Eight

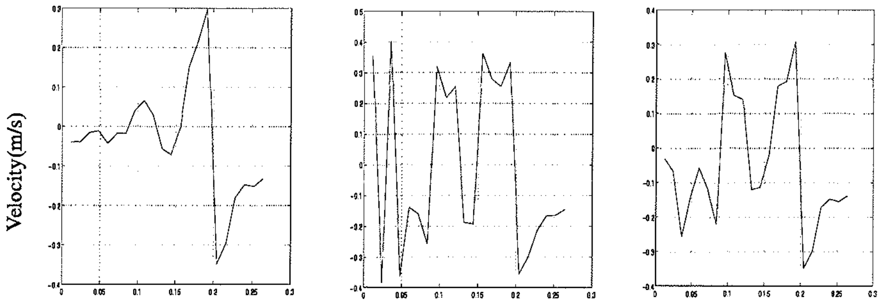

(a) first order FIR filter (b) second order FIR filter (c) 8th order FIR filter

Figure 12 The velocity estimation results when the FIR highpass filter is applied to *N*=**30** segment length. The FIR filter order (a) One, (b) Two, (c) Eight.

From the experimental results, it is seen that:

1. When the segment length is short (*N*=16, *N*=8), the regression filter gives better results than the FIR filter. When the segment length is increased to *N*=30, the regression filter and FIR filter give similar results.

2. When the segment length is short, the order of the regression filter should be low, because the high order filter can remove too much blood signal; hence, the velocity estimation results become worse. When the segment length is increased to *N*=16 and *N*=30, the lower order (first order) filter can not remove the clutter signal adequately, and the higher order filter gives better results.

3. The first and the second order FIR filter cannot suppress 40dB clutter adequately. From the above figures, the second order FIR filter gives better estimation results than the first order FIR filter. When segment length is increased to 16, the 8th order FIR filter can be used, but the estimation results are not as good as those of the regression filter. When *N*=30, there is no significant difference between the 8th order FIR filter and the third order regression filter.

D. Further Experimental Verification from 2-D Imaging

A further experimental evaluation of regression filters and FIR filters was performed. A set of RF data was collected by an ultrasound scanner (Vingmed SYSTEM FIVE). The data was from the mitral region of the heart. The experimental parameters were as follows:

Pulse repetition frequency (PRF)	Center frequency (f_0)	Beams per frame	Samples per beams	Depth averaging
5.976kHz	2.5MHz	24	30	2.8mm

The Nyquist limit was 0.9204m/s. Since the number of samples per beam is 30, it can be reduced to N by using only the first N samples. We use N=8, 16 and 30 in this study.
Figure 13 shows a power spectrum from one block of this data (depth=0.077m, angle 1.52π for this 2-D data set). The clutter in this block is about 20dB higher than the blood signal.

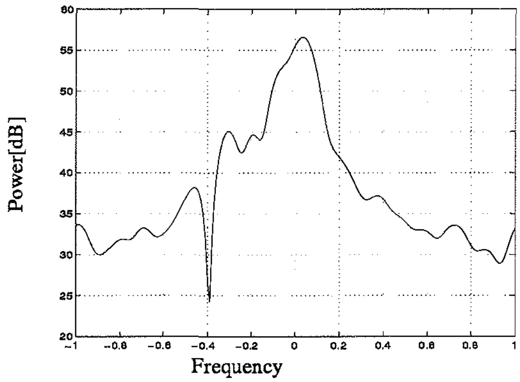

Figure 13 The power spectrum of part of the received data from the mitral region of the heart.

For simplicity, six velocity images were shown here in Figure 14. More velocity images were shown in the Appendix.

Table 3: A list of wall filter which used in the 2-D heart mitral data

Samples per beam	regression filter	FIR filter
N=8	the first order	the second order
N=16	the second order	the 8th FIR
N=30	the third order	the 8th FIR

In order to test the accuracy using different wall filters, the estimates obtained with the regression filter when N=30 were used as a reference. The bias and standard deviation of the error between the estimates and this reference were used as a measure of the estimation accuracy [7]. The results are listed in Table 4.

Table 4: Mean velocity estimation accuracy for the different wall filters. The results created by using the 3rd order regression filter when N=30 were assumed to be reference estimates.

	I	II	III	IV	V
bias [cm/s]	3.80	4.42	2.85	7.66	2.05
std.deviation [cm/s]	28.54	28.73	32.91	41.22	25.49
I: N=8, the first order regression filter. II. N=16, the second order regression wall filter. III. N=8, the second order FIR wall filter. IV. N=16, the 8th order FIR wall filter. V. N=30, the 8th order FIR wall filter.					

From the 2-D velocity images and the results in Table 4, it is seen that:

1. When N is 8, the first order regression filter gives better results than the second order FIR filter, which eliminates too much blood signal. The region with low blood velocity disappears in Figure 14 (b). From the frequency response in Figure 1, it can be predicted that the first order FIR filter will remove much more blood signal. However, high order FIR filters are not suitable to short segment case.

2. There is no significant difference between Figure 14 (e) and (f) when N=30. The bias and standard deviation between those two images is at a minimum as shown in Table 4.

3. In this experiment, a 3.5cm wide region of the mitral region of heart has been scanned. When N=30, the frames rate is 16*Hz*. When N=16, the frames rate is 31*Hz*. When N=8, the frames rate is 62*Hz*. With this high frame rate, the 2-D velocity image (Figure 14 (a)) still give a high quality image.

Conclusions

Experimental comparisons between the regression filter and the FIR filter have been performed based on the data from the subclavian artery and the mitral region of the heart. The results show that when the segment length is short (less than 16), the regression filter gives better results than the FIR filter. When the segment length is increased to 30, no significant difference exist between the FIR filter and the regression filter.

When the segment length is short, the low order regression filter is preferred because the high order regression filter may remove significantly blood signal. In this case, only the first or second order FIR filter can be used. However, they both eliminate too much blood signal.

In the experimental data from the mitral region of heart, a 3.5cm wide region has been scanned. When the pulse number per beam direction is 8, the frame rate per second is 62. A high quality image has been obtained by using the first order regression filter.

Further study will include using the third to eight order FIR filter and low order IIR filter with special initialization for comparison. The goal is to obtain an optimum clutter filter.

References

[1] Bjϕrn A. J Angelsen, "Waves, Signals and Signal Processing in Medical Ultrasonics," *Textbooks,* Trondheim, Norway, April, 1996.

[2] Hans Torp, "Clutter rejection filters in color flow imaging: A theoretical approach," *IEEE Trans. On Ultrasound, Ferroelectrics, and Frequency control,* Vol.44, No.2, March, 1997.

[3]A. P. G. Hoeks, Van de Vorst, J. J. W. Dabekaussen, A. Brands, P. J., Reneman, R. S., "An efficient algorithm to low frequency Doppler signals in Digital Doppler system," *Ultrasonic Imaging* 13, 135-144, 1991.

[4] A. Kadi and T. Loupas, "On the performance of Regression and Step-initialized IIR Clutters for colour Doppler systems in diagnosing medical ultrasound," *IEEE Trans. On Ultrasound, Ferroelectrics, and Frequency control,* Vol.42, No.5, pp.927-937, 1995

[5] R. B. Peterson, L. E. Atlas and K.W. Beach, "A Comparison of IIR initialization Techniques for improved color Doppler wall filter performance," *IEEE Ultrasonics Symposium*, Seattle, WA, 1994

[6] J. A. Jensen, "Stationary Echo Cancelling in Velocity Estimation by Time-domain Cross-correlation," *IEEE Trans. Med. Imag.*,Vol.12, no., pp.471-477, 1993

[7] Hans Torp and Steinar Bjaerum, "Quality versus Framerate in Color Flow Imaging: An Experimental Study Based on Offline Processing of RF-Signals Recorded from Patients," *Proceedings of IEEE Ultrasonics Symposium*, pp1229-1232, San Antonio, Texas, 1996.

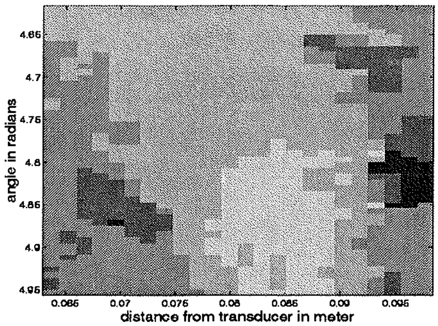

(a)N=8. The first order regression wall filter.

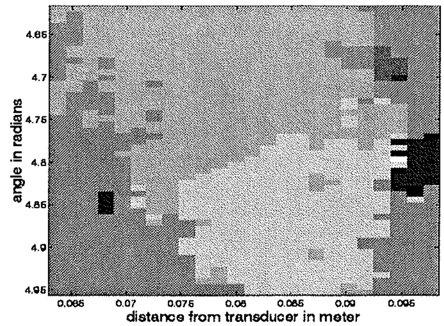

(b) N=8. The second order FIR wall filter

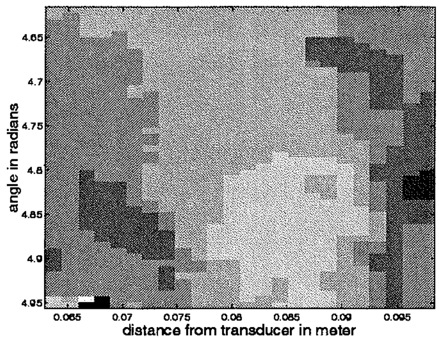

(c)N=16. The second order regression wall filter.

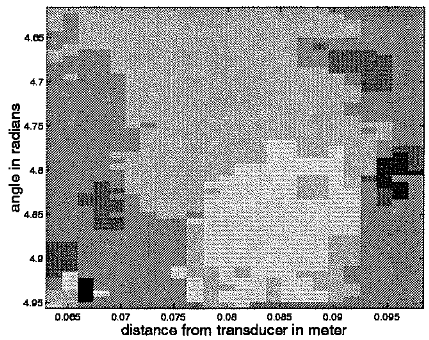

(d) N=16. The 8th order FIR wall filter

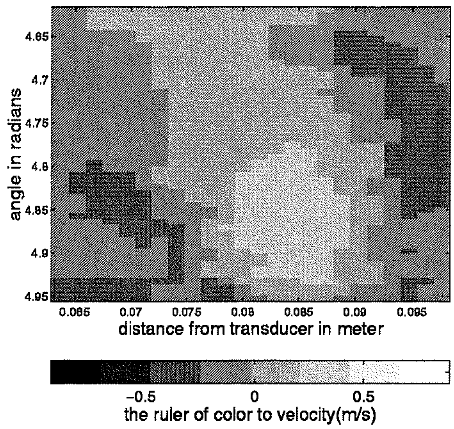

(e)N=30. The third order regression wall filter.

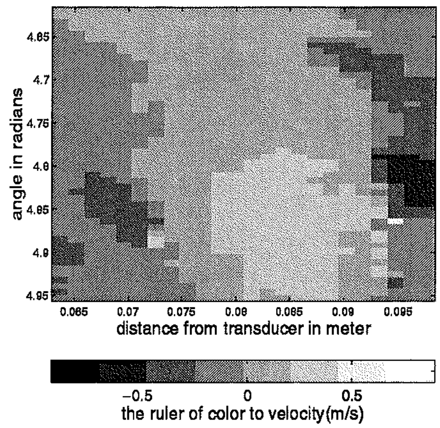

(f) N=30. The 8th order FIR wall filter.

Figure 14 2-D velocity imaging from the mitral region of the heart. The images are obtained by applying different wall filters prior to the velocity estimation.

Appendix: Velocity images using different wall filters

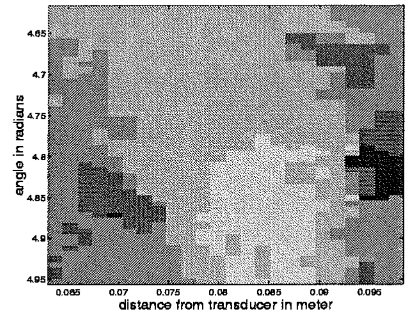

(a) The first order regression filter.

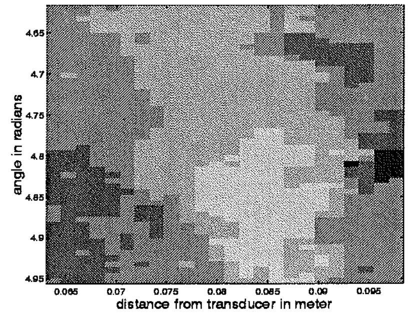

(b) The first order FIR filter

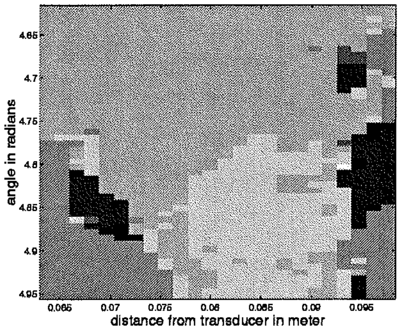

(c) The second order regression filter

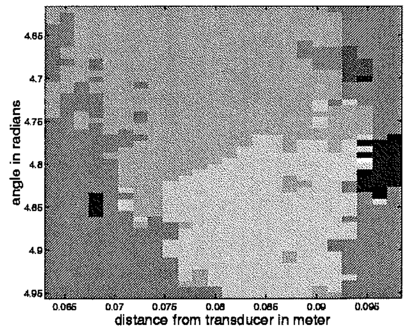

(d) The second order FIR filter

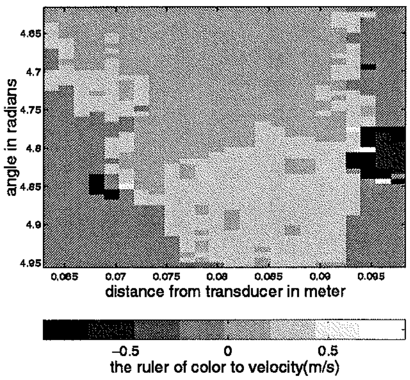

(e) The third order regression filter

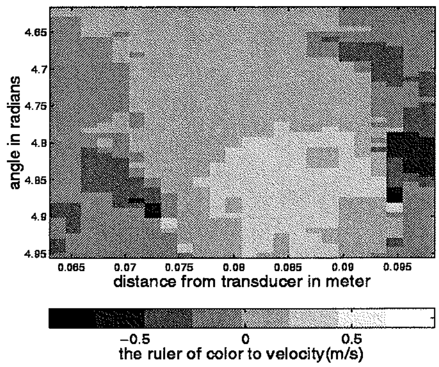

(f) The 8th order FIR filter

Appendix-1: Velocity images by using different wall filter when sample segment $N=8$.

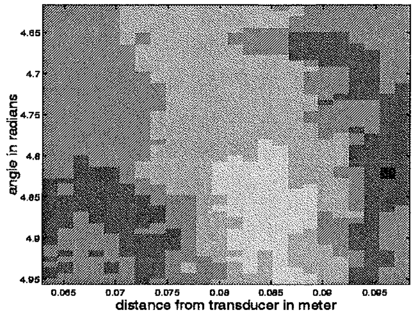

(a) The first order regression filter

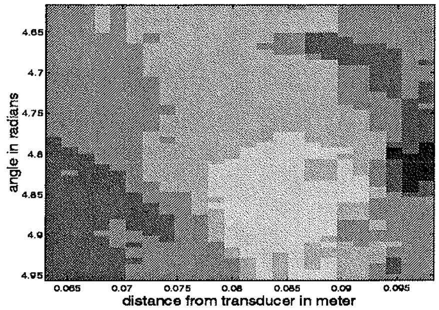

(b) The first order FIR filter

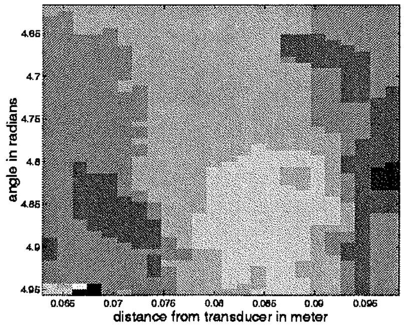

(c) The second order regression filter

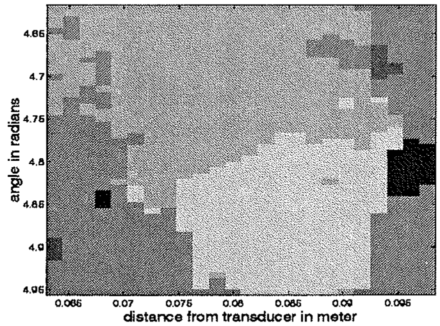

(d) The second order FIR filter

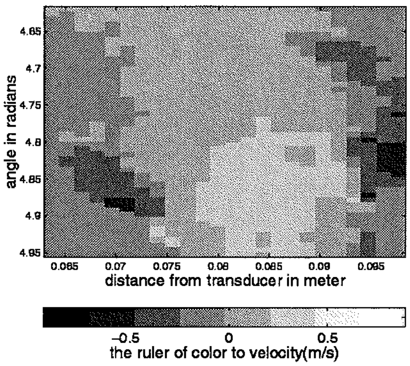

(e) The third order regression filter

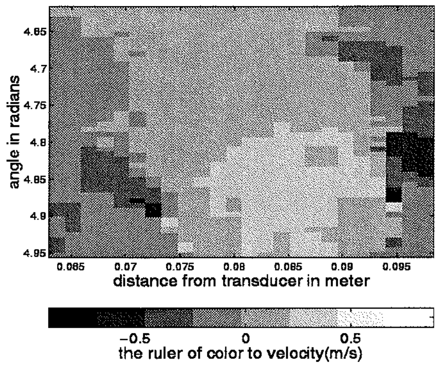

(f) the 8th order FIR filter

Appendix-2: Velocity images by using different wall filter when sample segment *N=16*.

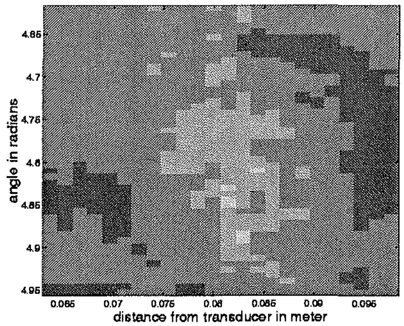

(a) The first order regression filter

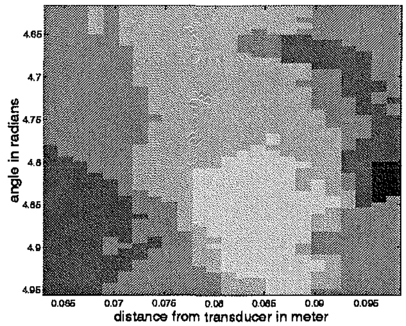

(b) The first order FIR filter

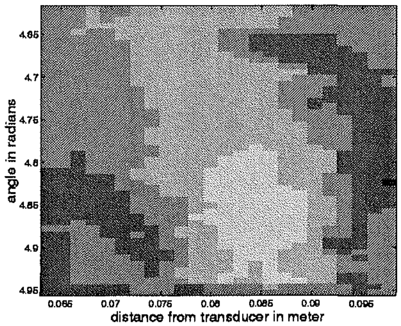

(c) The second order regression filter.

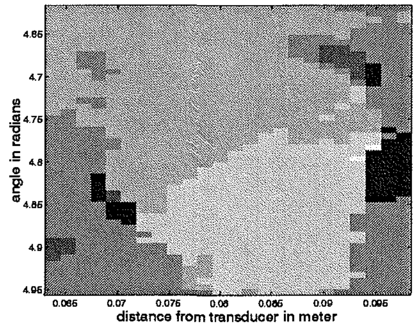

(d) The second order FIR filter

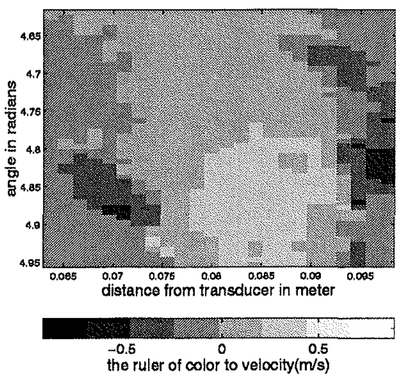

(e) The third regression filter.

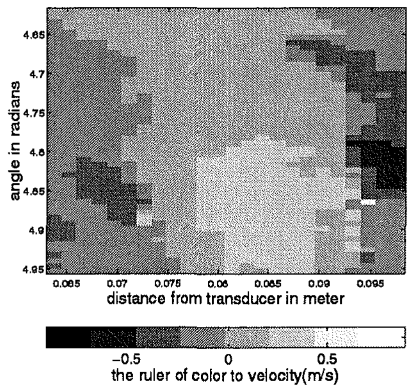

(f) The 8th order FIR filter

Appendix-3: Velocity images by using different wall filter when sample segment *N=30.*

Paper D

Effects of the Wall Filter on the Estimation of High Blood Velocity

A large part of this paper was published in: X. Lai, H. Torp, "Effects of the Wall Filter on the Estimation of High Blood Velocity", presented in *IEEE International Ultrasonics Symposium,* Toronto, Ontario, Canada, 1997.

Effects of the Wall Filter on the Estimation of High Blood Velocity

Abstract

In pulsed wave Doppler ultrasonic measurements, a highpass wall filter is used to remove the clutter signal prior to the blood velocity estimation. For high velocity measurements, the wall filter creates dead zones where the Doppler frequency equals multiples of the pulse repetition frequency (PRF). In this work, the effect of the wall filter has been studied for two different blood velocity estimators; the crosscorrelation method (CCM) and the extended autocorrelation method (EAM). When the pulse bandwidth is sufficiently high, the Doppler signal bandwidth will exceed the wall filter cut-off frequency due to the transit-time effect, and the dead zones are partially removed. However, the chance of velocity aliasing is increased in these zones due to the filtering, both for the CCM and EAM method. The effects of the wall filter have been studied by simulations with rectilinear velocities up to four times the Nyquist limit (v_{NY}). In this simulation, the pulse bandwidth is 2.5MHz. When the cut-off frequency of the wall filter is 0.1*PRF, no velocity aliasing has been observed. When the wall filter is increased to 0.2*PRF, there is 15% aliasing error occurring at velocity=2*v_{NY} and no velocity aliasing at v=4*v_{NY}. When the wall filter is increased to 0.25*PRF, there is about 70% velocity aliasing error at twice v_{NY}, and 15% velocity aliasing error at velocity four times v_{NY}. The simulation results have further been verified by experimental data from subclavian artery measurements with velocities up to twice the Nyquist limit.

I Introduction

Blood velocity is an important parameters in the clinical diagnosis of vascular disease. Ultrasound techniques have been shown to be a valuable tool for blood velocity measurement. The pulsed wave Doppler (PW) and multi-range gated (MRG) techniques are currently widely used, because they provide range resolution. To obtained Doppler information in PW and MRG techniques, multiple pulses are transmitted repeatedly at a set pulse repetition frequency (PRF). The blood velocity in the selected range of interest is estimated from the received multiple echoes. The received signal components from a range cell include blood flow signal, received noise and the echoes from boundaries and slow moving tissue which are commonly referred to as clutter or wall signals. This clutter signal may be more than 60 dB higher than from blood signal and it must be removed by a high pass wall filter prior to the velocity estimation.

Due to the sampled nature of the PW and the MRG method, the Doppler shift is periodical with a frequency PRF. This causes the velocity estimation ambiguity by conventional autocorrelation method. The highest estimated velocity is the velocity corresponding to a Doppler shift of PRF/2. This velocity is referred to as the Nyquist limit v_{NY}. Since blood velocities exceeding the Nyquist limit can be found under jet flow conditions, for instance, in heart defects, other velocity estimators such as CCM [1] and EAM [2] which are not subject to this limit must be used.

Due to the wall filter, any low velocity blood component of blood flow would also been removed. Thus, all the estimators suffer from the velocity dead zone around zero velocity. The frequency response of the wall filter is repeated with the PRF. This means it also removes some of the signal power whose velocities are centered about $2nv_{NY}$ $(n = 0, \pm 1, \pm 2\ldots)$. One of the question raised is whether the velocity dead zones are present around $2nv_{NY}$.

In this work, we investigate the effects of the wall filter on the high velocity estimation in the CCM and the EAM.

II. Theoretical Analysis

A. Effects of the Wall Filter When the Transit Time Effect is not included

In a 2-D blood signal model [4], the received RF signal $p(t,k)$ is a Gaussian random signal [4], where t is the elapsed time after a pulse transmission which corresponds to a certain depth from the transducer and k is the index of the transmitted pulse sequence. If we ignore the transit time effect of the received signal from successive pulses, the received echo from the k^{th} pulse differs from 1^{th} pulse only by a time delayed factor, i.e.,

$$p(t, k) = p(t-k\tau_v, 0) \qquad \tau_v = -\frac{2Tv\cos\theta}{c}$$

where T is the pulse repetition period, c is the velocity of sound. v is the blood flow velocity, θ is the angle between the ultrasound beam and the blood flow direction.

The 2-D Fourier transform of $p(t,k)$ can be expressed as [3]

$$G_1(\omega_1, \omega_2) = \int_t \sum_k p(t, k) e^{-j\omega_1 t} e^{-j\omega_2 k} dt = \tag{1}$$

$$\sum_k P(\omega_1) e^{-j\omega_1 k\tau_v} e^{-j\omega_2 k} = \sum_n P_1(\omega_1)\delta\left(\omega_2 + n\frac{2\pi}{T} + \tau_v\omega_1\right)$$

where $P_1(\omega_1)$ is the Fourier transform of $p(t,0)$. The 2-D power spectrum of $p(t,k)$ is given by:

$$G(\omega_1, \omega_2) = |G_1(\omega_1, \omega_2)|^2$$

It can be seen from (1) that $G_I(\omega_1,\omega_2)$ is periodic in ω_2 with a period of $2\pi/T$. It may be written as a sum of copies of the nonaliased part $G_0(\omega_1, \omega_2)$ and:

$$G(\omega_1, \omega_2) = \sum_n G_0\left(\omega_1, \omega_2 + n\frac{2\pi}{T}\right)$$

An example of a 2-D power density spectrum is shown in Figure 1.

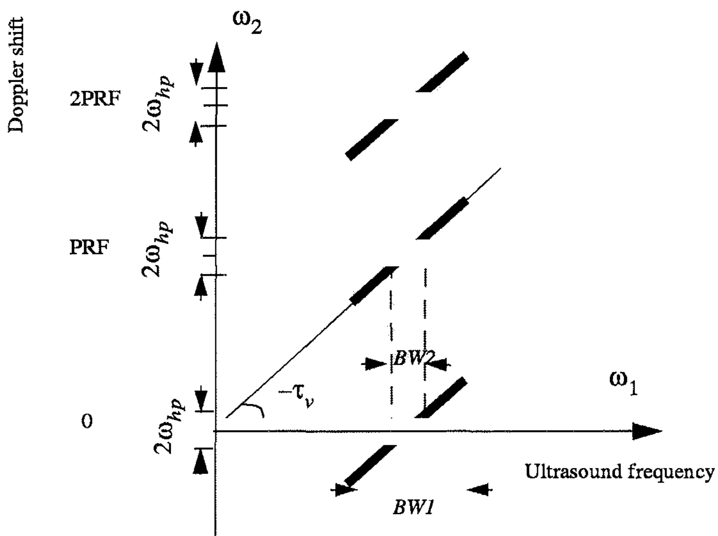

Figure 1 2-D power spectrum of pulsed wave Doppler signal without transit time effect

To estimate the blood velocity by CCM, we make use of the correlation coefficient $R_0(\tau,1)$ defined as the 2-D Fourier transform of the power spectrum. When a wall filter is applied, the 2-D correlation function will be:

$$R_o(\tau, 1) = \int_{-\infty}^{\infty} \int_{-\pi}^{\pi} G_0(\omega_1, \omega_2) H(\omega_2) e^{-j\omega_1\tau} e^{-j\omega_2} d\omega_1 d\omega_2 = \qquad (2)$$

$$2\int_0^{\infty} P(\omega_1) H(\omega_1\tau_v) \cos\omega_1(\tau - \tau_v) d\omega_1$$

Where $H(\omega_2)$ is the power transfer function of the wall filter and $P(\omega_1) = |P_1(\omega_1)|^2$

The CCM method uses the maximum point of $R_0(\tau,1)$ to calculate the velocity. Since the product $P(\omega_l)H(\omega_l\tau_v)$ is non-negative, an upper bound for the integral in (2) can be found:

$$\int_0^{\infty} P(\omega_1)H(\omega_1\tau_v)\cos\omega_1(\tau-\tau_v)d\omega_1 \le \int_0^{\infty} P(\omega_1)H(\omega_1\tau_v)d\omega_1 \tag{3}$$

From (3) it follows that the expected correlation function attains its maximum at $\tau=\tau_v$. This means that even though the shape of the correlation function (or the power spectrum) is changed, the time delay is able to be estimated, as long as the wall filter $H(\omega_1\tau_v)$ does not remove the power of ultrasound signal $P(\omega_1)$ completely, the estimation will be unbiased.

However, the wall filter does remove a portion of the signal power. It causes decorrelation in the signal and the envelope of the correlation function become smoother. On the other hand, the signal to noise ratio may also be reduced due to the wall filter which also cause the envelope of the correlation function become smoother. Thus, the probability of velocity aliasing may be increased.

Two special situations in which the wall filter $H(\omega_1\tau_v)$ may remove the power of $P(\omega_1)$ completely are worth mentioning here. The first case occurs when the blood velocity is low and $H(\omega_1\tau_v)$ acts as a highpass filter with a cut-off frequency is ω_{hp}/τ_v. When the blood velocity (Doppler shift) power distribution is within the cut-off frequency of the wall filter, all the blood signal power is removed. Therefore, the filter disable the velocity estimator.

The second special case occurs when the blood velocity is high and its Doppler shift power is approximately equal to PRF. Under these conditions the wall filter acts as a stopband filter.

When the blood velocity (Doppler shift) power distribution is within the stopband of the wall filter, all the blood flow signal power is again removed. This situation can only take places when

$$BW_2 > BW_1$$

where BW_1 is the RF signal bandwidth and $BW_2=2\omega_{hp}/\tau_v$ as shown in Figure 1. This condition can be expressed as:

$$\omega_{hp} < \frac{BW_1 \times \tau_v}{2} \tag{4}$$

(4) gives a threshold for the cut-off frequency of the wall filter. The above threshold frequency is proportional to the Doppler shift or the blood velocity. So that it is lowest for a Doppler shift frequency approximately one times the PRF and higher for shift frequencies equal to higher multiples of the PRF. When the Doppler shift is equal to the PRF, (4) can be rewritten as

$$\omega_{hp} < \frac{BW_1}{2f0} = \frac{1}{2Q} \tag{5}$$

where Q is a quality factor defined as f_0/BW_1. For high blood velocity estimation, the right side of (5) ($1/2Q$), gives a useful value for the upper-limit of the cut-off frequency of the wall filter.

The same analysis is valid for the EAM estimator, since the two methods give the same value [1], provided that the radial sampling frequency is sufficiently high.

We can also explain this in another way. From (21) and Appendix of Paper A, the time delay equals to the line slope passing through the origin of the frequency plane and point ($\varpi1$, ϖ), i.e.

$$\tau = \frac{\varpi}{\varpi 1} \tag{6}$$

$\varpi1$ is defined as:

$$\varpi 1 = \frac{\int_0^{\infty}\int_{-\pi+\varpi 1}^{\pi+\varpi 1} \omega_1 G(\omega_1, \omega_2) d\omega_1 d\omega_2}{\int_0^{\infty}\int_{-\pi}^{\pi} G(\omega_1, \omega_2) d\omega_1 d\omega_2} \tag{7}$$

ϖ was defined in (26) Paper A which gives:

$$\tau = \frac{\int_0^{\infty}\int_{-\pi+\varpi}^{\pi+\varpi} \omega_2 G(\omega_1, \omega_2) d\omega_1 d\omega_2}{\int_0^{\infty}\int_{-\pi+\varpi 1}^{\pi+\varpi 1} \omega_1 G(\omega_1, \omega_2) d\omega_1 d\omega_2} \tag{8}$$

If there is a wall filter, the output 2-D spectral density has been affected and the time delay should be

$$\tau = \frac{\int_0^{\infty}\int_{-\pi+\varpi 2}^{\pi+\varpi 2} \omega_2 G(\omega_1, \omega_2) H(\omega_2) d\omega_1 d\omega_2}{\int_0^{\infty}\int_{-\pi+\varpi 1}^{\pi+\varpi 1} \omega_1 G(\omega_1, \omega_2) H(\omega_2) d\omega_1 d\omega_2} \tag{9}$$

which can be further expressed as:

$$\tau = \frac{\int_0^{\infty}\int_{-\pi+\varpi 2}^{\pi+\varpi 2} \omega_2 |P(\omega_1)|^2 \delta(\omega 2 - \tau_v \omega_1) H(\omega_2) d\omega_1 d\omega_2}{\int_0^{\infty}\int_{-\pi+\varpi 1}^{\pi+\varpi 1} \omega_1 |P(\omega_1)|^2 \delta(\omega 2 - \tau_v \omega_1) H(\omega_2) d\omega_1 d\omega_2} \tag{10}$$

$$= \frac{\int_0^{\infty} (\tau_v \omega 1) |P(\omega_1)|^2 H(\tau_v \omega_1) d\omega_1}{\int_0^{\infty} \omega_1 |P(\omega_1)|^2 H(\tau_v \times \omega_1) d\omega_1} \equiv \tau_v$$

This means if $\varpi 1 \neq 0$, the slope of $\varpi/\varpi 1$ is still equal to the time delay τ_v even there is a wall filter. It also means that the time delay estimation is unbiased, or the wall filter will not affect mean value estimation of the time delay.

B. Effects of Wall Filter when the Transit Time Effect is included

So far, the effects of the wall filter are based on the ideal pulsed wave Doppler signal where the transit time effect has not been taken into account. The transit time effect is the spectral broadening along the Doppler frequency axis due to the scatterers entering and leaving the ultrasonic beam. A model for the 2-D spectrum was given in [4]:

$$G_0(\omega_1, \omega_2) = P(\omega_1) |B(\omega_2 + \tau_v \omega_1)|^2 \tag{11}$$

Here B is the Fourier transforms of the transversal two-way beam sensitivity function, $b(d)$, and d is the distance from the ultrasonic beam center axis to the scatterer. A typical example is shown in Figure 2

By comparing the 2-D power spectra between Figure 1 and Figure 2, we make the following observations.

a. In the case of high blood velocity, the requirement on the wall filter cut-off frequency when the transit time effect is absent can also be applied. This means that as long as the blood signal is not completely removed by the filter, the blood velocity can still be estimated.

b. The estimation of the blood velocity is biased when the Doppler shift is close to multiples forth PRF and when transit time effect is present. Since the clutter filter may remove some signal power, the mean Doppler frequency ϖ may have bias. The mean RF frequency $\varpi 1$ may also have a small bias. But it is not significant compared to bias of ϖ and it is neglected here. Therefore, the time delay $\tau = \varpi/(\varpi 1)$ has bias. The bias depends on the true velocity. When the Doppler shift is the same as PRF (Figure 3 (a)), the clutter filter removes power symmetrically around PRF. There is no velocity bias in this case. When the Doppler shift is higher than the PRF (Figure 3 (b)), the clutter filter removes more power from frequencies just

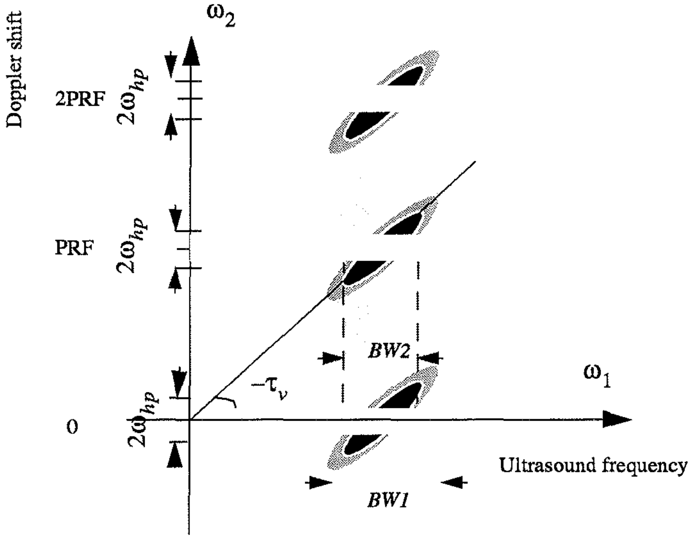

Figure 2 2-D power spectrum of pulsed wave Doppler signal with transit time effect

above PRF than below, the estimated ϖ will be smaller than the true value, causing a negative bias. Conversely, when the Doppler shift is higher than the PRF the bias is positive. An prediction for the velocity estimation bias is sketched in Figure 4. The results are valid in the absence of white noise

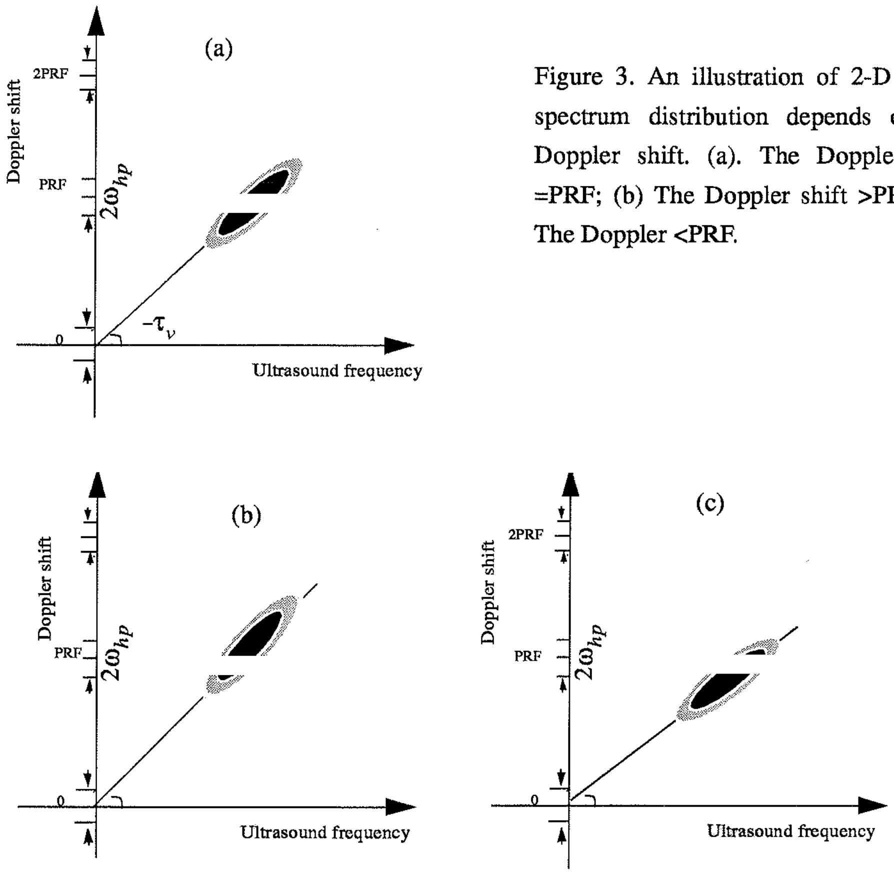

Figure 3. An illustration of 2-D signal spectrum distribution depends on the Doppler shift. (a). The Doppler shift =PRF; (b) The Doppler shift >PRF; (c) The Doppler <PRF.

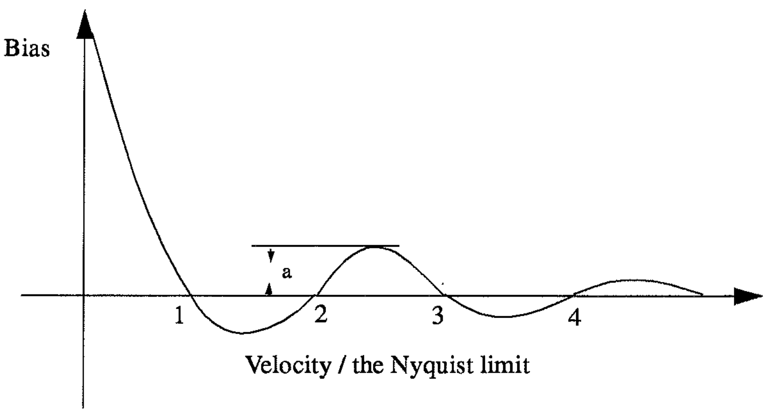

Figure 4 The illustration of velocity estimation bias due to the wall filter

c. The bias value 'a' in Figure 3 depends on the signal spectrum shape and the cutoff frequency of the wall filter. The bias is more pronounced when the bandwidth of the received signal is narrow.

III. Simulation Results

Flow signal was generated using the model in [1] including transit time effect. The following parameters were used: Pulse length: 0.8μs. The center frequency: $5MHz$, PRF: $6.564kHz$, giving a Nyquist limit v_{NY}: 1.0265m/s. The processing procedures include demodulation, wall filtering and velocity estimation. The depth and temporal averaging for each estimation is 2.4μs and 9.75ms, respectively.

The wall filter is a FIR filter with 20 taps and utilizes a Kaiser window. After wall filtering the data is weighted by a Hamming window. The velocity is calculated by the EAM method from 50 independent signal segments.

Case A: The velocity estimation result is shown in Figure 4 for a cutoff frequency $\omega_{hp} = 0.2\pi$, SNR=30dB. One can see that a large velocity estimation bias exists at very low velocities while higher velocities have a small bias. The bias is zero when the velocities are multiples of $2v_{NY}$. These results are consistent with the discussions in section above.

Case B: The velocity estimation result for a cutoff frequency $\omega_{hp} = 0.41\pi$, and SNR=30dB is shown in Figure 5. As the cutoff frequency increases, estimator bias and velocity aliasing around velocities equal to $2nv_{NY}$ increase as well. This latter finding can be explained on the basis of the wall filter removing part of the signal power which decreases the magnitude of correlation function and flattens its envelope. The probability of aliasing is maximum when the velocity is multiple of 2 v_{NY}, this is because the power removed by the wall filter approaches maximum. This is illustrated in Figure 8. In Figure 6, '--' marks where velocity aliasing occurred. In this case, no velocity aliasing is observed for velocities around four times v_{NY}.

Case C: The velocity estimation results for a cutoff frequency $\omega_{hp} = 0.5\pi$ and SNR=30dB are shown in Figure 7. It is evident that as the cutoff frequency increases, the bias around $2n$ v_{NY}, increases, while the velocity aliasing occurs not only around twice v_{NY}, but also around four times v_{NY}.

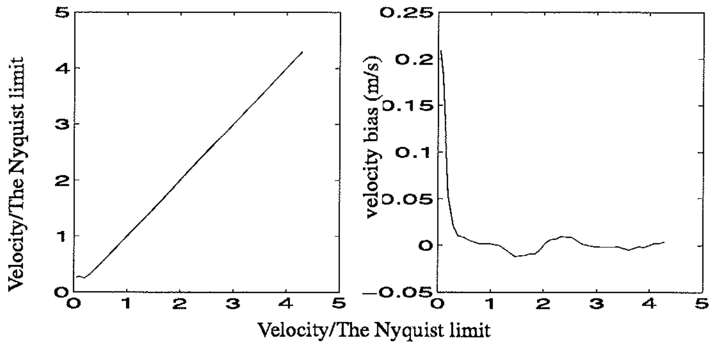

Figure 5 Simulation results for ω_{hp}=0.2π and SNR=30dB.

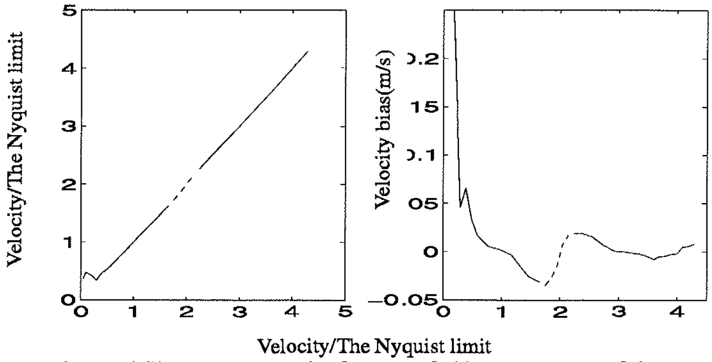

Figure 6 Simulation results for ω_{hp}=0.41π and SNR=30dB,

'--'marks where the velocity aliasing occurred.

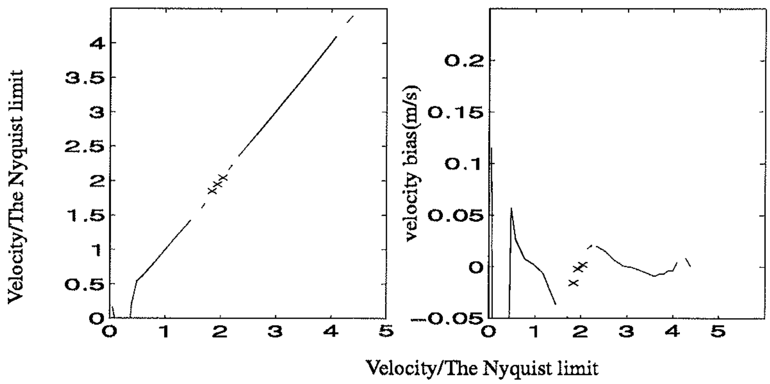

Figure 7 Simulation results for ω_{hp}=0.5π and SNR=30dB. '--' marks where velocity aliasing occurred. 'x' marks the velocity dead zones.

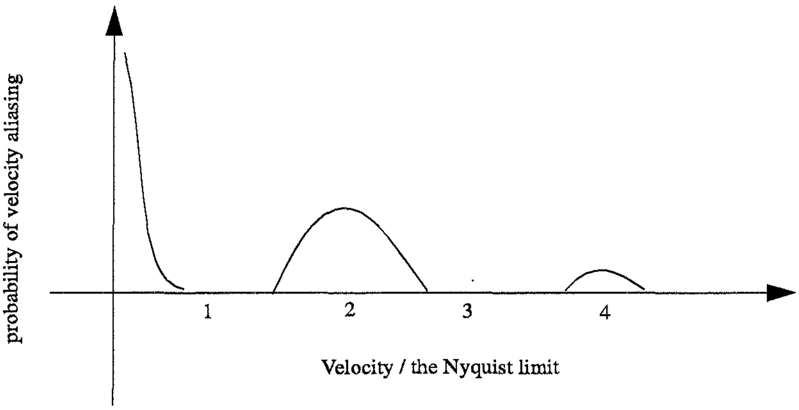

Figure 8 The illustration of the chance of velocity aliasing due to the wall filter

IV. Experimental Verification

Our conclusion regarding the wall filter effect has been verified by experimental ultrasound data taken from subclavian artery flow. Raw RF data from an ultrasound scanner (Vingmed CFM 800) was collected in real time via a custom data acquiescing system.

The parameters used in the experiment are the same as in simulation except that the PRF=4kHz. The processing procedures are also the same but a power threshold was used to discriminate between the noise from the blood signal. The data window for each estimation has the same as in the simulation study.

Case A. cutoff frequency $\omega_{hp} = 0.2\pi$,

Case B cutoff frequency $\omega_{hp} = 0.41\pi$,

Case C cutoff frequency. $\omega_{hp} = 0.44\pi$

Table1: Summary the experiment results

	Dead zones around multiple PRF	Estimated the highest velocity	Correspondin g non-aliasing Dopplershift	Estimated the lowest velocity	Corresponding non-aliasing Doppler shift
$\omega_{hp}=0.2\pi$	No	1.2307(m/s)	1.97π	-0.1201(m/s)	-0.19π
$\omega_{hp}=0.41\pi$	No	1.2141(m/s)	1.94π	-0.2434(m/s)	-0.39π
$\omega_{hp}=0.44\pi$	Yes	-0.6063(m/s)	-0.97π	-0.2665(m/s)	-0.43π

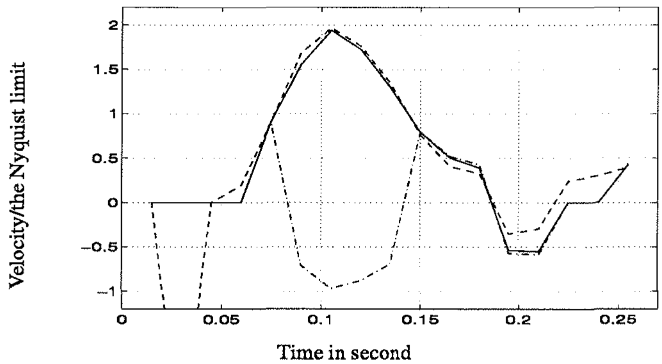

Figure 9 '--' is the results from Case A which $\omega_{hp}=0.2\pi$ '-' is the results from Case B which $\omega_{hp}=0.41\pi$ '-.' is the results from Case C which $\omega_{hp}=0.44\pi$.

The experiment showed similar performance as the simulations, and the results are summarized in Table 1 and Figure 9.

V. Conclusions

The influence of a wall filter to velocity estimators in both the CCM and the EAM is investigated. Theoretical analysis showed that both estimators are unbiased, when no transit-time effect is present, provided that the signal power is not completely removed by the wall filter. When transit-time effect was included, a theoretical estimator bias curve was calculated. When the cut-off frequency of the wall filter is below a upper limit, there will be no velocity dead zones around multiply $2v_{NY}$, but the probability of velocity aliasing will be increased. The highest aliasing probability occurring at the velocity = $2nv_{NY}$.

Accounting for transit time effects introduces a bias into the velocity estimates. Furthermore, this bias depends on velocity.

The occurrence of velocity aliasing and the velocity estimation bias depend mainly on the bandwidth of signal and the cutoff frequency of the wall filter. Other factors such as depth and temporal averaging, signal to noise ratio and velocity may also affect the estimation error. In order to reduce the occurrence of velocity aliasing and velocity estimation bias, the cut-off frequency of wall filter should remain as low as possible.

Those conclusions have been verified by simulations and experimental data.

References

[1] O. Bonnefous and Pesquė: "Time Domain formulation of Pulse-Doppler Ultrasound and blood velocity Estimation by cross-Correlation." *in Ultrasonic Imaging* 8. 1986

[2] X. Lai, H. Torp, and K. Kristoffersen, "An Extended Autocorrelation Method for Estimation of Blood Velocity, "*IEEE Trans. on Ultrasound, Ferroelectrics, and Frequency control,* Nov, 1997

[3] L. S. Wilson, "Description of Broad-Band Pulsed Doppler Ultrasound processing Using the Two-Dimensional Fourier Transform," *Ultrasonic Imaging* 13, 301-315, 1991

[4] H. Torp, K. Kristoffersen, "Velocity Matched Spectrum Analysis: A New Method for Suppressing Velocity Ambiguity in Pulsed-Wave Doppler," *Ultrasound in Med. & Biol.,* Vol. 21 No.7, pp.937-944, 1995

[5] J. A. Jensen, "Stationary Echo Cancelling in Velocity Estimation by Time-Domain Cross-Correlation," *IEEE Transactions on Medical Imaging,* Vol. 12. No. 3 September, 1993

[6] Thanasis Loupas, J. T. Powers and Robert W. Gill, "An Axial Velocity Estimator for Ultra-sound Blood Flow imaging, Based on a Full Evaluation of the Doppler Equation by Means of a Two-Dimensional Autocorrelation Approach," *IEEE Trans.on Ultrasound,Ferroelectrics,and Frequency control,* vol.42, NO.4. pp.672-689, July, 1995

EXTENDED AUTOCORRELATION METHOD FOR COLOR FLOW IMAGING

X-M. LAI, H. TORP, and K. KRISTOFFERSEN*,

Dep. of Biomed. Engineering, University of Trondheim, Norway,
*Vingmed Sound, Horten, Norway

SUMMARY

The conventional autocorrelation method for color flow imaging (CFI) is based on the phase estimation of the autocorrelation function with temporal lags. A new method for velocity estimation based on the autocorrelation function with lags both in temporal and axial direction, is presented. The new algorithm shows better performance than the conventional autocorrelation technique in the estimation variance and the capability of resolving velocity ambiguity. This can be explained by the axial information added in the estimation. The performance of this new algorithm is compared to the RF cross-correlation technique in the estimation variance and the ability to estimate the maximum velocity up to three times the Nyquist limit. The estimation variance is calculated by simulation using a theoretical signal model with different pulse bandwidth and signal-to-noise ratio. The improvement of this new algorithm is demonstrated by digitized ultrasound RF-data from a jet flow in a water-tank model.

INTRODUCTION

The conventional autocorrelation method for CFI is based on the phase estimation of the autocorrelation function. Parameters such as velocity, velocity spread and signal power are calculated from the autocorrelation function of the complex demodulated pulsed Doppler signal from each rang gate on the beam axis. They are coded into a color image which overlay with the standard gray level tissue image. This method was firstly developed for weather radar applications and applied to ultrasound blood velocity measurement in 1983 by a Japanese group [1]. There are mainly two limitations in this method. One is the velocity ambiguity problem caused by the sampled nature of pulsed Doppler. The other is the large variance of the velocity estimation. Because high range resolution need wideband transducer which leads to the increase of variance in the velocity estimation.

An alternative algorithm called crosscorrelation method for blood velocity estimation has been presented by Bonnefous [2]. The crosscorrelation algorithm is based on estimation of the time delays of the received echoes from the pulse-to-pulse from the crosscorrelation function of the RF signal. The two limitations of the conventional autocorrelation can be overcome by the crosscorrelation method [2]. Because the time delays is found by detecting the peak amplitude of the crosscorrelation function, the wrong peak detection can happen in some cases because of the estimation variance of the crosscorrelation function. In this paper, the velocity estimation error caused by wrong peak detection of the correlation function is called aliasing estimate error.

In this work, a new extended autocorrelation (EAM) is proposed. It uses both of the phase and the amplitude of the autocorrelation function to estimate the velocity. It uses firstly the phase of the autocorrelation function to give a limited number of candidates in time delays which is proportional to the velocity. Then it selects the candidate which corresponds to the maximum amplitude of the autocorrelation function. The true velocity is determined by the selected candidate, consequently. The similarity between the EAM and crosscorrelation method is analyzed theoretically, and a quantitative comparison for different velocity estimators is performed with computer simulations.

ALGORITHM DESCRIPTION

Assuming $x(t, k)$ is the received complex demodulated signal. The parameter t is the elapsed time after pulse transmission, which corresponds to a certain range distance from the transducer, and k is pulse number. If there is a frequency dependent attenuation, the signal spectrum of $x(t, k)$ is not symmetrical around zero frequency but around a frequency of $\Delta\omega$. This $\Delta\omega$ can be estimated by the phase of the autocorrelation function $\hat{R}_x(1, 0)$. If $x'(t, k)$ is the frequency shifted complex demodulated signal of $x(t, k)$ and assume the spectrum of $x'(t, k)$ is symmetrical around zero frequency. Then we have: $x'(t,k)=e^{-i\Delta\omega t}x(t,k)$. The relation between the autocorrelation functions is

$$\hat{R}_{x'}(\tau, m) = e^{-i\Delta\omega\tau}\hat{R}_x(\tau, m) \tag{1}$$

where τ is the arbitrary lag in range, and m in time (or pulse number).
The approximate relation between the correlation function of the RF signal $\hat{R}_s(\tau, m)$ and autocorrelation function $\hat{R}_x(\tau, m)$ was derived in a previous paper [3] as:

$$\hat{R}_s(\tau, m) \approx \frac{1}{2}Re\{e^{i\omega_0\tau}\hat{R}_x(\tau, m)\} \tag{2}$$

where ω_0 is the center frequency in the transmitted signal. From (1) and (2), we have:

$$\hat{R}_s(\tau, m) \approx \frac{1}{2}Re\{e^{i(\omega_0+\Delta\omega)\tau}\hat{R}_{x'}(\tau, m)\} \tag{3}$$

If the envelope of $\hat{R}_{x'}(\tau, 1)$ is sufficiently smooth, then the peak in the correlation function $\hat{R}_s$ occurs when $\tau = \tau_{max}$ i.e.

$$phase\{e^{i(\omega_0+\Delta\omega)\tau}\hat{R}_{x'}(\tau, 1)\} = 0 \tag{4}$$

So the following relation between the autocorrelation phase angle estimate and the 'peak crosscorrelation estimate' can be found as:

$$(\omega_0 + \Delta\omega)\tau_{max} \approx 2\pi n - phase\left\{\hat{R}_{x'}(\tau_{max}, 1)\right\} \tag{5}$$

In [4], it is shown that the phase of $\hat{R}_{x'}(\tau, 1)$ is independent of τ when there is only one velocity component inside the sample volume. That means we can use the phase of $\hat{R}_{x'}(\tau, 1)$ for any τ instead of the phase of $\hat{R}_{x'}(\tau_{max}, 1)$.
From (1) and (5), we have:

$$(\omega_0 + \Delta\omega)\tau_{max} \approx 2\pi n - phase\left\{\hat{R}_x(\tau_{max}, 1)\right\} + \Delta\omega\tau_{max} \tag{6}$$

The new method is firstly to estimate the phase of $\{\hat{R}_x(\hat{\tau}_{max}, 1)\}$ and find a number of the candidates which are:

$$\tau_n = \frac{1}{(\omega_0 + \Delta\omega)}\{2\pi n - phase\{\hat{R}_x(\hat{\tau}_{max}, 1)\} + \Delta\omega\hat{\tau}_{max}\}(n = 0, \pm 1 \ldots \pm K) \tag{7}$$

where $\hat{\tau}_{max}$ is the rough estimate of τ_{max}, because true τ_{max} is unknown in this step and $\hat{\tau}_{max}$ is found by maximizing the amplitude of $\hat{R}_x(\tau, 1)$. K is the number of the Nyquist repetition. Then, it uses the amplitude of $\hat{R}_x(\tau, 1)$ to determine which τ_n corresponds to the maximum amplitude of $\hat{R}_x(\tau, 1)$. The velocity is determined by the selected τ_n.

In a practical situation, the autocorrelation function is sampled in the radial coordinate τ. The amplitude of $\hat{R}_x(\tau, 1)$ for any τ can be found using some kind of interpolation technique.

SIMULATION RESULTS

To evaluate the velocity estimators, some simulation experiments were performed. In paper [4], a parametric model for the 2D signal from blood flow with constant, rectilinear velocity field is described. The signal is completely described by the single scatterer response, where the transmitted pulse waveform, beamwidth and velocity magnitude and direction can be selected. Two-dimensional blood flow signals were generated by convolution of a matrix of independent Gaussian random variables, with the ultrasonic system single scatterer response[3]. The simulation parameters in this paper were given as follows.

Transducer center frequency	2.5MHz	RF sampling rate	10MHz
Pulse repetition frequency	6564Hz	Ultrasonic measurement angle	30degree
Speed of sound	1540m/s	Temporal averaging	1.8ms
Nyquist velocity	1.0265m/s	Radial averaging	3 *2.4μs or 3 *0.8μs

The velocity estimators had been applied to simulated signals with constant velocity v=0.2 m/s, v=0.5m/s,v=1.2m/s, v=2.2m/s and v=3.2m/s from 50 independent simulations. The values in the table are standard deviation or the probability of aliasing estimate error of velocity estimators. The probability is denoted by "P" and it is defined as

$$P= \frac{\text{the number of aliasing estimate}}{\text{the total estimate number}} *100\%$$

The probability of aliasing estimate error will be displayed in the table instead of standard deviation when P>0.

The result shows that the EAM has less velocity estimate variance than the conventional autocorrelation method both for low bandwidth and high bandwidth. This is because the radial information has been added to the EAM. There is no significant difference between the EAM and the crosscorrelation method. Both of them have the ability to estimate the velocity which is beyond Nyquist limit and give the similar variance. The aliasing estimate errors have been observed in the case of low pulse bandwidth and low signal to noise ratio. This is because the correlation function of low pulse bandwidth or under poor SNR condition is flat compared to high pulse bandwidth and under high SNR condition, respectively. The estimation variance of the correlation function has heavy influence on the detection of the true peak in the correlation function and the aliasing error can occur.

Table 1: The variance of the velocity estimators

pulse length	velocity	Autocorr. SNR=∞	EAM SNR=∞	Cross-corr. SNR=∞	Autocorr. SNR=0	EAM SNR=0	Cross-corr. SNR=0
2.4μs	0.2m/s	0.0241	0.0120	0.0122	0.0573	10%(P)	10%(P)
2.4μs	0.5m/s	0.0344	0.0163	0.0164	0.1105	4%(P)	0.0192
2.4μs	1.2m/s	——	0.0177	0.0179	——	4%(P)	4%(P)
2.4μs	2.2m/s	——	0.0206	0.0209	——	8%(P)	10%(P)
2.4μs	3.2m/s	——	0.0237	2%(P)	——	6%(P)	4%(P)
0.8μs	0.2m/s	0.0317	0.0095	0.0094	0.1696	0.0136	0.0136
0.8μs	0.5m/s	0.0609	0.0165	0.0162	0.1149	0.0189	0.0194
0.8μs	1.2m/s	——	0.0178	0.0170	——	0.0207	0.0190
0.8μs	2.2m/s	——	0.0228	0.0221	——	0.0267	0.0258
0.8μs	3.2m/s	——	0.0196	0.0195	——	0.0241	0.0249

EXPERIMENTAL RESULTS

a. Water-tank model

Figure 1 shows a schematic diagram of the water-tank. It consists of an upper reservoir tank and a flow tank which has two rooms. There is a small jet aperture between the two rooms. The fluid flow from the upper reservoir tank to the left room of the flow tank by a tube with a valve. This valve is used to control the water pressure in the left room which determines the jet velocity. A pump in the right room is controlled by an adaptive water level regulator. The fluid is pumped back to the upper reservoir tank. Figure 2 is an illustration of the jet stream.

b. The parameters in this experiment

Transducer center frequency	2.5MHz	RF sampling rate	10MHz
Pulse repetition frequency	5670Hz	Acoustic velocity	1540m/s
Temporal averaging	2.1ms	Nyquist velocity	0.8732m/s
pulselength	0.8μs	Radial averaging	1.28μs

c. The gray flow imaging of the jet stream

Figure 3 is the velocity image estimated by the extended autocorrelation method.

Figure 4 is the velocity image estimated by the conventional autocorrelation method.

Figure 4 illustrates that the velocity aliasing occurs and only low velocities which are below the Nyquist limit are estimated correctly. Figure 3 shows that the EAM can estimate velocities up to three times the Nyquist limit. But the aliasing estimate error occurs at some places in Figure 3.

CONCLUSIONS

The extended autocorrelation method (EAM) of velocity estimation for color flow imaging has been presented. The performance of EAM, crosscorrelation and autocorrelation velocity estimators has been assessed by simulation using a theoretical signal model. The results show that the performance of EAM is better than the conventional autocorrelation method. The EAM and crosscorrelation method give a similar performance in the estimation variance and capability of resolving velocity ambiguity. Those two methods can work well for high pulse bandwidth. Therefore, the range resolution and accuracy of the estimated velocity are improved. For low pulse bandwidth and under the situation of poor signal to noise ratio, significant aliasing error occurred for both two methods.

REFERENCES

[1] C. Kasai, K. Namekawa, A. Koyano, and R. Omoto, "Real-time Two-Dimensional Blood Flow Imaging Using an Autocorrelation Technique" *IEEE Trans. Sonics Ultras., vol.SU-32, pp458-464, 1985*

[2] O.Bonnefous and Pesquė, "Time Domain formulation of Pulse-Doppler Ultrasound and blood velocity Estimation by Cross-Correlation," *in Ultrasonic Imaging 8. 1986*

[3] H .Torp, X. M. Lai and K. Kristoffersen, "Comparison Between Cross-Correlation and Auto-Correlation Technique in Color Flow Image" in *Ultrasonic Symposium. 1993, Baltimore*

[4] H. Torp, K. Kristoffersen and B. Angelsen, "Autocorrelation Techniques in Color Flow Imaging", *IEEE Trans.onUltrasound Ferroelectrics and Frequency control, vol.41, pp604-612,1994*

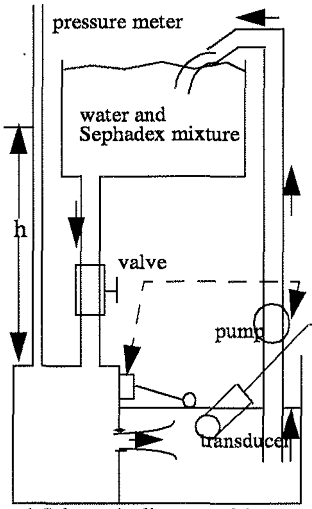

Figure 1 Schematic diagram of the water-tank

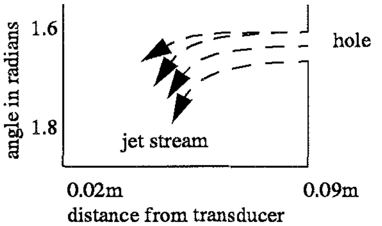

Figure 2 An illustration of jet stream

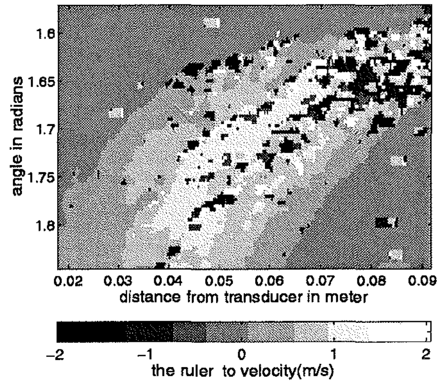

Figure 3 Velocity image of the jet stream using the EAM method

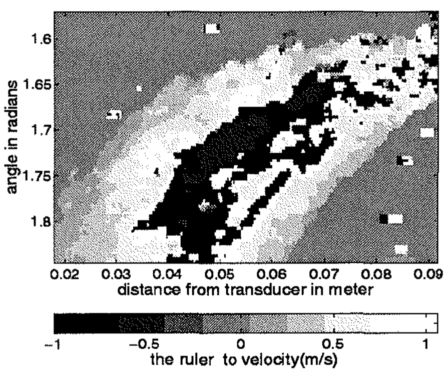

Figure 4 Velocity image of the jet stream using the autocorrelation method

Appendix A

Interpolation Method for Time Delay Estimation in the RF-signal Crosscorrelation Technique for Blood Velocity Measurement

X. LAI and H. TORP
Dep. of Cybernetics Eng., and Dep. of Physiology & Biomedical Eng.,
The Norwegian University of Science and Technology

Abstract

The cross correlation method (CCM) for blood flow velocity is based on the time delay estimation of the echoes from pulse-to-pulse. The sampling frequency is usually kept low in order to reduce computation complexity, and the peak in the correlation function is found by interpolating the correlation function. The parabolic-fit interpolation method introduces bias at low ratio of sampling rate to ultrasound center frequency. In this work, 4 different interpolation methods are suggested to improve the estimation accuracy.

1. Parabolic-fit with bias-compensation, derived from a theoretical signal model.
2. Parabolic-fit combined with linear filter interpolation to the correlation function.
3. Parabolic-fit to the correlation function of the complex signal envelope.
4. Matched filter applied to the correlation function interpolation.

The new interpolation methods are analyzed both by computer simulated signals, and RF-signals recorded from patient data with velocities up to 4 times the Nyquist velocity. The results show that these methods have similar estimation accuracy when signal to noise ratio (SNR) is high and the matched filter interpolation gives the better performance when SNR is low.

1. Introduction

The cross-correlation method of the time domain technique has been used for estimating the blood velocities [1], and has advantages over the Doppler method in many applications [2]. The CCM is by searching the maximum correlation coefficient $R(\tau, 1)$ (in depth and temporal direction) for the time delay τ_1, i.e, $\tau_1 = max_{\tau}(R(\tau, 1))$ where $R(\tau, 1)$ is a 2D RF correlation function model given in [6]. With the approximated Gaussian envelope, a theoretic correlation model is:

$$R(\tau, 1) = \exp\left(-\frac{(\tau-\tau_1)^2}{2\sigma^2}\right)\cos(2\pi f0(\tau-\tau_1)) \qquad (1)$$

$$\tau_1 = \frac{2Tv\cos\theta}{c} \qquad (2)$$

In which the standard deviation σ is given by the RMS bandwidth $B = 1/\sigma$. T is pulse repetition period, v is the blood velocity, c is the ultrasound speed, θ is the angle between the ultrasound beam and blood vessel.

In practice, the digital echo signal is discrete due to the sampling. The true location of the maximum correlation coefficient is not constrained to discrete increments, and may fall between the discrete sampling points; which results in the estimation inaccuracy. Interpolation is necessary to improved the time delay estimation accuracy [3].

The curve-fitting method of the parabolic-fit and the cosine-fit [4], [5]; the linear filter interpolation methods [4], [7] are usually used. The parabolic-fit method is usually simple but it has bias when the ratio of the sampling rate to the center frequency (*fs/f0*) is low [3], [4]. To reduce computation complexity, *fs/f0* is usually kept low (in the order of 4). In this situation the curve-fitting interpolation methods above suffer from large errors for velocities exceeding the Nyquist limit.

In this work, four other interpolation methods are proposed, and evaluated.

2. Parabolic-fit with bias-compensation

The parabolic-fit has been used in many applications. This method only requires a few operations. It works in densely sampled RF correlation function, but it has bias when the sampling rate is low. The bias introduced by parabolic-fit depends on the Q-factor ($Q = f_0/B$), *fs/f0* and the velocity (v) itself. The bias is denoted *b(v,fs/f0,Q)*, can be calculated from the theoretical correlation function model Eqn(1). Some examples are shown in Fig.1.

$$b\left(v, \frac{fs}{f0}, Q\right) = v - \hat{v} \quad (3)$$

where $\hat{v}$ is the estimated velocity by the parabolic-fit.

One method to reduce the estimated velocity bias is to compensate it by using the *priori* knowledge of the estimated velocity bias from the theoretical correlation function model. Rewrite Eqn(3) as:

$$v = \hat{v} + b\left(v, \frac{fs}{f0}, Q\right) \quad (4)$$

Using the zero order approximation:

$$b\left(v, \frac{fs}{f0}, Q\right) \approx b\left(\hat{v}, \frac{fs}{f0}, Q\right)$$

Eqn(4) become:

$$v = \hat{v} + b\left(\hat{v}, \frac{fs}{f0}, Q\right) \quad (5)$$

The blood velocity estimated by Eqn(5) is parabolic-fit with bias-compensation. The bias-compensation may be implemented by look-up table.

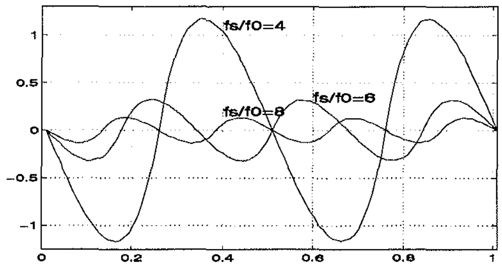

Fig.1 The velocity estimation bias by parabolic-fit for signal with Q=1 which is calculated from the theoretical correlation function model.

3. Parabolic-fit combined with linear filter interpolation

The parabolic-fit interpolation calculates a few correlation coefficients in the vicinity of the maximum discrete point. The true maximum amplitude could be missed when *fs/f0* is low and the false maximum from the subsidiary peak could be selected. In other word, the velocity aliasing occurs. It can be derived that the aliasing error is likely to occur when

$$\frac{fs}{f0} \leq \frac{2\pi}{\operatorname{acos}[\exp(-1/2(\sigma f_0)^2)]} \quad (6)$$

To avoid the aliasing error in the parabolic-fit, the *fs/f0* has to be increased. The digital approach of the linear filter interpolation is usually used to increase the sampling rate from *fs/f0* to *Mfs/f0* by using lowpass filter [7], where M is the interpolation rate. According to Eqn(6), the required M depends on the *Q*-factor of the signal and Mfs/f0>6.84, there will be no aliasing for *Q*=1 signal. That means for a signal with a central frequency=bandwidth (2.5MHz in our simulations later), an interpolation rate M=2 is required to avoid aliasing error.

This method is to increase the sampling rate with M=2 to the correlation coefficients before the parabolic-fit. It is more efficient than the reconstruct filter interpolation [4] in which the interpolation rate M has to be very high (M=50) to get the same estimation accuracy, furthermore the bias introduced by the parabolic-fit in this method is small.

A simple lowpass filter is halfband filter [7] in the linear filter interpolation with rate two. It satisfies the zero-crossing criterion of ideal filters and results in efficient designs in that every other coefficient is zero and need not be computed in a practical implementation.

4. Parabolic-fit to the complex envelope of the correlation function

Ultrasound scanner which use the conventional autocorrelation technique is based on the complex signal. The cross correlation function can be calculated in baseband, and remodulated to the RF domain, followed by interpolation and peak detection. But it is efficient to use parabolic-fit to the real part and the imaginary part of the complex correlation function, respectively, before remodulating.

5. Matched filter interpolation to the correlation function

5.1 Matched filter method

Time delay is a basic estimate in many applications. A generalized crosscorrelation for time delay estimation was given in the classic work [8]. The block diagram is

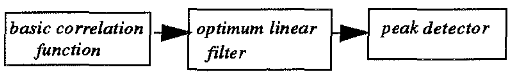

Fig.2. Diagram of time delay estimate

Because of the deteriorating effect of the noise on the time delay detection, a false peak may be produced and cause a false estimate of the time delay. The purpose of the optimum liner filter $w(\tau)$ is to minimize the occurrence of false peaks.

The received signal from two successive pulses is given by

$$z(t, k) = y(t, k) + n_1(t, k) \quad (7)$$

$$z(t+\tau, k+1) = y(t+\tau, k+1) + n_2(t+\tau, k+1) \quad (8)$$

where y is the blood signal, n_1, n_2 are the white Gaussian noise, z is the received signal. The correlation function is:

$$R_z(\tau, 1) = R_y(\tau, 1) + R_{y,n_1}(\tau, 1) + R_{n_2,y}(\tau, 1) + R_{n_1,n_2}(\tau, 1)$$

but due to the finite observation time, in general, $\langle R_{y,n}(\tau, 1)\rangle + \langle R_{n,y}(\tau, 1)\rangle$ and $R_{n_1,n_2}(\tau, 1)$ are not zero and thus contributes to the noise of the correlation function. The noise depends on the SNR of the signal and the length of the finite observation time. According to criteria of maximizing of expected signal peak *at* τ relative to the background noise, the resulting optimum filter [8] in term of signal and noise spectral density is:

$$W(\omega) = \Phi_y(\omega)/ \tag{9}$$

$$\Phi_{n_1}(\omega)\Phi_{n_2}(\omega) + \Phi_y(\omega)\left(\Phi_{n_1}(\omega) + \Phi_{n_2}(\omega)\right) + \Phi^2{}_y(\omega)$$

where $\Phi_y(\omega)$ is the Fourier transform of the correlation function R_y, $\Phi_{n_1}(\omega)$ and $\Phi_{n_2}(\omega)$ are the noise spectral densities.

From Eqn(9), it is seen that it is certainly difficult to design the true optimum filter since it has a complicated relationship to signal and noise spectral characteristics. The Eckart filter is used in practice. It uses the criterion that maximizes the ratio of mean correlator output due to the signal present to the variance of the correlator output due to noise alone. The resulting filter is

$$W(\omega) = \Phi_y(\omega)/\Phi_{n_1}(\omega)\Phi_{n_2}(\omega) \tag{10}$$

To the white noise, the spectral densities $\Phi_{n_1}(\omega)$ and $\Phi_{n_2}(\omega)$ are independent to ω. In this case, this suboptimum linear filter is matched filter with impulse response $w(\tau) = R_y(\tau, 1)$. The matched filter for estimating time delay is

$$m(\tau) = \int (R_z(\tau_1, 1))R_y(\tau - \tau_1, 1)d\tau_1 \tag{11}$$

The peak detector is performed on $m(\tau)$

5.2 Matched filter applied to the correlation function interpolation

It is shown that the match filter can also be used in the interpolation for estimation time delay when the RF-signal is sampled in low sampling rate. In this application the matched filter with high sampling rate is used as anti-imaging filter in the linear filter interpolation, therefore it is no necessary to use extra narrow bandwidth anti-imaging filter. So the matched filter has two functions, one is that it is a suboptimum linear filter to maximum the signal peak to output noise, the other is that it replaces narrow bandwidth filter to eliminate the image spectra produced in the zero padding in the interpolation.

5.3 Performance comparison between matched and linear filter interpolation

It is seen that the matched filter of Eqn(10) approximate the optimum filter Eqn(9) when SNR is low. Its performance is verified by the simulation. In the simulation, the matched filter interpolation method, linear filter interpolation method which includes the combined interpolation method and the reconstruct filter interpolation method are applied to the simulation signal. The error probability p is calculated as

$$p = \frac{number\ of\ abs(v - \hat{v}) > accuracy\ limit}{number\ of\ simulations} \tag{12}$$

where v is the true velocity and $\hat{v}$ is the estimated velocity, the accuracy limit varies from 5% to 50% of the Nyquist velocity. The error probability explains that the probability of making a false peak in the estimation of the time delay. The results in Fig.3 is from 2000 independent simulations and it shows that the error probability for those three methods are similar when SNR is high and the error probability for the matched filter interpolation is lower than others when SNR is low which means the performance by the matched filter method has been improved.

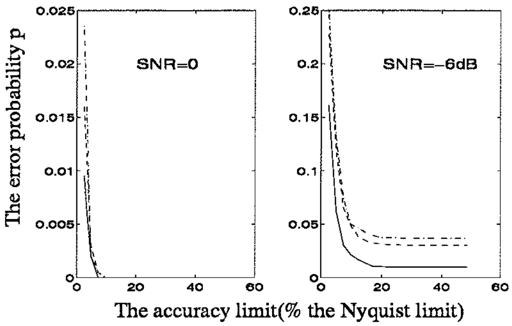

'-' matched filter interpolation, '--' reconstructive interpolation.'-.' combination interpolation.

Fig.3 Performance comparison between matched and linear filter interpolation

6. Simulation results

The interpolation approaches are verified by the computer simulations in this section. The simulation signal is generated from the model in [6]. The main parameters are given as follows.

Center frequency f0	2.5MHz
Sampling rate fs	10MHz
Bandwidth	2.5MHz
Pulse repetition frequency	6564Hz
Nyquist limit	1.0265(m/s)
temporal averaging	1.8ms
Depth averaging	2.4μs

If the blood signal is given by Eqn(7), the signal to noise ratio for the sampled received signal is defined as:

$$SNR = 10\log 10 \frac{\sum_n \sum_k y^2(n,k)}{\sum_n \sum_k n_1^2(n,k)} \tag{13}$$

The velocity estimation results are from 50 independent simulations.

Table 1 is the results of the method parabolic-fit with bias compensation. The results show that the velocity estimation bias has been reduced significantly by compensation comparing to the parabolic-fit without compensation. Because the parabolic-fit method has aliasing error when applied to the signal fs/f0=4, only the estimation results to the velocities within the Nyquist limit are given.

Table 1: The velocity estimation bias and standard deviation (SD)(% Nyquist velocity) with parabolic-fit (A) and parabolic-fit with bias compensation(B). SNR=30dB

	A		B	
	0.2m/s	0.5m/s	0.2m/s	0.5m/s
bias	-2.192	0.322	-0.059	-0.056
SD	1.289	1.159	1.033	1.419

Table 2 is the results of the method parabolic-fit combined with linear filter interpolation. The velocities up to 4 times the Nyquist limit have been estimated.

Table 2: The velocity estimation bias and standard deviation(SD)(% Nyquist velocity) with parabolic-fit combined with linear filter interpolation. SNR=30dB

	0.2m/s	0.5m/s	1.2m/s	2.2m/s	3.2m/s	4.2m/s
bias	-0.308	-0.583	0.483	0.521	0.787	0.330
SD	1.141	1.459	1.877	1.935	2.519	3.080

Table 3 is the results of the method parabolic-fit to the complex correlation function. The results show that the estimation error and variance are similar to results in **Table 2**

Table 4 is the results of the method matched filter applied to the correlation function interpolation. The results show that there is no significant difference to the results in **Table 2** and **Table 3**

Table 3: The velocity estimation bias and standard deviation (SD)(% Nyquist velocity) with parabolic-fit to the complex correlation envelope. SNR=30dB

	0.2m/s	0.5m/s	1.2m/s	2.2m/s	3.2m/s	4.2m/s
bias	-0.093	-0.049	0.097	0.010	0.195	0.023
SD	0.922	1.442	1.724	1.812	2.289	2.871

Table 4: The velocity estimation bias and standard deviation(SD)(% Nyquist velocity) with matched filter interpolation. SNR=30dB

	0.2m/s	0.5m/s	1.2m/s	2.2m/s	3.2m/s	4.2m/s
bias	0.434	0.591	0.818	0.880	0.721	0.418
SD	1.007	1.474	1.841	1.938	2.565	3.079

7. Experiment evaluation

The interpolation approaches are verified by the experimental data from subclavian artery in this section.

A. The parabolic-fit with bias-compensation applied to experimental data from subclavian artery which velocities are within the Nyquist limit.

The first method parabolic-fit with bias-compensation has velocity aliasing error when applied to the signal with fs/f0 =4. In this experiment, the Nyquist limit is 1.0265m/s and the velocities are limited within the Nyquist limit. The results are in Fig.4.The results show that there is difference between parabolic-fit without compensation and with bias-compensation and there is no significant different between parabolic-fit with bias-compensation and cosine-fit interpolation[5]

B. The interpolation methods applied to the experimental data with velocities up to 2 times the Nyquist limit

The second, the third and the forth approaches can estimate high velocities beyond the Nyquist limit when fs/f0=4.

Fig.5 has the results for these interpolation methods applied to the experimental data from the subclavian artery with the velocities up to 2 times the Nyquist limit (The Nyquist limit is 0.6255m/s). The results show there is no significant difference between them.

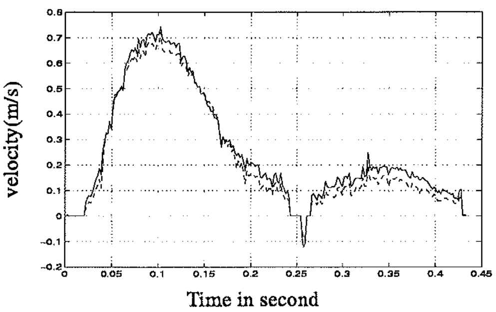

'-' parabolic-fit with bias compensation,
'--' the parabolic-fit without compensation.

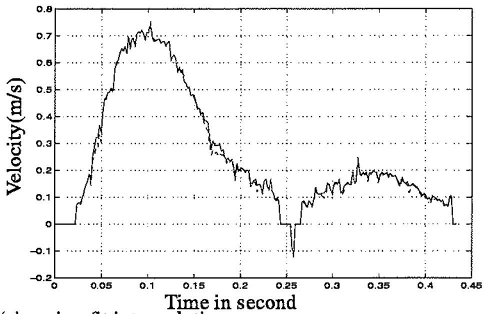

'-' cosine-fit interpolation,
'--' parabolic-fit with bias-compensation.

Fig.4 Experimental evaluation of Parabolic-fit with bias-compensation, parabolic-fit and cosine-fit interpolation.

C. The methods applied to the experimental data with velocities up to 4 times the Nyquist limit

This experimental data were obtained from the data which were used in velocity image Fig. 5 by decimating the RF data to reduce the pulse repetition frequency, so a lower Nyquist velocity was obtained (The Nyquist limit is 0.3128m/s). This decimation was done before the wall motion filter. The results are shown in Fig.6.

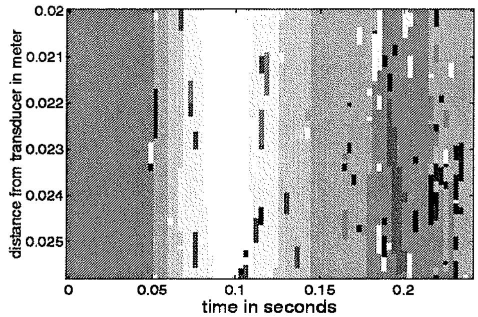

Velocity image obtained with method 2 parabolic-fit combined with linear filter interpolation.

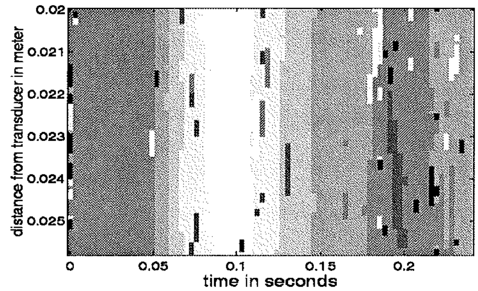

Velocity image obtained with method 3 parabolic-fit to the complex correlation envelope.

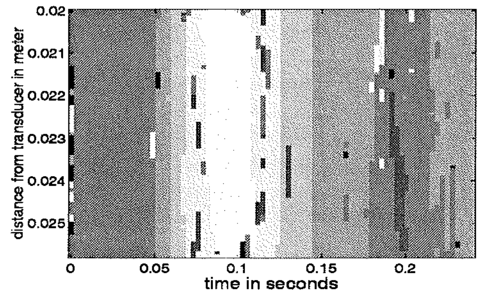

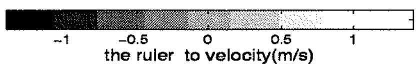

Velocity image obtained with method 4 matched filter interpolation to the correlation function

Fig.5. Experimental evaluation: Method 2, method 3 and method 4 applied to the experimental data with velocities up to 2 times the Nyquist limit.

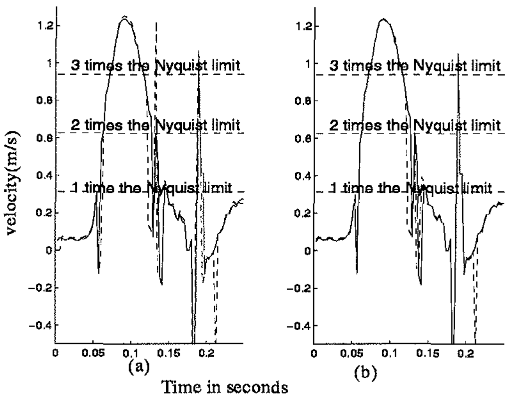

'--' in (a) parabolic-fit to the complex correlation envelope
'-' in (a) matched filter interpolation.
'--' in (b) parabolic-fit combined with linear filter interpolation.
'-' in (b) with the matched filter interpolation

Fig.6. Experimental evaluation: Method 2, method 3 and method 4 applied to the experimental data with velocities up to 4 times the Nyquist limit.

Conclusions

Four interpolation methods for time delay estimation in the RF-Signal crosscorrelation technique for blood velocity measurement are presented. All the methods give similar performance to the blood signal with high SNR(> 0dB) and has higher accuracy than the parabolic-fit when fs/f0 is low. The estimation accuracy is improved from 2.5% to 1% of the Nyquist velocity compared to the parabolic-fit interpolation method when *fs/f0*=4 and Q=1. The matched filter interpolation applied to the correlation function gives better performance than other methods when SNR is low.

The first method; parabolic-fit with bias-compensation method; has least computation, but suffers from aliasing errors when *fs/f0* =4. The second method parabolic-fit combined with linear filter interpolation method avoids the aliasing error by interpolating the correlation function to a higher sampling rate. It requires less computation than method 3 and method 4. The third method; parabolic-fit to the complex correlation function envelope method; has similar performance as method 2, but requires intensive computations modulating baseband signal to RF-band. Using an iterative approach, the computation can be reduced greatly. The forth method which uses matched filter interpolation to the correlation function gives best performance when SNR is low.

References

[1] O. Bonnefous and Pesqué. "Time Domain formulation of Pulse-Doppler Ultrasound and blood velocity Estimation by Cross-Correlation.". *in Ultrasonic Imaging 8. 1986*

[2] I. A. Hein, William D. O'brien, "Current Time-Domain Methods for Assessing Tissue Motion by Analysis from Reflected Ultrasound Echoes--A Review". *IEEE Trans.on Ultrasound, Ferroelectrics, and Frequency control,* vol. 40, NO.2. March, 1993

[3] Foster, GT.C., Embree, M. P. and O'brien,W.D., "Flow velocity profile via time-domain correlation: error analysis and computer simulation", *IEEE Trans.on Ultrasound, Ferroelectrics, and Frequency control,* vol.37, 164-174, 1990

[4] I. Cespedes, Y.Huang et al "Method For Estimation of Subsample Time Delays of Digitized Echo Signals" Ultrasonic Imaging 17, 142-171 (1995)

[5] P.G.M de Jong, T.Arts, A.P.G.Hoeks,and R.S Reneman, Determination of Tissue Motion Velocity by Correlation Interpolation of Pulsed Ultrasonic Echo Signals, *Ultrasonic Imaging* 12, 84-98 (1990)

[6] X.Lai, H.Torp et al, "An Extended Autocorrelation Method for Estimation of Blood Velocity", Submitted to *IEEE Trans.on Ultrasound,Ferroelectrics,and Frequency*

[7] Jae S. Lim, Alan V. Oppenheim, "Advanced Topics in Signal Processing", Prentice Hall,Englewood Cliffs, NJ, 1988

[8] J. C. Hassab and R.E.Bouchek, "Optimum estimation of time delay by a Generalized Corrector", *IEEE Trans. Acoust, Speech, Signal processing,* vol ASSP-27 pp. 373-380, Aug, 1979

Acknowledgments

The authors would like to thank for Vingmed Sound A/S, Horten, Norway, where this study was done.